# SEDIMENTOLOGY AND RESERVOIR CHARACTERISTICS OF MIDDLE JURASSIC DHRUMA FORMATION, OUTCROP APPROACH, CENTRAL SAUDI ARABIA

BY

**IBRAHIM MOHAMED YOUSIF MOHAMED**

A Thesis Presented to the
DEANSHIP OF GRADUATE STUDIES

**KING FAHD UNIVERSITY OF PETROLEUM & MINERALS**

DHAHRAN, SAUDI ARABIA

In Partial Fulfillment of the
Requirements for the Degree of

## MASTER OF SCIENCE

In

**GEOLOGY**

**May 2017**

KING FAHD UNIVERSITY OF PETROLEUM & MINERALS
DHAHRAN- 31261, SAUDI ARABIA
**DEANSHIP OF GRADUATE STUDIES**

This thesis, written by **IBRAHIM MOHAMED YOUSIF MOHAMED** under the direction of his thesis advisor and approved by his thesis committee, has been presented and accepted by the Dean of Graduate Studies, in partial fulfillment of the requirements for the degree of **MASTER OF SCIENCE IN GEOLOGY.**

Dr. Mohammad H. Makkawi
(Advisor)

Dr. Abdulaziz M. Al-Shaibani
Department Chairman

Dr. Osman M. Abdullatif
(Member)

Dr. Salam A. Zummo
Dean of Graduate Studies

Dr. Waleed Abdulghani
(Member)

4/05/12

**Date**

# Dedication

To my loving parents, who pray, encourage and guide me all the way

To my all family members

To my fiancée

To my friends and colleagues

# ACKNOWLEDGMENTS

I would like to acknowledge King Fahd University of Petroleum & Minerals (KFUPM) for providing me this opportunity to pursue my graduate studies. The Geosciences Department at College of Petroleum Engineering and Geosciences (CPG) is highly appreciated for support and laboratory facilities to carry this research. I would like also to extend my deep thanks and gratitude to my advisor Dr. Mohammad Makkawi for his guidance, support, efforts, and encouragement all the time. Great thanks to my committee members Dr. Osman Abdullatif and Dr. Waleed Abdulghani for their invaluable comments and guidance through my research work.

Special thanks go to Mr. M. Bashari, Mr. H. Elzain, Dr. A. Adam, Mr. A. Abdelkarim, Mr. M. A. Altawab, Mr. M. Mahgob and Mr. A. Alqubalee for their assistance and huge efforts during fieldwork as well as their invaluable discussion.

Many thanks goes out to Dr. Ali Eisaw, the head of the Petroleum Geology Department, Faculty of Petroleum and Minerals at Al Neelain University, Khartoum, Sudan for his continuing support and encouragement all the way.

Thanks also goes out to King Abdulaziz City of Science & Technology (KACST) for providing enough fund for this research as a part of National Plan for Science, Technology, and Innovation (MAARIFAH) – King Abdulaziz City of Science & Technology – through the Science and Technology Unit at KFUPM, the Kingdom of Saudi Arabia, award number 14-OIL310-04.

Above all, my deepest gratitude is due to Allah for giving me energy, patient, and knowledge to succeed in this wonderful and fruitful journey at KFUPM.

# TABLE OF CONTENTS

# LIST OF TABLES

# LIST OF FIGURES

# ABSTRACT

Full Name : Ibrahim Mohamed Yousif Mohamed

Thesis Title : Sedimentology and Reservoir Characteristics of Middle Jurassic Dhruma Formation, Outcrop Approach, Central Saudi Arabia

Major Field : Geology

Date of Degree : May 2017

The current study aims to characterize the lithofacies, paleoenvironment, high-resolution stratigraphic architecture and reservoir characteristics of Dhruma Formation in outcrops in central Saudi Arabia. Accessible and well-exposed outcrops of Dhruma Formation were analyzed for this purpose. The outcrops are located southwest of Riyadh city near Khashm Mi'dad area in central Saudi Arabia. The lithofacies analysis and stratigraphic architecture have been carried out mainly based on petrography and high-resolution outcrop photo mosaic analysis. Nine lithofacies types (LFTs) have been identified. Fissile shale (LFT3) represents the most dominant lithofacies type in studied sections of Dhruma Formation and constitutes about (36%) which followed by skeletal peletal spiculitic wackestone (LFT1) and skeletal foraminiferal peloidal packstone (LFT8) with (15%) and (12%) respectively. The rest of the lithofacies types have abundance range from (<1 to 7%). The identified lithofacies types were grouped into five major carbonate environment that range from distal-to-proximal carbonate ramp setting. However, the detailed lithofacies and stratigraphic analysis of studied sections of carbonates Dhruma Formation show that they

belong to the D5 and D6 Members based on lithofacies and biocomponent especially benthic foraminifera.

The detailed stratigraphic analysis revealed around 53 cycles and cycle sets with $5^{th}$ to $6^{th}$ order magnitude. The thickness of parasequences range from centimeters up to six meters with an average thickness of 1.5 meters. Those are stacked to form four high-frequency sequences (HFSs) with thickness range from one meter up to fourteen meters. The latter were grouped into a single depositional sequence of $3^{rd}$ order magnitude. The signature of carbon and oxygen stable isotope ratios are depleted in transgressive dominated intervals compared with that in regressive dominated part. The abrupt shift in $\delta$ 18O values seems to be an indication of a subaerial exposure surface which located just above the thick amalgamated unit of cross-bedded peloidal skeletal oolitic grainstone and oolitic grainstone lithofacies. The Jurassic maximum flooding surface (MFSJ30) has been placed and indicated within the thick transgressive shale/mudstone of the D5 Member.

Different pore types were recognized which include: fracture, intraparticle, moldic and intercrystalline porosities. The dominant pore types are fracture and intraparticle porosities. The moldic porosity and intraparticle porosity are the dominant ones in the upper most part of the vertical composite stratigraphic section which is equivalent to Lower Fadhili reservoir in the subsurface. The factors that enhancing reservoir quality include dissolution and dolomitization. The factors that reducing the reservoir quality include: cementation, grain compaction and stylolites. The meteoric calcite cementation significantly blocked most of the original pore space in grainy rock texture. However, diagenetic alterations such as dedolomitization is changeable and it is difficult to interpret their effects on porosity evolution and reservoir quality of the D5 and D6 Members. As result of intensive meteoric

dissolution, porosity and permeability logs along vertical stratigraphic section are relatively high for the two lagoonal lithofacies: skeletal foraminiferal peloidal packstone (LFT8) and skeletal foraminiferal wackestone (LFT9) in the upper most part of the section which represent an outcrop equivalent of the Lower Fadhili reservoir in the subsurface. The micro porosity was also observed in the same interval. Three groups have been established based on rock texture: grain-dominated, muddy-grainy and mud-dominated. It show scattered pattern and their boundaries are not sharp and they cross each other due to complexity in pore geometry. Therefore, nine hydraulic flow units and five global hydraulic elements (GHE1-GHE-5) have been introduced for the D5 and D6 Members which have flow zone indicator range from (0.0938 to 1.5). The correlation between carbon and oxygen stable isotope signatures and the porosity log along vertical stratigraphic section shows clearly the positive trend of these variables. However, the transgressive part is dominated by heavier isotope composition compared with the regressive dominated part. The 3D outcrop lithofacies model was established by using sequential indicator simulation algorithm (SIS) and it shows layer cake in low-resolution. However, thin layers cause a problem in upscaling of the field data. The petrophysical models were generated by assigning the average porosity and permeability values for each lithofacies in the three-dimensions outcrop lithofacies model. Relatively good reservoir quality has been observed in the upper most part within the zone 1 which is mainly lagoonal deposits and it have been subjected to intensive phreatic meteoric dissolution and created abundant moldic pores in this interval. The lithofacies and porosity models also show that within the potential reservoir units there are porosity and permeability barriers which are lithologically and diagenetically controlled.

The findings of this high-resolution outcrop analog scale analysis provide detailed insight into reservoir description, architecture and quality prediction within the actual inter-well spacing of the D5 and D6 Members in the subsurface. Consequently, this might also serve to optimize reservoir exploration and development of subsurface equivalent reservoirs.

# ملخص الرسالة

**الاسم الكامل**: ابراهيم محمد يوسف محمد

**عنوان الرسالة :** الخصائص الترسيبية و صخور المكمن لمتكون ضرما في التكشفات السطحية, الجوراسي الاوسط, وسط المملكة العربية السعودية

**التخصص:** جيولوجيا

**تاريخ الدرجة العلمية**: مايو 2017

تحتوي صخور الكربونات لمتكون ضرما والتى تنتمي للعصرالجوراسي الأوسط مكامن نفطية هامة في حقول النفط في المنطقة الشرقية بالمملكة العربية السعودية ومنطقة الخليج العربي. ومع ذلك، فإن تعقيد صخور الكربونات والقصور المصاحب للبيانات والتقنيات التحت سطحية المستخدمة تعيق الفهم العميق والتقيم لجودة المكامن وتركيبتها الداخلية في حدود المسافة المعروفة بين الأبار في الحقول النفطية. تهدف الدراسة الحالية الى تحديد خصائص السحنات، البيئة القديمة، البناء الداخلي الطبقي عالي الدقة وخصائص المكامن النفطية لمتكون ضرماء في التكشفات السطحية. في هذه الدراسة تم إستهداف التكشفات سهلة الوصول وجيدة التكشف لمتكون ضرما. تقع هذه المتكشفات في جنوب غرب مدينة الرياض بالقرب من منطقة خشم مداد بوسط المملكة العربية السعودية. تحليل السحنات والتكوين الداخلي الطبقي تم إجرائه اساساً إستناد على وصف الشرائح الرقيقة تحت المجهر والصور المدمجة عالية الدقة. تسع سحنات رسوبية تم التعرف عليها. الطفل الإنشطاري يمثل السحنة الغالبة بنسبة حوالي (36%) في المقاطع التى تمت دراستها من متكون ضرما و الذي يليه من حيث الوفرة سحنة الواكستون المحتوي على هياكل، بيليت وشوكيات و سحنة الباكستون المحتوي علي هياكل وفورمنيفرا وبوليدز بنسبة (15%) و (12%) علي التوالي. بقية السحنات لديها وفرة تتراوح من (اقل من 1 الي 7%). تم تجميع السحنات التى تم تحديدها الي خمس بيئات كربوناتية والتى تتراوح من المنطقة القريبة الي البعيدة من المنحدر الترسيبي ذو الزاوية المنخفضة. على كل حال، السحنات المفصلة والتحليل الطبقي للمقاطع المدروسة

لتكوين ضرما اظهر انها تنتمي الى العضو الخامس والسادس بناءاً على السحنات و المحتوي الإحيائي خصوصاً المنخربات القاعية.

أوضح التحليل التفصيلي الطبقي حوالي 53 دورة واطقم دورة من الدرجة الخامسة والسادسة. سمك المتواليات (الباراسكونسس) يتراوح من سنتمرات الي 6 امتار بمتوسط سمك يبلغ متر ونصف. هذه البارسكونسس تتجمع مع بعضها لتكون اربع متواليات عالية التردد بسمك يتراوح من متر واحد حتي 40 متراً. تم تجميع المتواليات عالية التردد في متوالية رسوبية واحدة من الدرجة الثالثة. نسب أثر النظائر المستقرة للكربون والأكسجين استنفذت فى الفترات التى يسودها تقدم البحر مقارنة بالجزء الذي يسوده تراجع البحر و يبدو أن التحول المفاجئ فى قيم نظير الاكسجين 18 تدل على تكشف تحت هوائي والذي يقع فوق الوحدة السميكة المتراكبة لوحدة الحجر الحبيبي الاوولايتي ذو الطبقات المتقاطعة المحتوية علي هياكل وبليدز مع الحجر الحبيبي الاوولايتي. وقد تم وضع سطح الحد الأقصي للفيضان رقم 30 في الجوراسي في نطاق صخور الطفلة/ الطين السميكة في العضو الخامس.
تم تحليل جودة المكمن للعضو الخامس والسادس بالإعتماد على الملاحظات المستقاة من دراسة الشرائح الرقيقية، قياسات المسامية والنفاذية، المجهر الإلكتروني الماسح، تشتت الحيود السيني، وميض الحيود السيني و اثار النظائر المستقرة للكربون والاكسجين. تم التعرف على انواع مختلفة من المسام والتى تشمل: الكسور, داخلية الحبيبات, القالبية و تلك التى بيين البلورات. المسامية السائدة هي مسامية الكسور وداخل الحبيبات. تعتبر المسامية القالبية و داخل الحبيبات هي المسامية السائدة في الجزء العلوي الأقصى في القطاع الرأسى المركب والذي يعتبر مكافئ لمكمن فاضيلى الاسفل التحت السطحي. تشمل التغييرات الناشئة من عمليات النشأة المتأخرة والتى تتحكم فى جودة المكمن للصخور الكربوناتية لمتكون ضرما مايلي: الحفر والتخدد، السمنتة، الإنحلال، الدلمتة/ الدلمتة العكسية والدفن. هذه المتغيرات لها تأثيرات مختلفة على تطور جودة الخزان. قيم المسامية والنفاذية على طول القطاع الطبقي الرأسى عالية نسبياً لسحنتين من سحنات البحيرة المالحة هما: سحنة الباكستون المحتوي علي هياكل وفورمنيفرا وبوليدز وسحنة الواكستون المحتوي على هياكل وفورامنيفرا فى الجزء العلوى الأقصى والذي يمثل مكافئ سطحي لمتكون فاضيلي الأسفل تحت سطح الأرض. ويرجع السبب فى ذلك الى الإذابة المكثفة لمياه الأمطار والتى أدت الى تكون مسام كثيرة والتى تظهر وفرة في نسب الكربون والأكسجين. أيضا لوحظت المسامية الدقيقية فى نفس هذا النطاق. فى اجزاء معينة من القطاع، الكالسيت الكثيف سمنت و أغلق معظم المسام الاولية الاصلية وهذا قلل من جودة الخزان بدرجة كبيرة فى الصخور

ذات النسيج الحبيبي مثل سحنة الحجر الجيري الحبيبي الاوولیتي وسحنة الشوكيات ذات النسيج الباكي الحبيبي. التغيرفي المسامية المرتبط بالدلمتة العكسية متغيرة ومن الصعب تفسيرها. عملية الدلمتة تبعتها عملية دلمتة عكسية وتمت ملاحظتها في بعض الاجزاء من القطاع الطبقي الرأسى. عملية النشأة المتأخرة المرتبطة ايضا بالدفن قللت من جودة المكمن للعضو الخامس والسادس. السحنات التى تم التعرف عليها تم تقسيمها الى ثلاث مجموعات اعتماداً على النسيج الصخري: سائدة الحبيبات, طينية-حبيبة و سائدة الطين. هذه الثلاث مجموعات تظهر نمط متناثر والحدود بينها ليست حادة وتتقاطع فيما بينها. هذه الإختلافات فى نفس النسيج الصخري يعزى الى التعقيد في هندسة المسام. لذلك تم تقديم 9 وحدات تدفق هيدروليكيه اعتماداً على معامل جودة الخزان وقيم المسامية المعتادة. تم استخدم طريقة او نهج جديد والتى تعرف بالبتروتايبينغ و العناصر الهيدروليكيه ( عنصر هيدروليكي-1 الى عنصر هيدروليكى-5) للعضو الخامس والسادس والتي لديها مؤشر نطاق تدفق يتراوح من (0.0938 الي 1.5). المضاهاة بين اثار نظائر الكربون والاكسجين ومجس المسامية على طول القطاع الطبقى الرأسى تظهر بوضوح اتجاه ايجابي لهذه المتغيرات. ومع ذلك, فإن الجزء المتكون فى فترة تقدم البحر يسوده تكوين نظائري أثقل بالمقارنة مع ذلك المتكون في فترة يسودها إنحسار البحر. لتتبع و تخريط البناء الداخلى و جودة المكمن فى ثلاثة أبعاد, قمنا بإنشاء نموذج ثابت ثلاثي الابعاد للسحنات الرسوبية و خصائصها البتروفيزيائية. تم إنشاء نموذج ثلاثي الابعاد للسحنات الرسوبية للمتكشف بإستخدام خوارزمية محاكاة المؤشر المتتابعة والتى اظهرت شكل الكعكة الطبقية في دقة منخفضة. علي كل حال، سببت الطبقات الرقيقة مشاكل في تعميم البيانات الحقلية للنموذج. تم إستحداث النماذج البتروفيزيائية عن طريق توقيع قيم متوسط المسامية والنفاذية لكل سحنة فى النموذج الثلاثى الأبعاد للسحنات الصخرية، والتوزيع المكاني للوحدات السحنية تحكمت فيها السحنات نفسها. نسبياً جودة خزان جيدة تمت ملاحظتها فى الجزء الاقصى العلوي فى النطاق رقم واحد والذي تسودها رسوبيات ذات تكوين بحيري مالح والتى تعرضت لإذابة شديدة بمياه الامطار والتى كونت مسام غالبة كثيرة في هذا الجزء.

توفر نتائج هذه الدراسة على التكشفات السطحية نظرة تفصيلية لوصف المكمن, التكوين الداخلى, والتنبوء بجودة المكمن ضمن المسافة الاعتيادية بين الأبار للعضو الخامس والسادس تحت سطح الأرض. ونتيجة لذلك يمكن أن يؤدي ذلك الى الإستفادة المثلى للمساعدة فى استكشاف وتطوير المكامن المكافئة التحت سطحية

# CHAPTER 1

# INTRODUCTION

## 1.1 Introduction

Carbonate rocks have great economic significant since it contains a vast amount of the world's oil and gas reserves. It contains more than 60% of the world's oil reserves and 40% of its gas reserves. However, there are great challenges in interpretation and prediction of their architecture and reservoir quality. The heterogeneity of carbonates is controlled by both lithofacies and their subsequent diagenetic overprint, which causes great variability in petrophysical parameters (Schlumberger, 2007). Subsurface reservoirs models have limitations to show the real geologic characteristics (Eltom et al., 2013). The Jurassic carbonate reservoirs in Saudi Arabia have considerable economic significance, so they have been subjected to detailed studies in order to understand and enhance their reservoir characterization and modeling. Several important factors should be considered when it comes to evaluate carbonate reservoirs such as lithofacies, pore types, and sequence stratigraphy (Jordan and Wilson, 1994). The Middle Jurassic Dhruma Formation of Bajocian to Bathonian age hosts several subsurface carbonate oil reservoirs in the Eastern Saudi Arabian fields. These are from bottom to top: Faridah, Sharar, and Lower Fadhili reservoirs (Hughes, 2009a). For optimum exploration, development, and exploitation of these reservoirs, it is critical to characterize the lithofacies, depositional environment, and related diagenesis. Obviously, subsurface data source methods are limited to reveal critical

high-resolution stratigraphic and architectural elements. This is mostly related to two main reasons; the low resolution of 2D and 3D coverage of seismic data and the large inter-well spacing within oil fields. Nevertheless, the high cost associated with the acquisition, processing, and interpretation of the subsurface data has also a prime contribution. The outcrop analog acts as a quantitive approach where reservoir lithofacies, architecture and quality can be evaluated within the real inter-well spacing. Vertical and lateral profiles can be achieved easily and studied in detail. Moreover, the 3D geostatistical modeling of lithofacies and petrophysical properties (i.e. porosity and permeability) can be obtained to understand their spatial distribution. The well-exposed Phanerozoic outcrops in Saudi Arabia provide a good opportunity for outcrop analog to subsurface formations and reservoirs (Alsharhan and Kendall, 1986). They provide a complete stratigraphic context where the individual beds can be traced laterally for large distances. These outcrops also allow close description and evaluation of rocks variabilities and their effect on quality and architecture of the reservoir. This can be achieved by utilizing geological, petrophysical, and geostatistical approaches. Similar approaches being utilized by Eltom et al. 2014, 2013 to characterize and model the upper Jurassic Arab-D reservoir in outcrops. The contribution of high-resolution sedimentological and stratigraphical analysis, which is performed on outcrop scale, will allow capturing reservoir heterogeneity in a meter scale and predicting reservoir quality of equivalents. Therefore, this study integrates sedimentological, stratigraphical, petrophysical and geostatistical data to characterize the reservoir rocks within Dhruma Formation. The findings of this study might help to understand and predict the reservoir quality and architecture of subsurface equivalent within the real inter-well spacing.

## 1.2 Scope and Objectives

The current study aims to characterize and model the detailed microfacies, Paleoenvironments, reservoir quality and architecture in carbonate Dhruma Formation using outcrop analog from central Saudi Arabia. The well-exposed outcrops of Dhruma Formation will be examined from the sedimentological, stratigraphical and petrophysical point of view. The geostatistical approach will be utilized to develop a static model for lithofacies and petrophysical properties. The model will enable better assessment and prediction of analog quality and architecture. Therefore, a set of specific tasks are followed to develop the model which include:

1. Describe the detailed microfacies and interpret their depositional environment.
2. Establish high-resolution stratigraphic framework.
3. Characterize reservoir characteristics and quality.
4. Construct a static model for lithofacies and petrophysical properties.

## 1.3 Study Area

The area of the study is situated in the central Saudi Arabia near Riyadh city, the capital of Saudi Arabia (Figure 1.1). It is located in a road-cut to Saudi White Cement Factory between 46° 17' 50.21" & 46° 17' 39.80" East and 24° 18' 15.82" & 24° 18' 34.92" North (Figure 1.2). The main direction of Dhruma outcrop sections is NW-SE and having a total thickness of about 58 meters and extend laterally for a distance of more than 680 meters. Accessible and well-exposed outcrops of carbonate Dhruma Formation are located near Khashm Mi'dad area. Collected samples were systematically analyzed in details from sedimentological, stratigraphical, and reservoir quality point of view. The lateral profiles have been generated to enable capturing and mapping lithofacies and architecture within the real inter-well spacing through the outcrop photo mosaic (Figure 4.24).


Figure 1.1: Satellite image showing the study area in central Saudi Arabia (after Google Earth, 2017).

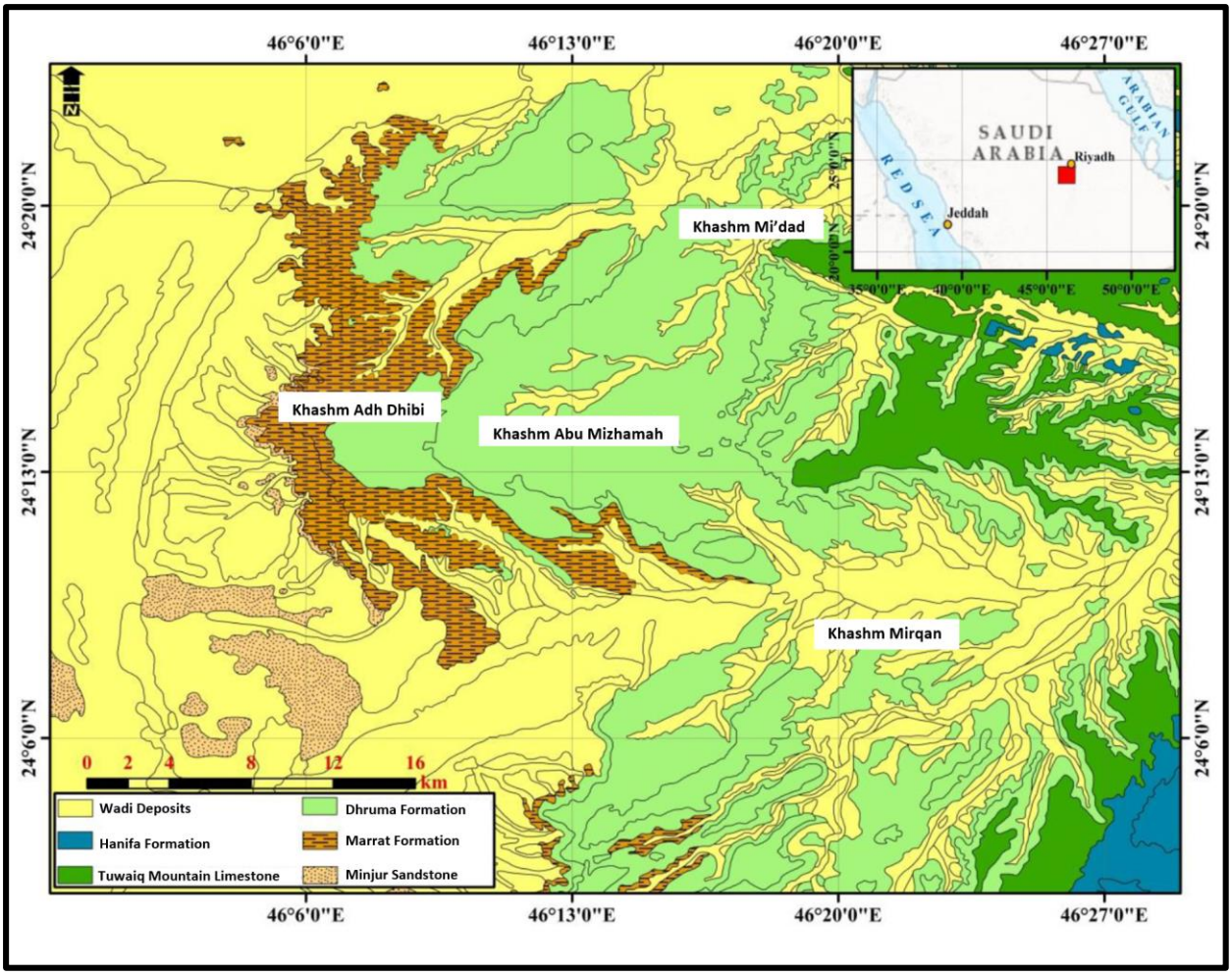


Figure 1.2: Geological map shows the study area and outcrops of Dhruma Formation in central Saudi Arabia (modified from EL-Sorogy et al., 2017).

## 1.4 Geologic Setting

The ongoing tectonic evolution of the Arabian Plate has a significant control on the Phanerozoic depositional setting, sediment types, and sediment distributional patterns throughout the Arabian Plate (Bell, 2004; Konert et al., 2001). In addition to the tectonic evolution, eustatic sea level changes and climatic changes were also believed to have an important control on the Phanerozoic sedimentary record of the Arabian Plate.

The Arabian Plate has been developed over five tectonic stages. These tectonic phases are responsible for wide unconformities in the stratigraphic column of the Arabian Plate. Sharland et al., 2001 related the large-scale unconformity-bounded sedimentary sequences to tectonic phases and named them as tectono stratigraphic mega-sequences (TMS) that affected either all or most of the plate (Figure 1.3). Eleven (11) Tectono Stratigraphic Megasequences were recognized (AP1–AP11) and extend from Late Proterozoic to Tertiary time. The Jurassic sequences have been linked to the AP7 phases which lasted for 33 Ma and was dominated by Jurassic carbonate platform, ramp, and basins within the shelf.

The intra-shelf basins were developed as result of subsidence of basement blocks during Middle Jurassic (Callovian) to Late Jurassic (Middle Oxfordian), and the subsidence was stated by extension in the N-S main fault system. Three-stress regime have been considered to control the structural evolution, intra-continental basins development, and the depositional patterns and style of the Arabian Platform (Edgell, 1992). These were evolved during the mid-Proterozoic, Proterozoic-Mesozoic, and Cenozoic.

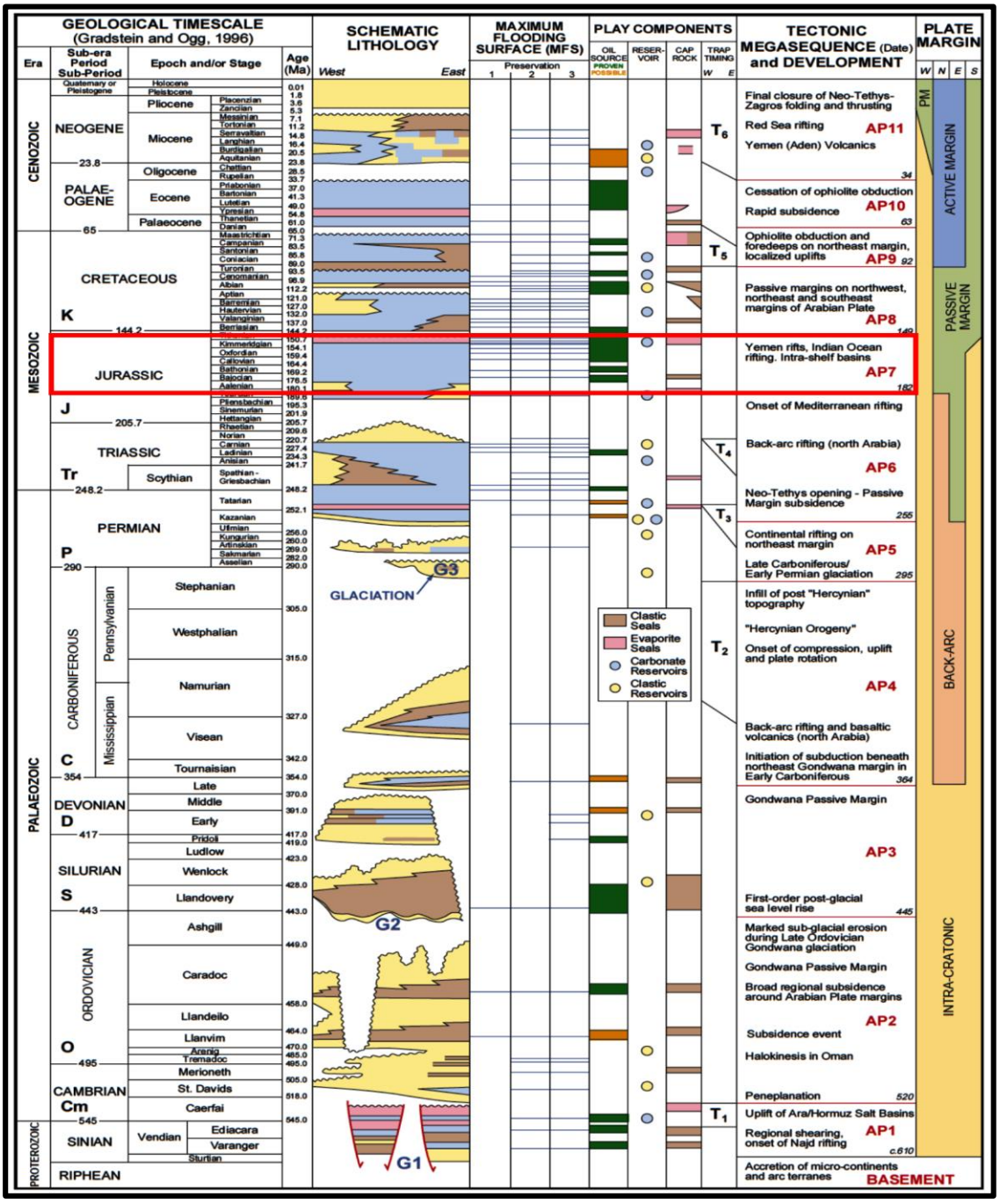


Figure 1.3: Schematic diagram summarizes the Arabian plate sequence stratigraphy covering the time from Precambrian to Phanerozoic. Twelve Tectono-stratigraphic Megasequence (TMS) have been established and their related geological events which affect the development of the stratigraphy and petroleum system. The Jurassic sequence has been linked to AP7, and it appears in the highlighted red square (Sharland et al., 2001).

The Mid-Proterozoic stress regime resulted in the formation of three structural trends; these include; 1) north-trending structures, 2) northwest-trending structures, 3) and northeast-trending structures. The north-trending structures are located in the eastern Arabian Plate and they have regular space. They include Summan Platform, Dibdibah Trough, Ghawar Anticline, and Qatar Arch, and they believed to be formed during Amar Collision (640–620) Ma. Following Amar collision, widespread extensional break down of the Arabian-Nubian Shield took place between (620-530) Ma due to A-type granitic pluton (Al-Husseini, 2000). The northeast-trending structures located around the Arabian Gulf and include the NE-oriented intra-continental rift basins of Oman, Zagros Mountains, and Arabian Gulf, these were described as pull-apart basins and they associated with the left-lateral dislocation induced by the Najd fault system (Al-Husseini, 2000). Later these basins were filled by a thick succession of clastic, carbonates and salt rocks. During the Cenozoic time, the Arabian Plate subjected to drift towards NNE and it is broken up from Africa from Oligocene onward, a new set of stress conditions dominated in the basement and has resulted in the formation of two major vertical shear (Edgell, 1992). During the Late Devonian- Early Carboniferous times, the Hercynian orogeny took place and was lasted for about 25 Ma and causes erosion of several kilometers of sediment above uplifted areas (Alsharhan and Nairn, 2003; Konert et al., 2001; Sharland et al., 2001). Throughout the late Early Permian, a major continental rifting and crustal stretching and thinning took place in West Pangaea. This rifting phase has separated what is so called Cimmerian continent from Gondwana and resulted in the formation of Neo-Tethys Ocean at the expense of the Paleo-Tethys (Alsharhan and Nairn, 2003). The extension of the Neo-Tethys Ocean was associated with a regional uplift in the Arabian Plate and hence resulted in the

formation of a Plate-wide unconformity, which is the so-called Pre-Khuff unconformity. Besides the continental uplifting, this opening was associated with the first critical regional marine transgressive event on the Arabian Plate, which has established the first Plate-wide carbonate succession of Khuff formation (Al-Jallal, 1995). Following the Late Permian opening of the Neo-Tethys, is the formation of series of intra-shelf basins (e.g., Arabian and Gotnia Basins), these were most probably of tectonic and/or eustatic origin with the later sediment load playing a role in increasing subsidence rate (Alsharhan and Nairn, 2003; Sharland et al., 2001; Ziegler, 2001). The intra-shelf basins which developed in Jurassic were associated with reservoir and source rocks. In the Early Late Cretaceous, the closing onset of the Neo-Tethys Ocean and the formation of significant and widely spread unconformity, which is the so-called Pre-Aruma Unconformity (Sharland et al., 2001). Following the subduction of the Afro-Arabian Plate beneath Eurasia (consumption of the Neo-Tethys Ocean), the continental collision took place along the present-day Zagros fold belt (Alsharhan and Nairn, 2003; Sharland et al., 2001). The present-day boundaries of the Arabian Plate comprise all the whole types of tectonic styles (Figure 1.4).They encompass rifting and spreading of the sea floor in the Red Sea and the Gulf of Aden, collision along the Zagrous and Bilits sutures, subduction along the Makran zone, and transform motion along the Arabian Plate from the interior Iranian microplates (Konert et al., 2001).

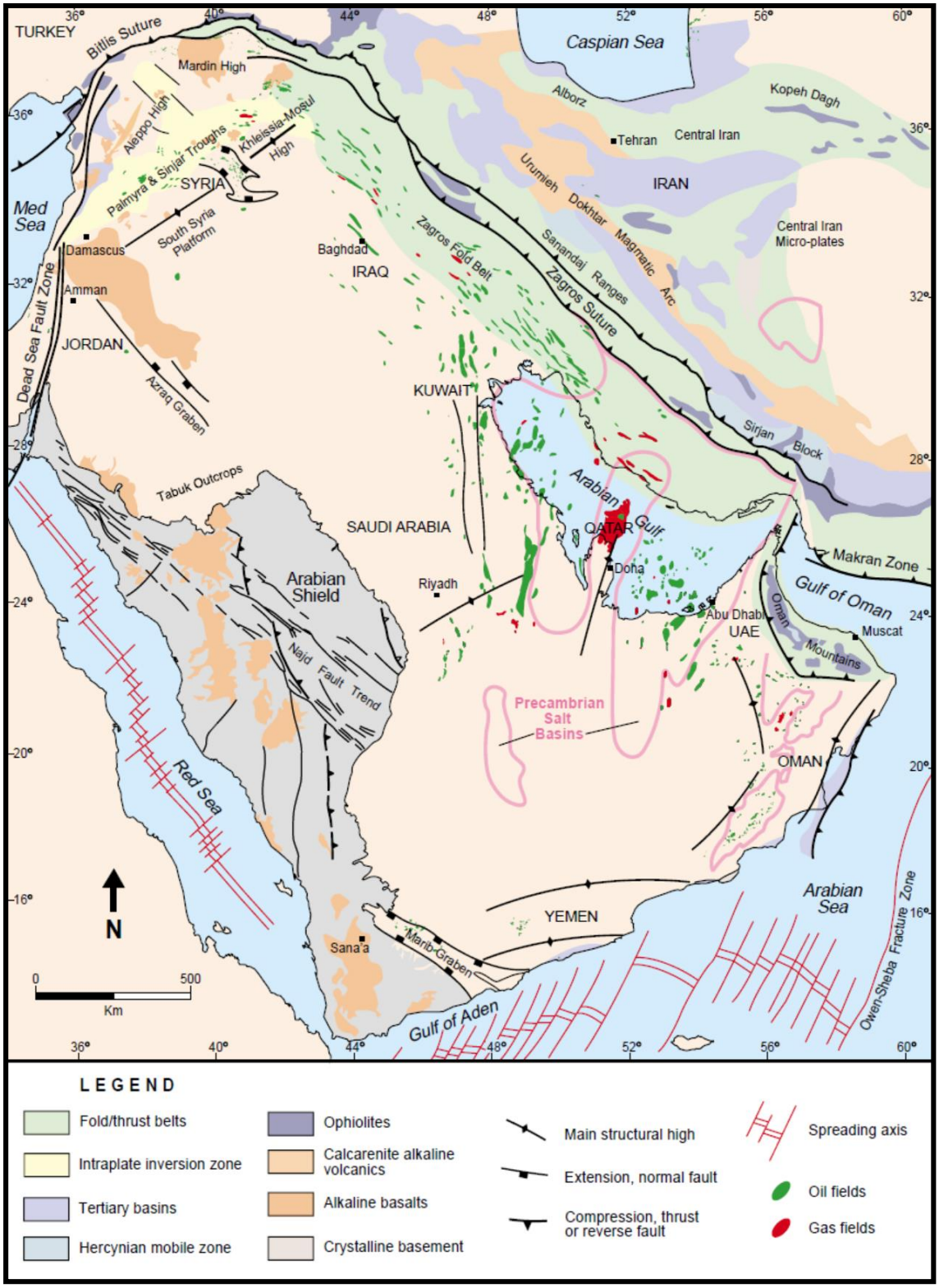


Figure 1.4: Location and the main tectonic elements of the Arabian Plate with the present-day Arabian Plate boundaries (Konert et al., 2001).

## 1.5 Paleo-plate Position

In addition to the tectonic evolution, climatically-controlled eustatic sea level and climatic changes were also believed to have significant control on the Phanerozoic sedimentary record of the Arabian Plate. These were extensively controlled by the paleo-Plate positions (Figure 1.5). Throughout the Late Precambrian times, the Arabian plate was located close to the equator with East-West orientation (Konert et al., 2001). In the Early Paleozoic, the plate moved into the southern latitudes. By the Silurian to Late Carboniferous time, a major clockwise rotation of about $100^{o}$ without significant latitudinal translation took place. During the Early Jurassic, the Arabian Plate standstill at an equatorial position (Al-fares et al., 1998). This equatorial position was essential for the intensive carbonate sedimentation during the Jurassic time. The paleogeography of the Arabian Plate during the Early to Late Jurassic was a warm, arid climate representing the southern edge of the Tethys Ocean (Al-Husseini, 1997) (Figure 1.6).

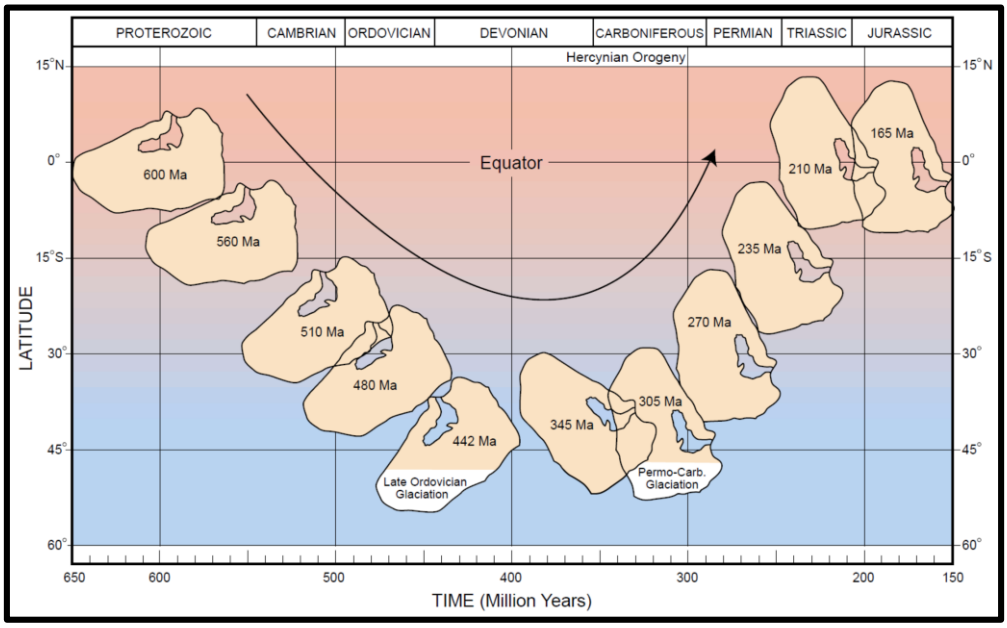


Figure 1.5: Paleo-plate position of the Arabian Plate (Konert et al., 2001).

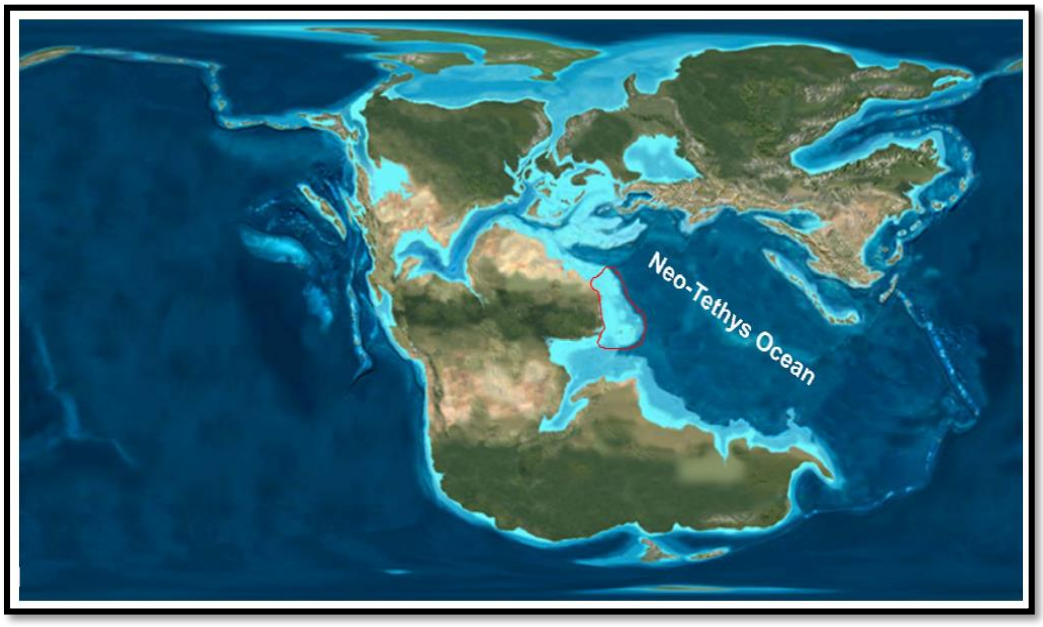


Figure 1.6: The Jurassic Paleogeography map, the Arabian plate colored with red (After Ron Blakey website).

# CHAPTER 2

# LITERATURE REVIEW

## 2.1 Introduction

This chapter will discuss the carbonate succession of Jurassic Shagra Group in Saudi Arabia in term of sedimentology, stratigraphy, and hydrocarbon reservoirs significance with a concentration on Dhruma Formation and its members. Other aspects will be discussed also include porosity and permeability characteristics and their heterogeneity. The concept of hydraulic flow units and rock petro-typing will be utilized for more quantitative estimation of the static reservoir properties. Finally, the static model of the lithofacies will be generated to understand the spatial distribution of reservoir bodies and their petrophysical patterns.

## 2.2 The Jurassic Shaqra Group

The lithostratigraphy of the Jurassic Shaqra group in Saudi Arabia was first defined by (Vaslet, 1987) and incorporates the seven formations set up by (Powers, 1962, 1968) and Powers et al. (1966), which interrupted by disconformities. The Jurassic Shaqra group has a great economic significance since it contains thirteen hydrocarbon reservoirs. The group includes seven formations from bottom to top Marrat, Dhruma, Tuwaiq Mountain, Hanifa, Jubaila, Arab, and Hith anhydrite formations (Figure 2.1) and each of which is considered to be a third-order cycle whereas the entire composited sequence from Marrat

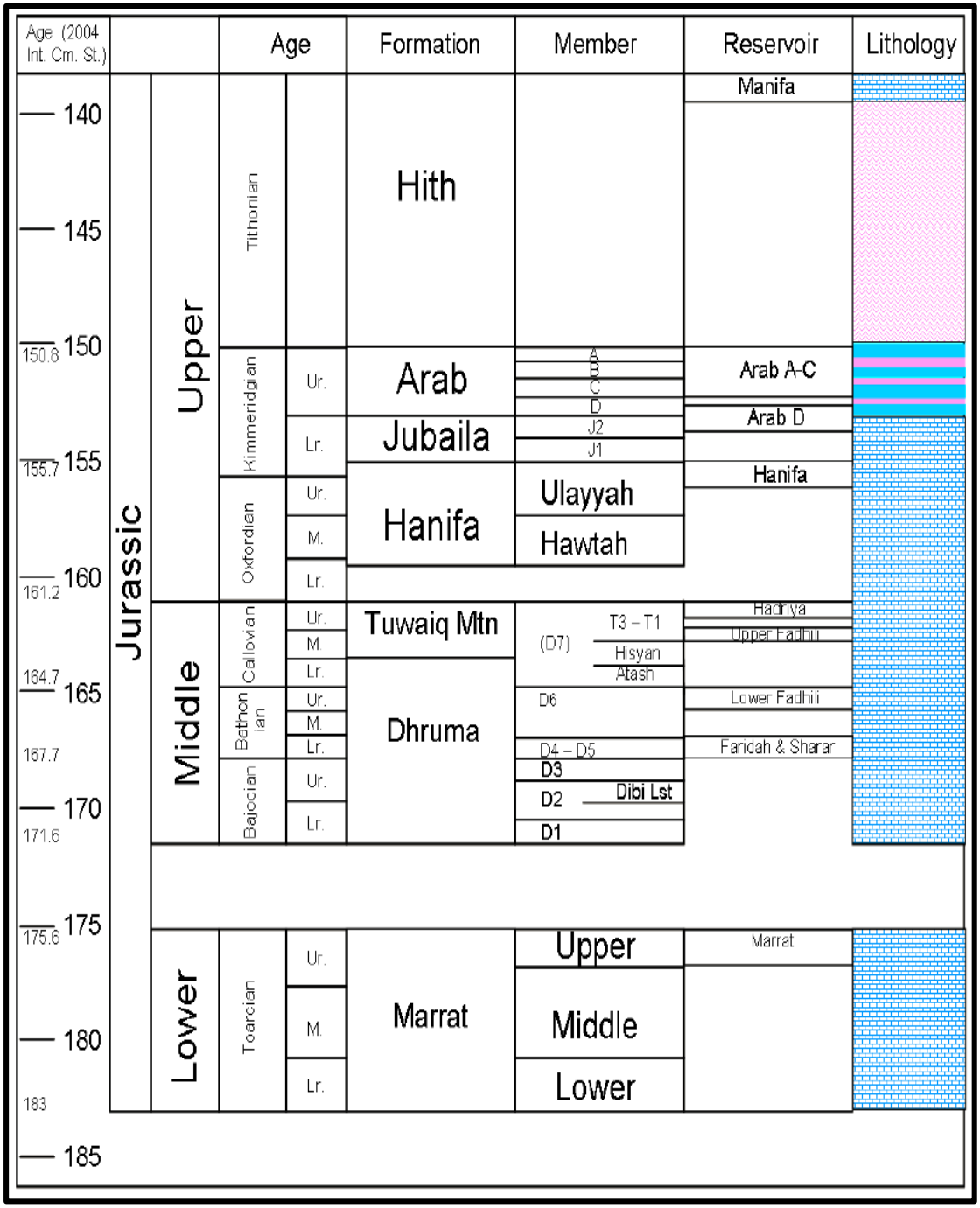


Figure 2.1: The Jurassic Shaqra Group its formations, lithostratigraphy, and reservoirs. The group encompasses seven formations and thirteen reservoirs. The Middle Jurassic carbonate Dhruma Formation hosts three reservoirs which include Faridah, Sharar and Lower Fadhili reservoir (Hughes, 2009b). The entire sequence from the Lower Dhruma to Hith constitutes Megasequence AP7 of Sharland et al. (2001).

to Hith anhydrite was described as a single second-order depositional sequence cycle (Al-Husseini, 1997). The majority of formations within the group are composed of carbonates, while the others partly contain interbedded carbonates and evaporates, and end with thick evaporates succession of Hith Formation (Hughes, 2009a).

The deposition of Shaqra Group passes up from shallow marine deposits of Marrat to deeper marine carbonates and marls of Dhruma Formation then passes up again into shallow marine carbonates (Tuwaiq, Hanifa, and Jubaila formations) and finally into Arab-D Member. Deposition continued with the shallow deposition of the interbedded carbonate and evaporates of Arab Formation and subsequently the deposition of the Hith Formation. The reference section of Jurassic lithostratigraphic units is situated in the central region around Riyadh city, where the most developed marine facies are encountered (Enay et al., 1987). The tectonoeustatic and probably glacioeustatic act as controlling factors on cyclicity of deposition that possibly exerted and affected the development of the major unconformities within the Shaqra Group.

The Jurassic sequence in Saudi Arabia exposed in a curve belt along the basement of the Arabian Shield on the western flank. The total thickness of the group in outcrop belt is 1130 meters, and the thickness increases remarkably in the subsurface equivalent in the eastern part of the Saudi Arabia. The succession developed as result of intensive carbonates deposition on a wide shallow marine platform (Hughes, 2009) (Figure (2.2).

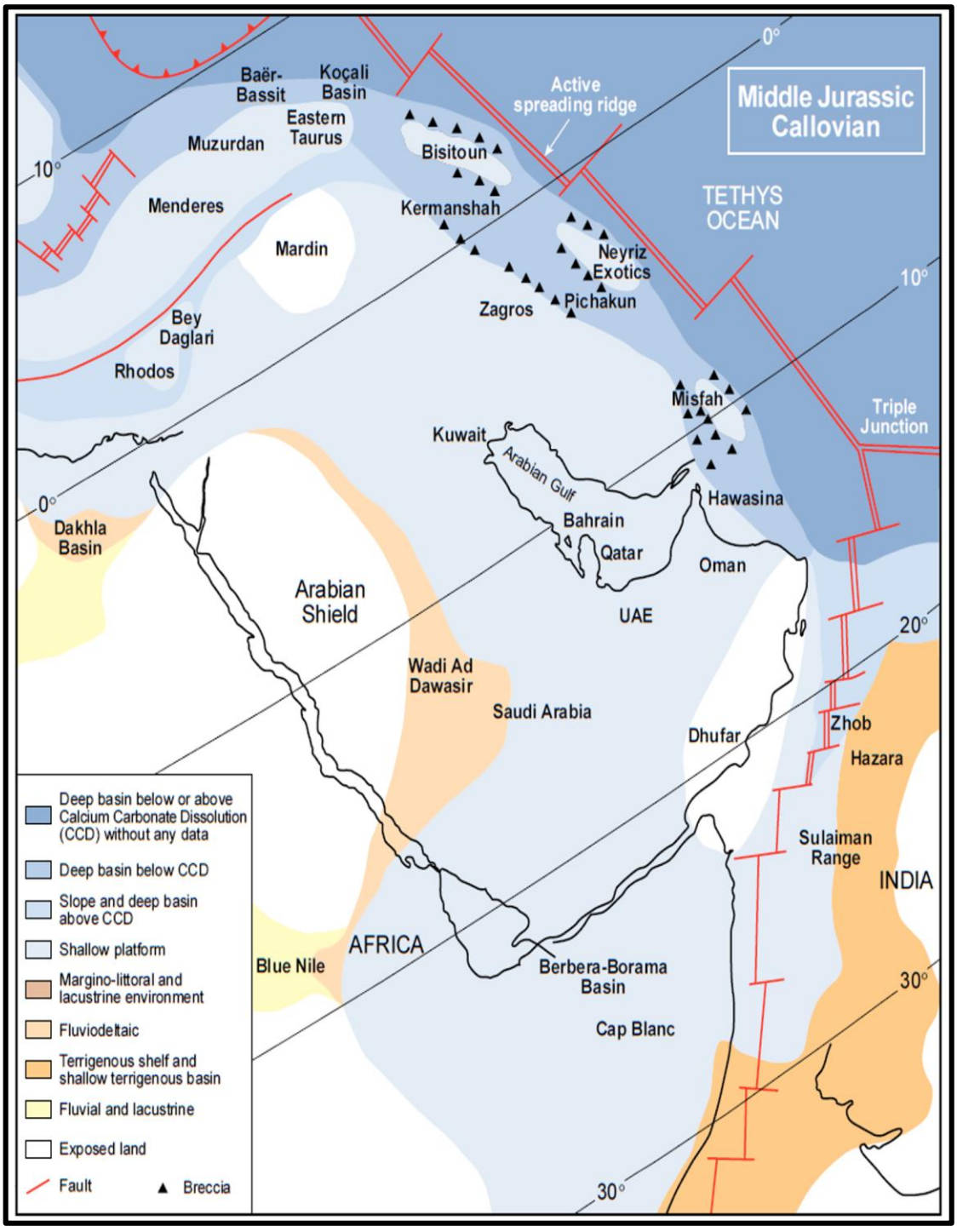


Figure 2.2: Interpreted paleoenvironment and reconstructed tectonic setting of the Middle Jurassic, Callovian (162-158 Ma) (Al-Husseini, 1997), displaying the flooding of the Arabian Plate by the marine transgression (Le Nindre et al., 1987; Enay et al., 1993). During this period the Upper Dhruma and Tuwaiq Mountain were deposited.

The Jurassic carbonates of Saudi Arabia have been studied since the early fifties from different aspects such as sedimentology, stratigraphy, paleogeography, paleoenvironments, geostatistical modeling and reservoir quality by Steineke and Bramkamp, 1952; Powers, 1962; Powers, 1966; Wilson, 1981; Le Nindre et al., 1987; Mitchell et al., 1988; Vaslet et al., 1989; Enay and Mangold, 1994). Numerous recent studies include those by Meyer et al., (1996), Hughes (1996; 2004, 2006), Al-Dhubeeb, (2005), Lindsay et al., (2006), Al-Mojel, (2010), Busbaid et al., (2010), Eltom et al. (2013) and Elzain et al (2015). Generally, at their outcrops equivalent, the entire Jurassic succession could be subdivided into three lithofacies. The lower succession is dominated by mudstone sediments (mostly Dhruma and Tuwaiq Mountain) with vertically scattered grain-dominated sequences (the grainy units of Dhruma and Tuwaiq Mountain), the middle succession is grain-dominated at the first-half and interbedded grainstone and anhydrite at the second-half (Arab Members), the upper section is dominated by salina anhydrite deposits (Hith Formation). Based on Hughes (2008), the thickness of Marrat Formation is 102.5 Meters, and it is unconformably overlain the Triassic Minjur Formation and comprises of an interbedded sequence of marine sandstone, carbonate, and claystone. The thickness of Dhruma Formation is 336 meters and unconformably overlain the Marrat Formation. The formation comprises of carbonate in the subsurface and carbonate and claystone around Riyadh area, and siliciclastics were described in the northern and southern outcrops. The Tuwaiq Mountain is about 295 meters thick and dominated by shallow-marine lagoonal and stromatoporoid carbonates of Middle to Upper Callovian age. The Upper Jurassic lithostratigraphy includes Hanifa, Jubaila, Arab, and Hith formations. The Hanifa Formation is about 126 meters thick and composed of muddy carbonate deposits in the lower unit and lagoonal

and stromatoporoid carbonate in the upper unit. The thickness of Jubaila Formation is about 89 meters which disconformably overlain the Hanifa Formation and is dominated by deep marine carbonate sediments in the lower part and shallow marine stromatoporoid in the upper part. The Arab Formation is about 54 meters thick in the surface outcrops and comprises of four stacked shallow marine carbonates and evaporates cycles. The uppermost Hith Formation consists mostly of 90 meters anhydrite but has carbonate unit in the top most part as described by Hughes and Naji (2009). The paleoenvironment maps as introduced by Ziglar, 2001 assumed that the Arabian plate was located at the edge of the Neo-Tethys Ocean where an extensive shallow marine platform was developed. Because of their chronological significant, ammonites remain the only accepted biostratigraphic zoning faunas for the entire Jurassic succession in Saudi Arabia. Ammonites results were complemented by data came from foraminifera, nannofossils, nautiloids, brachiopods, ostracod, gastropods, echinoid, pelecypod, and calcareous algae. These were believed to be strongly influenced by palaeoenvironmental factors (Alméras, 1987; Enay et al., 1987). The Jurassic foraminifera and their associated bio components were used to determine subtle variations in the Jurassic depositional environment (Hughes, 2009b). Particularly, the detailed, thin section-based, semi-quantitative micropaleontological and micropaleontological analysis of the Jurassic carbonates has revealed six paleoenvironmental regimes (Hughes, 2009), and these ranges from intertidal, shallow lagoon, deep lagoon, bank complex, transition bank-basin, and open marine to intra-shelf basin. The interpretation of the Jurassic sequence in Saudi Arabia has been understood within different sequence stratigraphic scope by Le Nindre et al. (1990), Al-Husseini (1997), Sharland et al. (2001) and Haq and Al-Qahtani (2005) of which mostly linked the

sequence to the fluctuations in sea level curve that established by Haq et al. (1988). Sharland et al. (2001) by applying the concepts of sequence stratigraphy of Galloway (1989), recognized the maximum flooding surfaces (MFS) from different source of data (wireline logs and outcrops) and correlated them across the Arabian plate in order to divide the widely distributed sedimentary succession of the plate into isochronous packages of sediment that are genetically related stratigraphic sequences.

## 2.3 The Dhruma Formation

The Dhruma Formation was first defined by Max Steineke in 1937 at Dhruma Town (latitude 24$^{o}$ 36' N and longitude 46$^{o}$ 07' E) as a Member of Tuwaiq Mountain Formation. The formation is termed the Sargelu in Kuwait and the Uwainat in Qatar. The outcropping strata of Dhruma formation extends for about 900 Km, from western Jordan, Al Arid town (latitude 19$^{o}$ 20' N) to Iraq al Mazhur (latitude 27$^{o}$ 05' N) with maximum width of about 25 to 20 Km (Powers et al., 1966; Enay et al., 2009).

The early subdivision of the Dhruma Formation was mainly based on sedimentological and biostratigraphical (mainly ammonites) characteristics (Bramkamp and Steineke, 1952). In 1945, Bramkamp has upgraded the Dhruma Member to Formation. The Dhruma Formation was subdivided by (Powers et al., 1966; Powers, 1968) into three units lower, middle and upper, with a total thickness of 447 meters. The succession is composed of intercalation between shales, sandstones, and limestones. The carbonate represents the dominant component in the subsurface, while in the central part of the exposed strata it is mostly composed of carbonate and claystone, and siliciclastics in outcrops towards the north and component in the subsurface, while in the central part of the exposed strata it is mostly composed of carbonate and claystone, and siliciclastics in outcrops towards the north and

south. The formation span in time from Bajocian to Bathonian age, and hosts the Faridah, Sharar, and Lower Fadhili reservoirs (Hughes, 2009a). Powers et al. (1966) added the informal Dhibi limestone to the lower unit of Bramkamp and Steineke (1952), and the formal Atash and Hisyan to the upper formation. The Hisyan Member is above and the Atash Member is below. The Hisyan Member is termed after Wadi al Hisyan. The upper limit of Hisyan Member is lithologically change from shale interbedded with thin limestone beds in the lower part to limestone interbedded with thin shale in the upper part, while the lower boundary of the member is firmly fixed at the shift from yellow-gray shale on top to yellowish brown calcarenite of the 'Atash Member at the bottom. The Atash Member of the Dhruma Formation contains the Lower Fadhili reservoir and it has been micropalaeontologically examined in the Berri and Qatif fields (Hughes, 2004). Hughes (2004) found that the open marine, ammonite-rich Hisyan Member is considered to be a genetically associated with the Tuwaiq Mountain Formation. The underlying ammonite-barren Atash Member is considered to be a genetically represents the shallowest and final sediment of the Dhruma sequence. Vaslet et al. (1983) introduced the lithology, members, and units of Dhruma Formation (Figure 2.3). The BRGM Group proposed seven informal units, from bottom to top D1 to D7, and this subdivision was mainly based on biostratigraphy. The highlighted reservoirs were interpreted and captured in a photo mosaic that taken by Hughes in February 2007 (Figure 2.4). The all units of Dhruma Formation from D1 to D7 are cropping out in central Saudi Arabia near Riyadh city.

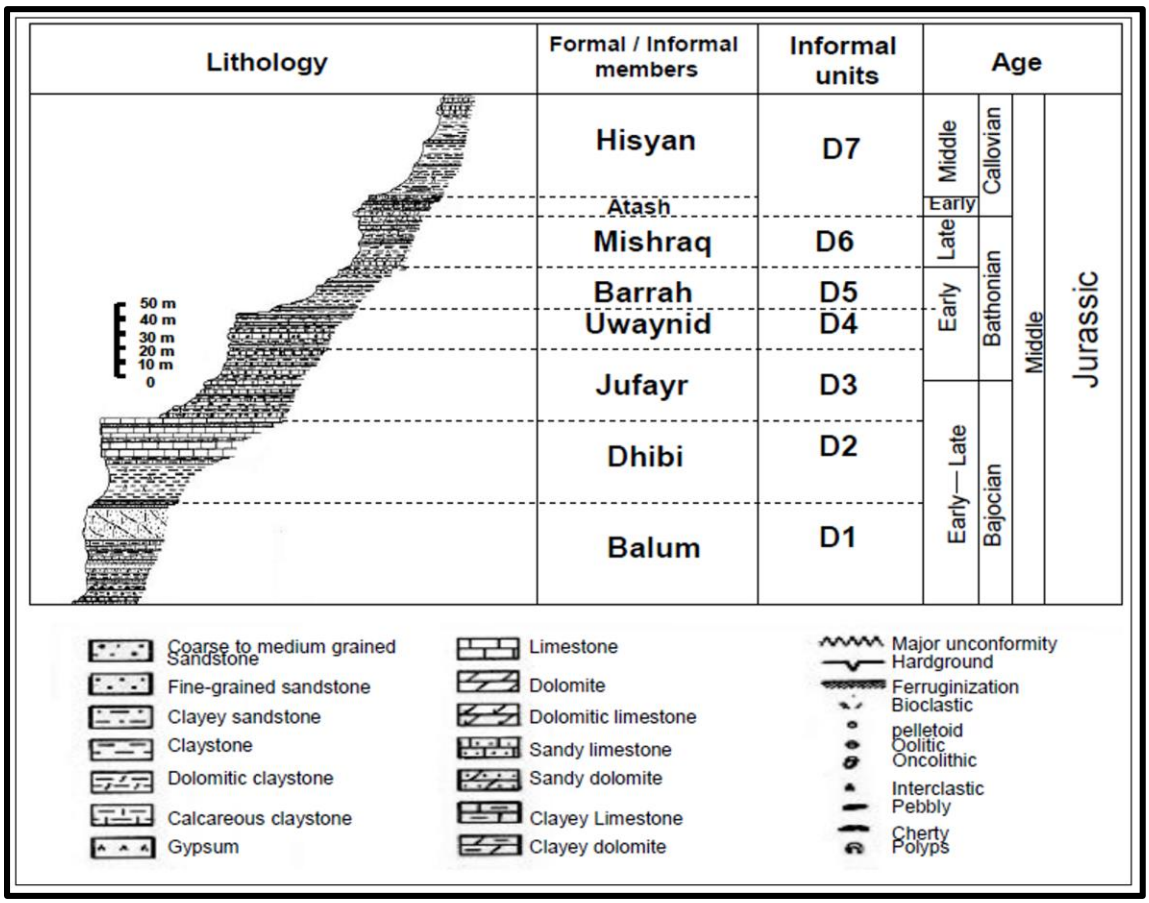


Figure 2.3: Lithology and age of the Members and Units of Dhruma Formation (Vaslet et al., 1983).

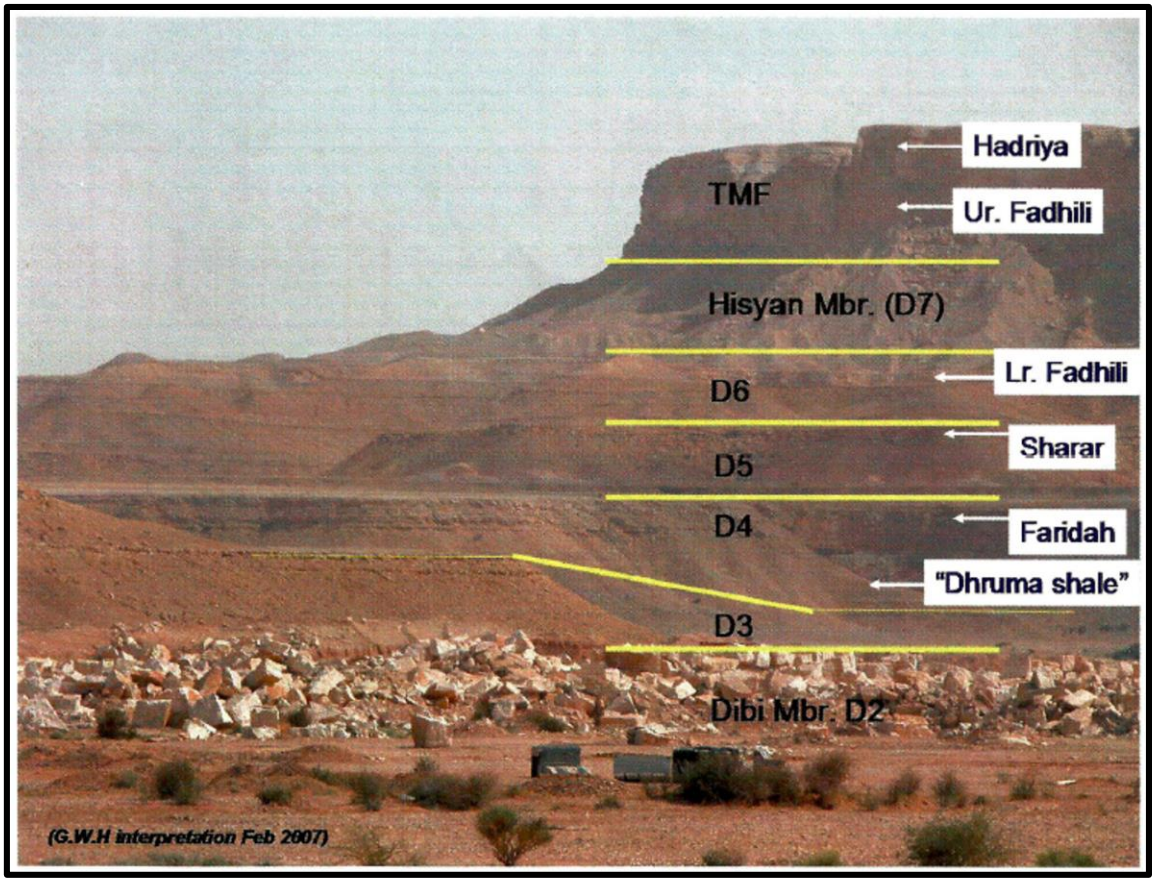


Figure 2.4: An interpreted Members of Dhruma Formation from D2 to D7 and equivalent reservoirs (Photo by W. Hughes, 2007).

Vaslet et al. (1983) proposed the Balum Member to represent the entire D1 unit. The Faridah and Sharer limestone reservoirs are considered to be hosted in the subsurface equivalents of the uppermost D4 and D5 units respectively. At Wadi al Hawtah (latitude 23° 33' N) and Ar Raghbah area (latitude 25° 09' N), three units of the formation were lithologically described early by Powers et al. (1966). The Lower Dhruma composed of shale with some limestone, near Khashm adh Dhibi, and the unit has a thin layer of gypsum at the base and a bed of massive limestone (Dhibi limestone) at the upper part. The Middle Dhruma composed of clean calcarenite limestone capped with oolite bed. The Upper Dhruma unit consists of limestone at the basal part (Atash member), and this overlain by

shally unit (Hisyan member). The most prominent lateral lithological change of the Dhruma Formation is the southward change from carbonate dominated sequences to sandstone dominated sequences (Powers, 1962).

The Dhruma Formation has been assigned to be better defined without the D7 unit, which includes Atash and Hisyan Members. The proposed modification will placed the D7 unit into the basal part of the Tuwaiq Mountain Formation instead to be a part of upper Dhruma Formation (Hughes, 2009). Latest reconsideration of the upper Dhruma and Tuwaiq Mountain Formation, partially proposed by Hughes (2004) and approved by discussion in early 2006 with Dennis Vaslet, would assign the D7 unit of Dhruma Formation which composed mainly from mudstone genetically within the basal Tuwaiq Mountain Formation and contains the lower Atash member and Middle Callovian nannofossils.

The middle Jurassic Dhruma Formation was deposited in shallow marine, warm-water carbonates condition and composed of several sequences separated by significant unconformities (Powers, 1968; Nindre et al., 1990). Le Nindre et al. (1990) and Vaslet et al. (1991) described the lower Dhruma shale has been deposited during the prominent Bajocian transgressive event LZA1.1, whereas the Dhibi limestone and the middle Dhruma member correspond to LZA2.1 and LZA2.2 respectively. The upper Dhruma and lower Tuwaiq Mountain have been assigned to a single sequence, the LZA3.2 sequence (Le Nindre et al., 1990). Unit D5 and D6 were believed to be deposited during a period of sea-level highstand (Al-Husseini, 1997). A depositional hiatus was placed between the middle and upper Dhruma, represent a period of the sea-level low stand and corresponds to LZA2.3, 2.4, and 3.1 sequences (Figure 2.5).

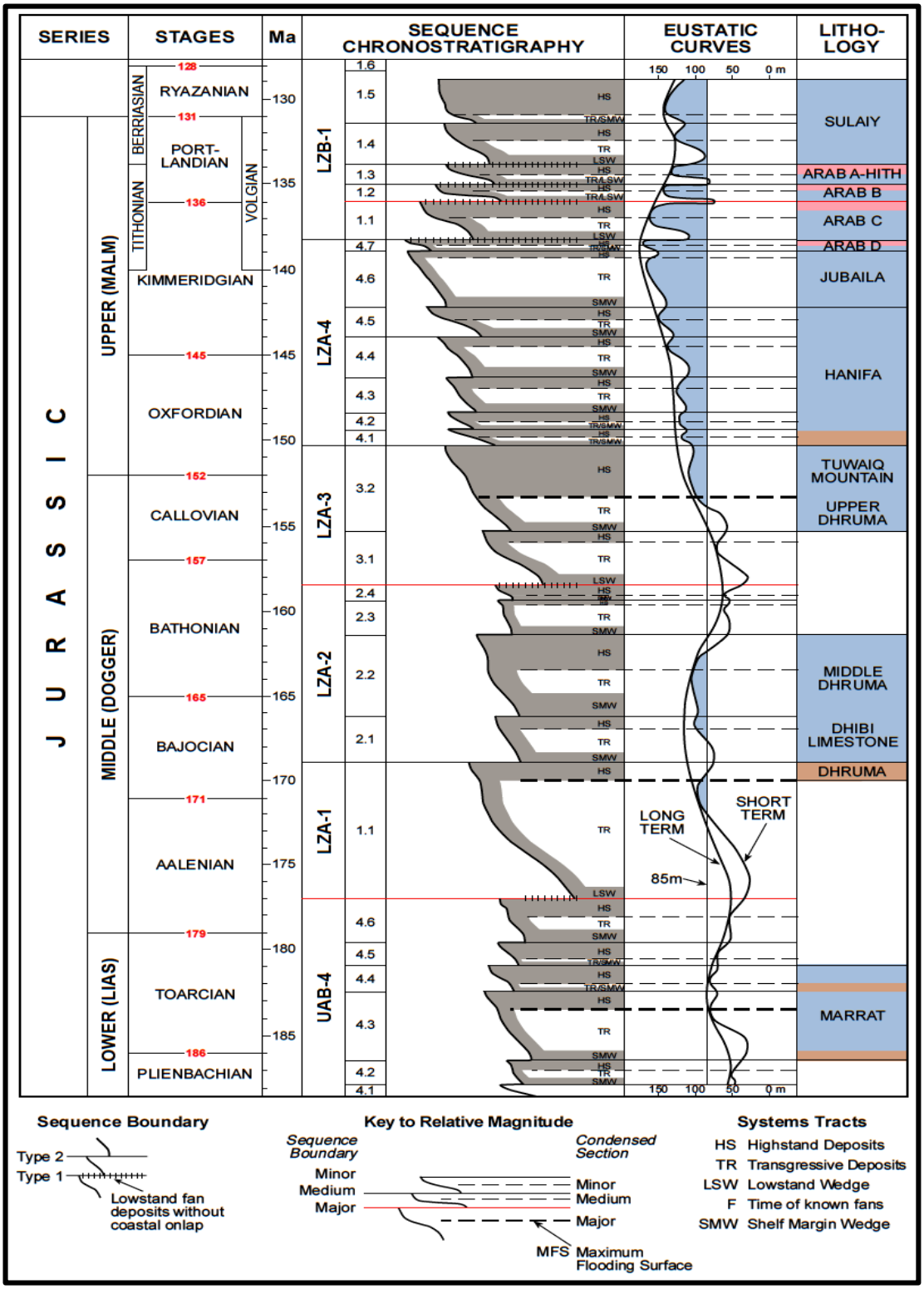


Figure 2.5: Sequence stratigraphic framework of the formations and members of central Saudi Arabia as interpreted by Le Nindre et al. (1990) and Vaslet et al. (1991).

Enay et al. (2009) investigated and interpreted the sequence stratigraphy framework of the Tuwaiq Mountain limestone and three units of Dhruma Formation (D3 to D7) (Figure 2.6). By utilizing the biostratigraphy study, they have been able to interpret the shale of the lower Bathonian D5 unit to represents a maximum flooding surface. The upper part of D5 was considered to be a regressive system tract. The proposed Wadi ad Dawasir "delta" was placed between D5 and D6 Members. The latter D6 unit and Wadi ad Dawasir "delta" have not been considered as members.

Recent work has been conducted by Schlaich and Aigner in (2015) and (2016) to investigate the geology and sequence stratigraphic framework of the Middle Jurassic Dhruma Formation in outcrops of the Oman mountains (Sultanate of Oman). Several Wadi sections with total thickness of about 240 meters were logged. The methodologies that were used include sedimentological and stratigraphical analysis supplemented by spectral gamma-ray measurements (SGR) and thin-section petrography. The study revealed twelve lithofacies, which grouped into five to four lithofacies association. The identified lithofacies range from a low energy mud-dominated lagoon to a high-energy environment, which recognized by peloids and ooids components. The identified lithofacies were deposited in an epeiric carbonate ramp with a very low inclination. The established high-resolution sequence stratigraphic framework and 2D correlation clearly show clearly a vertical change in lithofacies and cyclicity with characteristics gamma-ray response. The succession also shows a clear diversity in the bio component towards the top. The thickest and larger cyclicity is tens of meters and can be traced for a distance of 25 Km in the studied sections.

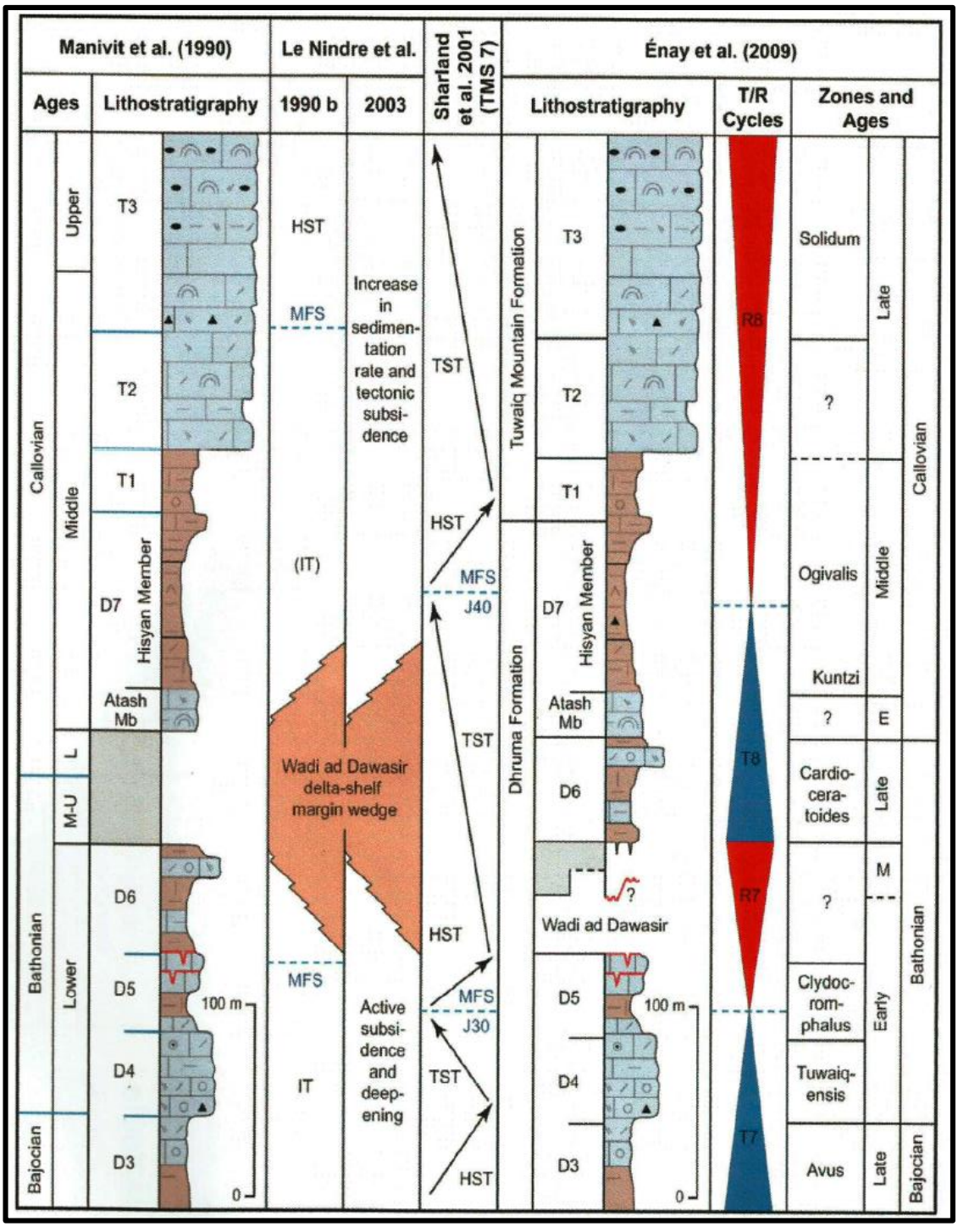


Figure 2.6: An interpreted stratigraphic framework of the Tuwaiq Mountain limestone and part of Dhruma Formation units from (Enay et al., 2009). The proposed Wadi ad Dawasir "delta" was placed between the D5 and D6 units.

## 2.4 The Petrophysical Characteristics

Porosity and permeability are essential to define reservoir quality which relatively distinguished by high porosity and permeability values. For this purpose, it is important to strictly predict the distribution pattern of porosity and permeability and determine the main factors control them. Understanding the statistical distributions and correlations between the petrophysical properties offer substantial intuition into reservoir rocks. Therefore, every zone or bed within a reservoir may provide a distinguished set of porosity and permeability values with distinctive statistical distribution (Saner and Sahin, 1999). The well understanding of permeability and its distribution is important for the effective description of the reservoir. This can be achieved usually from core data. The cross-plot between porosity and permeability can be used in the prediction of permeability values from porosity data with a high degree of accuracy (Saner and Sahin, 1999; Sahin and Saner, 2001). However, porosity is generally independent of particle size, while permeability is highly dependent on grain size (Amaefule et al., 1993). For instance, the cross-plot between porosity and permeability in a reservoir may have a directly proportional relationship. So far, within the same reservoir for same porosity values, there are low and high permeability zones in a reservoir. Accordingly, this classical cross-plot cannot be used reliably to evaluate actual permeability from porosity data set (Amaefule et al., 1993). The investigation of the porosity and permeability relationship, distribution patterns and variability with their depositional texture, mineral composition, and diagenesis will help to predict reservoir heterogeneity and quality. This subsection focuses on understanding the statistical distributions of porosity and permeability and correlations between the two variables (porosity and permeability).

Fitch et al. (2015) published a review study to define and describe the application of integrated approach to understand the heterogeneity of porosity and permeability. In this review article, the authors were discussed important aspects such as characterizing the variability in the data sets and the quantification evaluation of heterogeneity in petrophysical data by using heterogeneity measures. Also, different case studies have been discussed regarding heterogeneity of porosity and permeability in carbonates and clastic reservoirs. To examine the concept of variability, Fitch et al. (2015) performed across plot between bulk density and neutron porosity data for two carbonate formations (Formation A & B). The two formations show different distribution and reflect two populations (Figure 2.7). The Formation (A) is diversified in the distribution of values which indicates greater heterogeneity in character when it compared with Formation (B). The latter has a narrow and clustered distribution. From this fact, the two formations are different in facies and porosity system. The Formation (A) composed of dominant wackestone and packstone facies, while Formation (B) consists of grain rich carbonate facies.

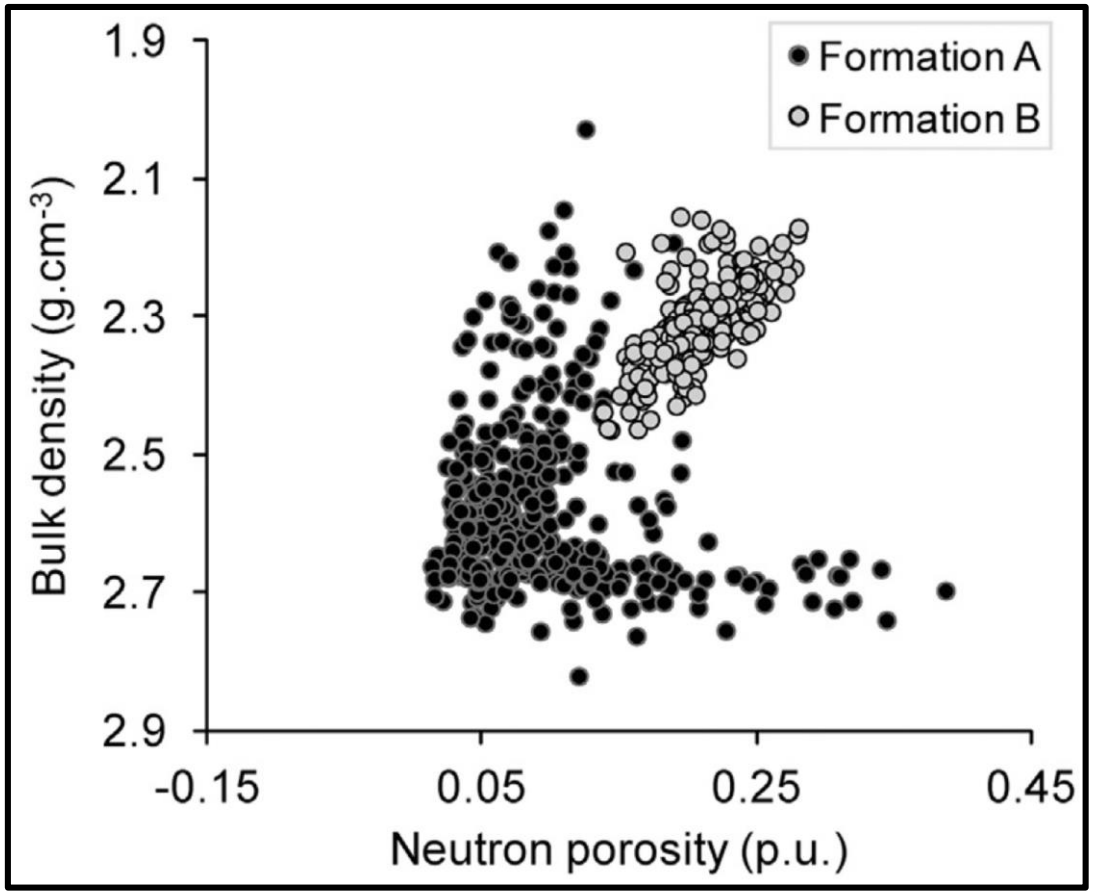


Figure 2.7: Cross plots between bulk density and neutron porosity data for the two Formations (A and B) (Fitch et al., 2015).

The porosity of the giant reservoirs of the Middle and Late Jurassic has been recorded widely as being remnant primary/ intergranular porosity, which ranges from about 15% to 30% in shoal carbonates as defined by Powers (1962); Wilson (1985) and Mitchell et al. (1988).

Several studies were conducted in this area which include: Alsharhan and Nairn, (1997); Grover (1993); Kompanik et al. (1993); Alsharhan and Magara, (1995). Alsharhan and Magara (1995) discussed the nature and distribution pattern of porosity and permeability in carbonate reservoirs of the Arabian Gulf basin. The authors indicated that the Jurassic reservoirs of the main oil fields in the Arabian Gulf basin are characterized by an exhibit exceptionally high porosity up to 30% (Figure 2.8). However, they conclude that the good reservoir quality is associated with grainy units. Also, they found that the distribution of porosity is quite irregular and complex.

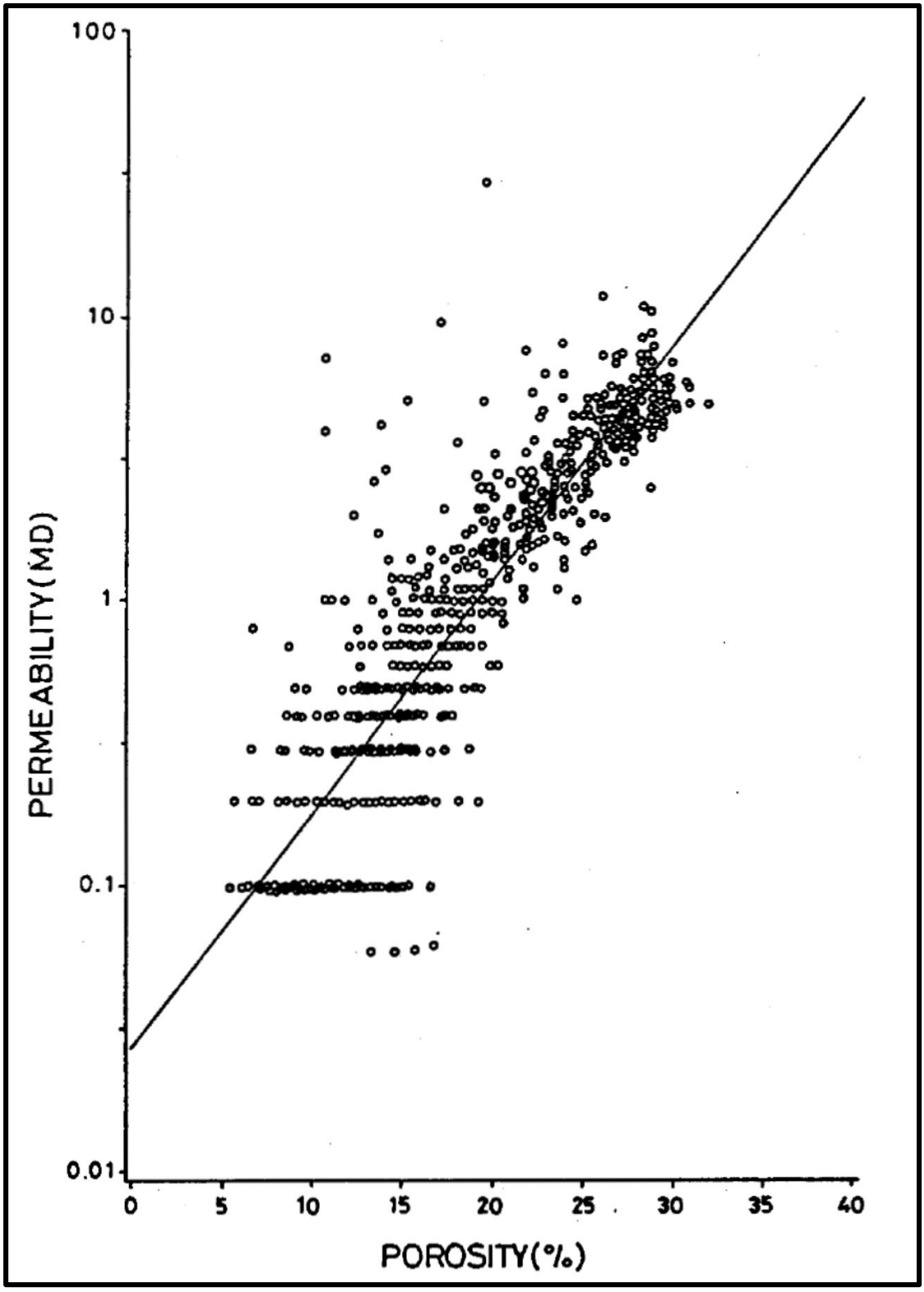


Figure 2.8: Cross plot between porosity and permeability data set from Hanifa reservoir, Abqaiq Field, Saudi Arabia (from Grover, 1993).

Saner and Sahin (1999) investigated the lithology, pattern of porosity and permeability distribution and reservoir zones in the Arab-D reservoir in Uthmaniyah Field, Saudi Arabia. They concluded that the porosity and permeability distribution patterns are lithologically controlled. They classified lithofacies into three groups: granular, muddy-granular and muddy facies based on the pattern of distribution of porosity and permeability in addition to their correlation. The first group (Granular facies) shows constant porosity and permeability distribution which is characterized by high porosity and permeability values. While the other two groups (muddy granular and muddy facies) demonstrate the bimodal distribution of porosity and permeability and indicate more heterogeneous nature with low values of porosity and permeability. The pattern of distribution of porosity and permeability are consistent. Despite the apparent linear correlation between porosity and permeability, the data sets are more scattered on the both side of the regression line (Figure 2.9).

Sahin and Saner (2001) also examined the statistical distribution and correlations of porosity and permeability for three productive zones (1-3) in the Arab-D reservoir in Abqaiq oil field, the eastern province of Saudi Arabia. In this study, they used data sets of well-log porosity and core porosity and permeability. The constructed histograms of well logs and core porosity data are similar for each zone**.** The calculated statistical parameters are comparable with exception means**.** However, the coefficient of variation (Cv) is fairly low for porosity (<0.50 in all cases with the exception in zone 3), which indicates less heterogeneity of porosity. The comparison between the vertical (Kv) and horizontal (Kh) permeability for each zone exhibits generally similar distribution**.**

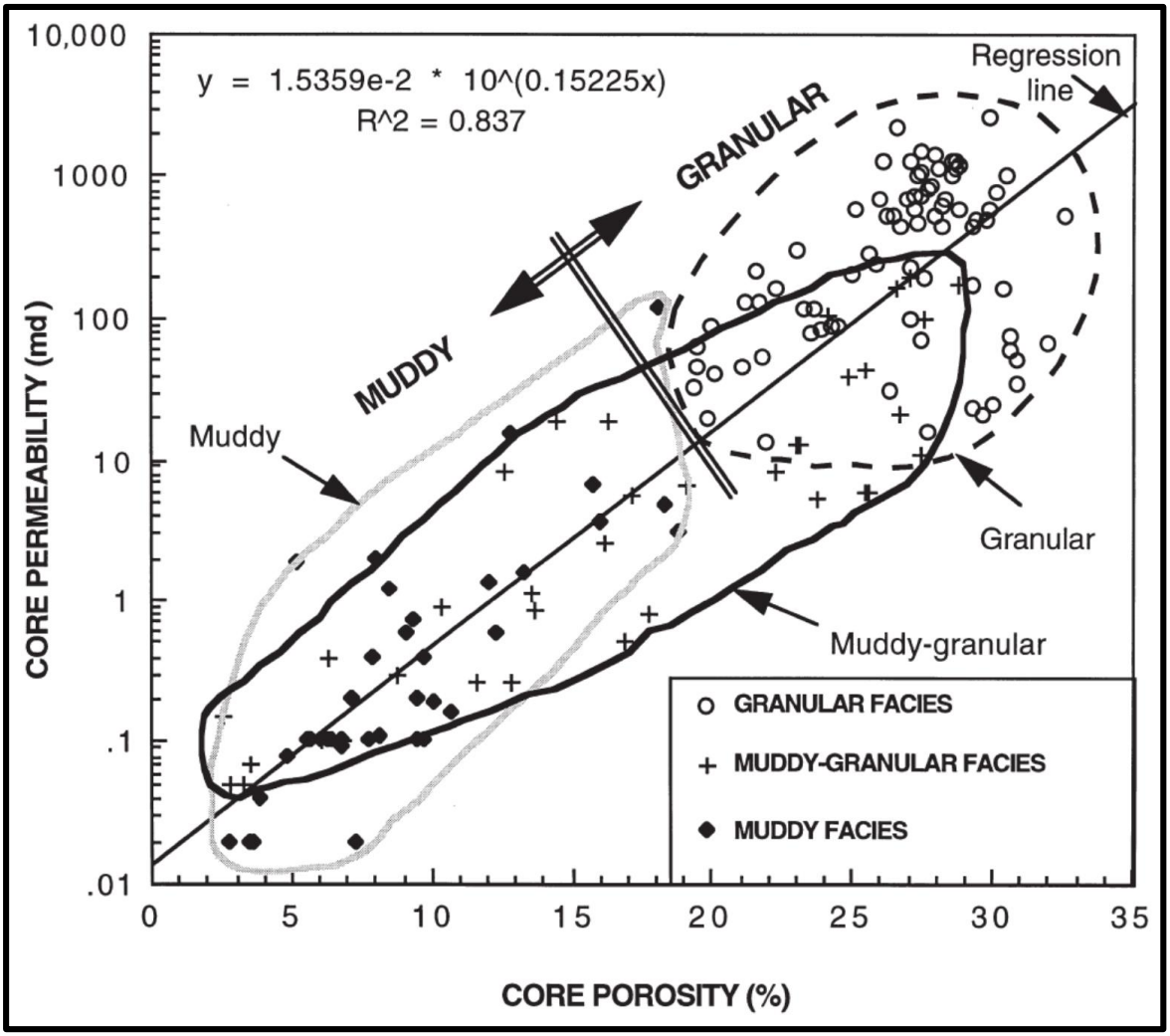


Figure 2.9: Porosity-Permeability relationship showing the distributions of the three lithofacies of the Arab-D reservoir in Uthmaniyah Field, Saudi Arabia (Saner and Sahin, 1999).

The distribution is symmetrical for zone 1 and skewed for zone 2 and zone 3. Coefficient of variation (Cv), indicated that the permeability is highly heterogeneous. The distribution of both porosity and permeability are quite similar to each other. The correlation between porosity and permeability shows that greater values of porosity have a tendency to be related to higher values of permeability and vice versa.

Abdulkadir et al. (2010) conducted a statistical analysis to understand the distribution pattern of petrophysical parameters of two units of Dibsiyah Member (Wajid Sandstone), southern western of Saudi Arabia. The histograms of both units exhibit an approximately symmetrical distribution of porosity due to moderately sorting of sand grains, which represent the major controlling factors of porosity**.** The vertical and horizontal permeability histograms show positive skewness, which indicate the heterogeneous nature of the distribution.

The majority of previous work done on Dhruma Formation either descriptive or quantitative studies. In this study, an integration between the two aspects will be utilized to enhance the static reservoir description with comparison with other Jurassic reservoirs such as Arab-D and Khuff reservoirs. The pattern of these petrophysical parameters and correlation will be discussed within the stratigraphic framework as well as diagenetic environments, and this will give a better picture concerning reservoir quality. Moreover, data comes from isotopes will be utilized to test the porosity evolution within the diagenetic environment and stratigraphic framework and related reservoir quality.

## 2.5 Reservoir Heterogeneity (Heterogeneity Measures)

It has been suggested that the majority of reservoirs were developed by mass of water through a long time, which encompasses different depositional environments. Following the deposition, the sediments may be subjected to subsequent physical and chemical changes, such as cementation, dissolution, compaction, and dolomitization, hence the reservoir quality changes accordingly. Consequently, the most part of reservoir heterogeneity subordinate upon the depositional environment and subsequent diagenetic processes. It is important to understand that homogeneous reservoirs does not exist, but different degrees of heterogeneity (T. Ahmed, 2006).

The simple definition of heterogeneity as introduced by Oxford Dictionaries (2014) is something that varied in character or content. There are other expressions may be used along with or substitute of heterogeneity term which includes variability, complexity, randomness, deviation from norm and discontinuity (Fitch et al., 2015).

Ahmed (2006) defined heterogeneity as a variation in properties of a reservoir as a function of space. The difference between homogeneity and heterogeneity is often relative and it depends upon the economic significance (Nurmi et al., 1990). The scale of heterogeneity ranges from gigascopic (basin scale) to microscopic (Thin-section scale) and the methods of investigation is different based on the heterogeneity scale itself.

The heterogeneity measures are measures used for quantitative assessment of variability by utilizing geostatistical approaches to offer a single value to characterize the variability of the dataset (Fitch et al., 2015). The heterogeneity measures which includes the coefficient of variation (CV) and the Lorenz Coefficient have been widely used in most scientific disciplines. They are commonly used in exploration operation to generate models

of porosity and permeability (e.g. Dykstra and Parsons, 1950; Sahni et al., 2005). In this sub section, three heterogeneity measures will be discussed with an outline of advantages and disadvantages of each measure.

Fitch et al. (2015) established a synthetic data set in order to clarify and understand the influence of different kinds of variability in data set on the three heterogeneity measures (Coefficient of variation, Lorenz Coefficient, and Dykstra- Parsons Coefficient) (Table 2.1). The Table (2.1) shows clearly that data set (i) is homogeneous, data set (ii) consists of two different sets of values high and low, data set (iii) contains values increasing linearly in a simple way, data set (iv) the values increases in an exponential style.

Table 2.1: An artificial data set that utilized to examine the influence of variability in data on the heterogeneity measures (Fitch et al., 2015).

| Depth (m) | Set (i) | Set (ii) | Set (iii) | Set (iv) |
|---|---|---|---|---|
| 100.50 | 1 | 2 | 2 | 10,000 |
| 101.00 | 1 | 2 | 1.8 | 1000 |
| 101.50 | 1 | 2 | 1.6 | 100 |
| 102.00 | 1 | 2 | 1.4 | 10 |
| 102.50 | 1 | 2 | 1.2 | 1 |
| 103.00 | 1 | 1 | 1 | 0.1 |
| 103.50 | 1 | 1 | 0.8 | 0.01 |
| 104.00 | 1 | 1 | 0.6 | 0.001 |
| 104.50 | 1 | 1 | 0.4 | 0.0001 |
| 105.00 | 1 | 1 | 0.2 | 0.00001 |

### 2.5.1 The Coefficient of variation (Cv)

Determined by dividing the standard deviation by the mean, and it used as a heterogeneity indicator and calculated by using the following equation:

$$Cv = \frac{\sqrt{\sigma^2}}{\bar{x}}$$

Where:

**Cv** : Coefficient of variation.
$\sqrt{\sigma^2}$ : Standard Deviation.
$\bar{x}$ : Mean.

The Cv values of permeability that less than 0.5 indicate homogeneous distribution, while values ranged between 0.5-1.0 reflect heterogeneous nature. Whereas the values greater than 1.0 represent very heterogeneous nature of distribution (Corbett and Jensen, 1992). As for the dataset in (Table 2.1), the Cv increases with heterogeneity. The dataset (i) is homogenous and data set (iv) is very heterogeneous. Therefore, the coefficient variation of homogeneous formation is zero and the value increase with increasing variability in the dataset.

### 2.5.2 The Lorenz Coefficient (Lc)

The first Lorenz approach was settled to quantify the degree of imbalance in the distribution of fortune over a population (Lorenz, 1905). The Lorenz curve has been modified by Schmalz and Rahme (1950) to be applicable in petroleum engineering through creating a plot between cumulative flow capacity and cumulative thickness, as functions

of porosity and permeability values obtained from core samples. They proposed a single parameter or value to define the degree of heterogeneity in productive zone of a reservoir. The Lorenz coefficient ranged from 0 to 1, zero for the entirely homogeneous reservoir and one for the heterogeneous reservoir (Figure 2.10). Therefore, the Lorenz curve is very helpful to describe the degree of heterogeneity in porosity and permeability in a reservoir.

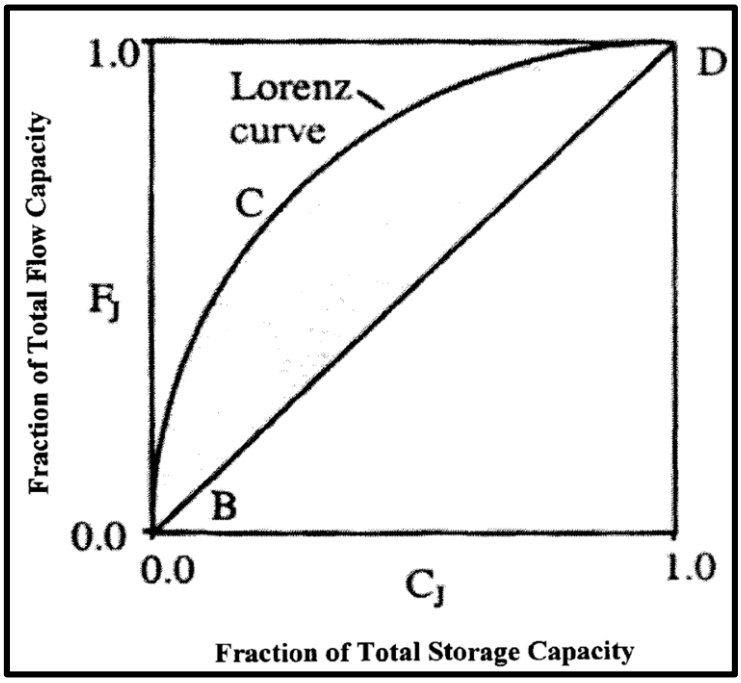


Figure 2.10: Lorenz plot to describe the heterogeneity (After Jensen, 1997).

The curve BCD in (Figure 2.10) known as the Lorenz curve. If we consider (A) is the area between the curve BCD and the diagonal line BD, then the Lorenz coefficient is defined as twice this area:

$$L_c = 2A$$

To calculate the fraction of total storage capacity (CJ) and flow capacity (FJ), the following equations can be used:

| | | |
|---|---|---|
| Fraction of Storage Capacity | $C_j = \frac{\sum_{i=1}^{j} \Phi_i h_i}{\sum_{i=1}^{n} \Phi_i h_i}$ | (j = 1, 2, 3, … n) |
| Fraction of Flow Capacity | $F_j = \frac{\sum_{i=1}^{j} k_i h_i}{\sum_{i=1}^{n} k_i h_i}$ | (j = 1, 2, 3, … n) |

Then the two obtained values CJ and FJ will be plotted on a linear graph paper.

Fitch et al (2015) examined the implementation of the Lorenz approach directly to porosity and permeability data (Figure 2.11). Regarding the synthetic data set in (Table 2.1), the Lorenz coefficient can be estimated by the arranging of the data in descending order, then make a plot between cumulative of the property under investigation (e.g., porosity) against cumulative measured depth increasing (Figure 2.11B). For this data the value of Lc is rising with heterogeneity in the dataset, dataset (i) correspond the line of best fit with a maximum value of Lc assigned to the data set (iv).

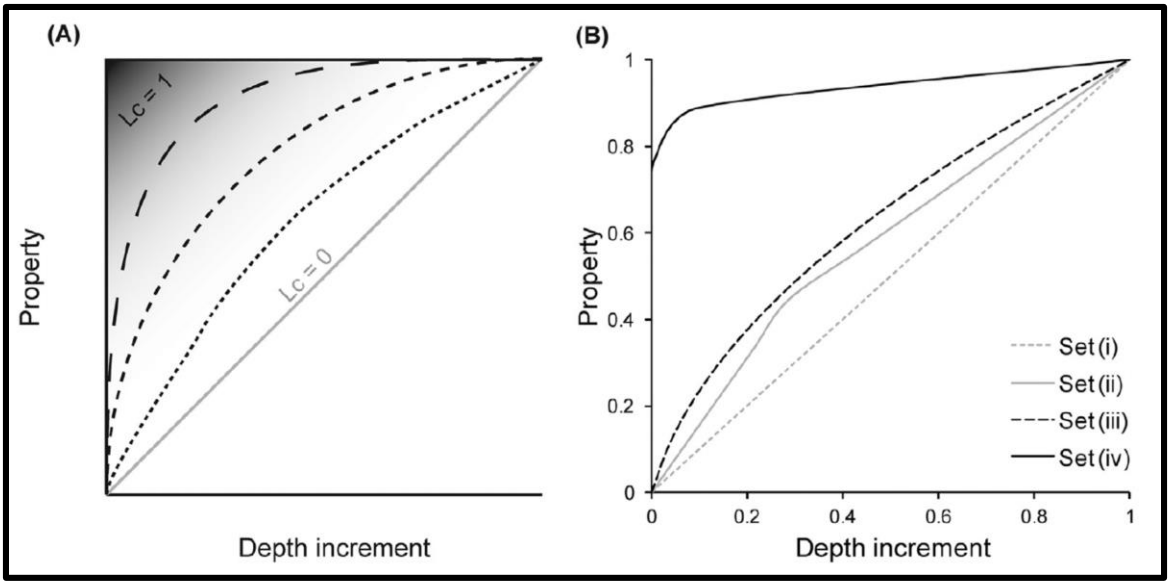


Figure 2.11: (A) Lorenz plot as examined by Fitch et al (2015) and (B) Different Lorenz plots generated by using a synthetic data set in Table 2.1.

### 2.5.3 The Dykstra-Parsons Coefficient ($V_{DP}$)

The technique has been introduced by Dykstra and Parsons (1950) to describe and evaluate the variation in permeability. The approach for calculating $V_{DP}$, gave by Jensen et al. (2000), starts by arranging the property under investigation (e.g., permeability) in descending order. The permeability data will be plotted on a log probability chart with cumulative probability values. The intersection of line of best fit for all dataset, from this plot, is then used to read two corresponding values 50% and 84.1% for the property of interest. The acquired values will be calculated using this equation:

$$V_{DP} = \frac{k_{0.50} - k_{84.1}}{k_{0.50}}$$

As there are increases in heterogeneity, the slope of the line of the best-fit increase. The Dykstra-Parsons coefficient for completely homogeneous reservoirs equal zero, and close to one for extremely heterogeneous reservoirs. For the synthetic data sets in (Table 2.1), it is clearly shown considerable variation in the generated Dykstra-Parsons plot (Figure 2.12(. Tiab and Donaldson (2015) introduced the term reservoir heterogeneity Index for Dykstra and Parsons coefficient.

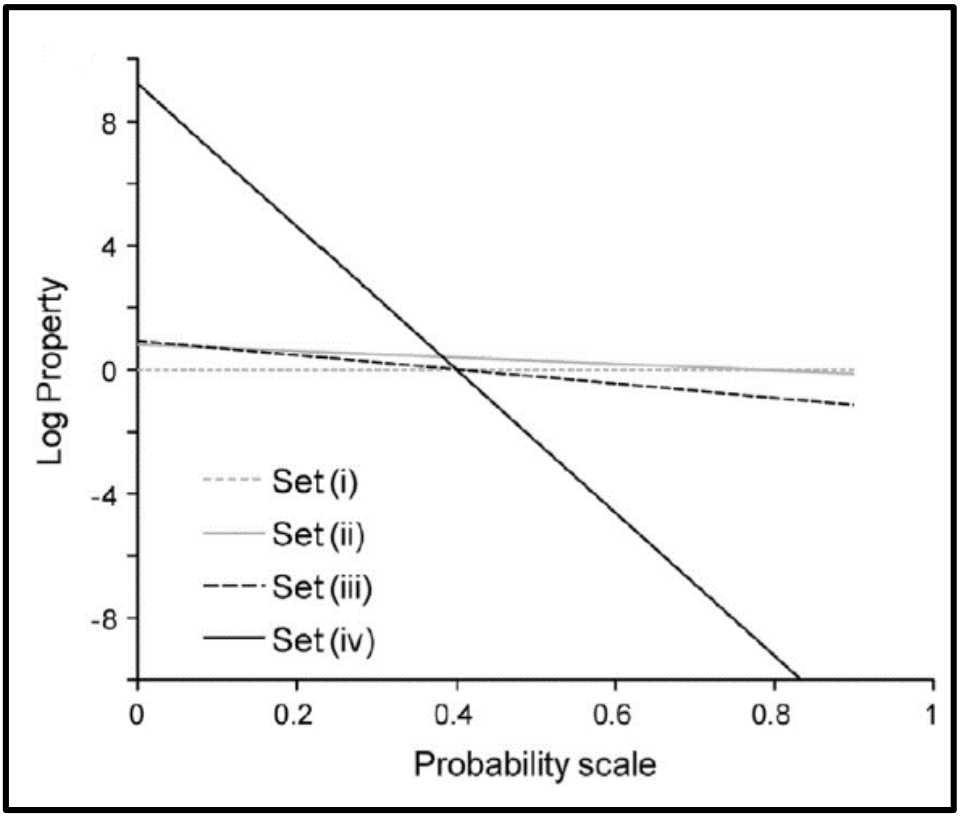


Figure 2.12: Dykstra-Parsons plot for the synthetic data sets in (Table 2.1) Fitch et al. (2015).

To sum up, the most significant advantages for utilizing heterogeneity measures is the capability to evaluate the variability in the data set by providing a single value which will allow direct correlation between diverse kinds of data, reservoir units, and fields. The simplest heterogeneity approach is the coefficient of variation (Cv) since it is not required preprocessing of the data set, but it has also limitations regarding no upper limit for heterogeneity. Lake and Jensen (1991) recommended that a great benefit of applying the coefficient of variation to measure the heterogeneity in the data set is that its ability to recognize extreme variability. The Lorenz coefficient is more precise and allow graphical visualizing of data set and quantification estimation of heterogeneity as well as provides a direct mean to compare between different types of data set. The last heterogeneity measure, Dykstra-Parsons coefficient, might be considered as more powerful statistical approach. However, it is complex and requires extra application of mathematical and statistical approaches (i.e., probability functions). Furthermore, in contrast to Lorenz plot, the Dykstra-Parsons does not give straightforward graphical representation to allow visualizing and make a comparison between datasets. A brief summary of the three static parameters is shown in (Figure 2.13).

Fitch et al. (2015) commented that the heterogeneity measures can be compared using the same techniques, however, it is not recommended that to compare between heterogeneity measures by using different techniques.

| Heterogeneity measure | Summary | Advantages | Disadvantages |
|---|---|---|---|
| Coefficient of variation (Cv) | Homogeneous = 0<br>Heterogeneous = ∞<br>$Cv = \frac{\sqrt{\sigma^2}}{\bar{x}}$ | Simple statistical technique,<br>No pre-processing of data required.<br><br>Easily applied to any data. | No maximum value, different measurement scales may influence heterogeneity results.<br><br>Limited comparison between different datasets |
| Lorenz Coefficient (Lc) | Homogeneous = 0<br>Heterogeneous = 1<br> 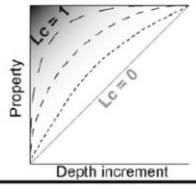 | Simple,<br>Graphical plot for comparison,<br>Easily applied to any data.<br><br>Direct comparison for different tools, formations and reservoirs. | Possible user error in sorting & normalization,<br><br>Negative values may complicate processing, but uncommon on well log datasets. |
| Dykstra-Parsons Coefficient ($V_{DP}$) | Homogeneous = 0<br>Heterogeneous = 1<br> 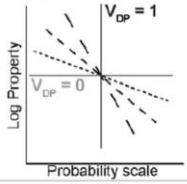 | Strong statistical basis, classification scheme established for interpretation.<br><br>Direct comparison for different tools, formations and reservoirs. | Complicated pre-processing required (probabilities),<br><br>Percentile values used in calculation are based on best fit line, rather than actual data. |

Figure 2.13: Advantages and disadvantages of the heterogeneity measures as discussed by Fitch et al. (2015).

## 2.6 Hydraulic Flow Units

Many difficulties still exist in numerical modeling and reservoir simulation. These difficulties are due to the limitations of techniques that are used to understand the detailed reservoir description and it is internal architecture and heterogeneity. The enhancement of reservoir description will reduce the quantities of hydrocarbon left in the reservoir (Amaefule et al., 1993). Therefore, understanding complex variabilities in the geometry of the pores is crucial in order to improve reservoir characterization (Amaefule et al., 1993). The core data can be used to obtain information on the effect of the depositional and diagenesis on pore geometry. These variabilities in pore geometry define different flow units in a unique way (Amaefule et al., 1993). The classical methods to differentiate between rock types was based on cross-plot between log of permeability and porosity. However, for any single porosity value within a given lithofacies type, permeability can differ by several orders of magnitude, which marks the presence of many flow units (Amaefule et al., 1993). The authors proposed a novel practical and theoretically correct approach to identify and characterize the hydraulic flow units within identifiable and traceable units (facies). The approach was based on and modified from the formula of Kozeny-Carmen as well as the idea of the mean hydraulic radius. The introduced method has been successfully applied for both clastic and carbonate lithofacies in different part of the world.

The flow units are characterized by two main important processes; depositional environment and later diagenetic overprint that affect the reservoir quality and its inflow behavior. It is critical to describe and characterize the reservoir zones and its conduits for movement of fluids. Reservoir engineers can utilize this important geological information

in reservoir simulation without extremely increasing its complexity. The concept of flow units was proposed to combine the geological data with engineering attributes in one system for the purpose of the reservoir description (Ebanks, 1987). There are several definitions introduced by many authors for flow units. Bear (1972) determined the flow units as a representative initial volume of the total reservoir body through it there is a consistent pattern in geological and petrophysical parameters. Ebanks (1987) introduced the flow units as a mappable volume of the total reservoir body through it both geological and reservoir properties that control the flow of fluids are internally steady and predictable compared to other flow units which have different properties.

The great benefit of this integrative approach for reservoir characterization and zonation in reservoir simulation is the ability to use this information to define and construct the layer of the model which is based on the vertical distribution of the porosity and permeability that obtained from both core measurement and log data (Ebanks, 1987).

According to Tiab and Donaldson (2004), the main aspects usually utilized to identify and characterize the flow units inside the reservoir rocks include Reservoir Quality Index (RQI), Flow Zone Indicator (FZI) and Tiab Flow Unit Characterization Factor ($H_T$). The measured petrophysical properties will be used in identification and characterization of flow units within the reservoir bodies. In the current study, the researcher is going to focus only on the first two parameters (RQI and FZI). The three parameters (RQI, $Ø_z$, and FZI) are based on porosity and permeability values which were measured from core plugs (Amaefule et al., 1993).

### 2.6.1 Reservoir Quality Index (RQI)

The concept was introduced by Amaeful et al., (1993). The concept of (RQI) applied with consideration of pore-throat, pore and grain-size distribution along with other microscopic parameters. The following Formula which was introduced by Amaeful et al., (1993) can be used to calculate the RQI:

$$RQI\,(\mu m) = \text{Reservoir Quality Index} = 0.0314\sqrt{\frac{k}{\Phi_e}}$$

The unit of RQI is micrometers (µm), k is permeability in (mD) and Øe is effective porosity in (fraction).

### 2.6.2 Flow Zone Indicator (FZI)

The second parameter to calculate and identify the flow units is FZI. The FZI can reflect the effect of depositional environment and related diagenetic alterations that control the reservoir geometry and its flow properties. The FZI values can be calculated from the following formula:

$$FZI = \frac{RQI}{\Phi_z}$$

Where $Ø_z$ is the ratio of the pore volume to grain volume and can be obtained from the following equation:

$$\Phi_z = \left( \frac{\phi_e}{1 - \phi_e} \right)$$

Once the above parameters are calculated, it is possible to identify the different flow units by making a plot between RQI versus $Ø_z$ in the log-log plot. In such plots, similar samples will be on the same straight line, which are characterized by similar pore-throat and hence comprise a flow unit. The good reservoir quality is associated with higher values of RQI and FZI and vise versa.

## 2.7 Petro-typing and Global Hydraulic Units (GHUs)

Several definitions for the concept of 'rock typing' were proposed in the literature, from two different aspects, geological (lithotype) and petrophysical (hydraulic units) point of view. This subsection is completely based on Corbett & Potter (2004) work and findings. The concept of 'petrotype' has been proposed by Corbett & Potter (2004) to be utilized in the determination of a particular set of petrophysical rock types. In other words, the concept is based on the orderly classification of petrophysical parameters versus international standard reference, and this will act as means in comparative reservoir description and its estimation. Also, it might be helpful in 3D models comparison. The concept of rock-typing is based on previously defined set of global hydraulic elements (GHE), and the latter was determined by a systematic advancement in values of the flow zone indicator (FZI). The plotting of the data on GHE base map (Figure 2.14) will easily allow to determine the existence of any trends in the dataset and the reservoirs to be compared. In addition to the

comparison between wells, fields, and others. However, different reservoirs can be described as a single GHE or to be restricted to a mix of GHEs.

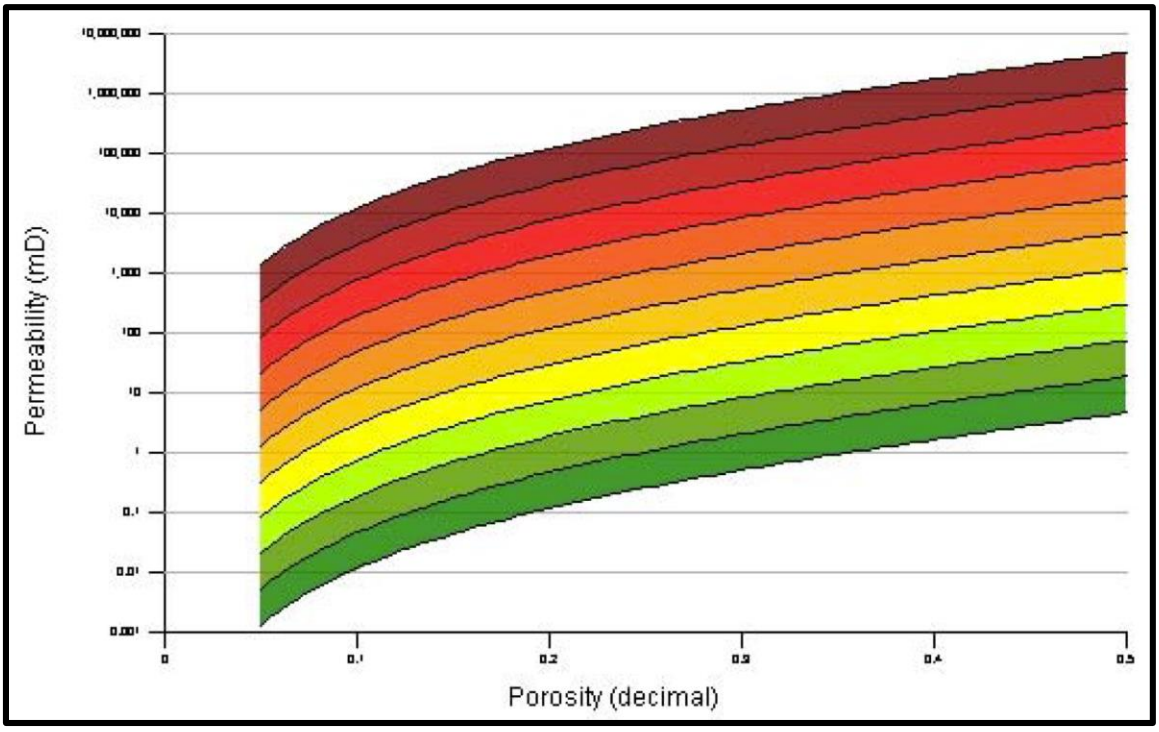


Figure 2.14: Template base map of the Global Hydraulic Elements (GHES) illustrate the ten zones with standard colors (Corbett and Potter, 2004).

The carbonate reservoirs of the Middle East for an example comprising many of the global hydraulic elements (GHEs) and these reservoirs were described as multi-petrotype reservoirs (Figure 2.15).

The identified trends can be utilized to predict the permeability. For any given porosity value, and it is possible to account for a permeability using the following equation:

$$K = \phi \left( (FZI)\, x \left( \frac{\phi}{1-\phi} \right) \Big/ 0.0314 \right)^2$$

The above equation can be also used to determine the constant lines of FZI values, which can be used also to assign the boundaries of hydraulic units and to define the Global Hydraulic Elements (GHEs) of the porosity and permeability (Table 2.2).

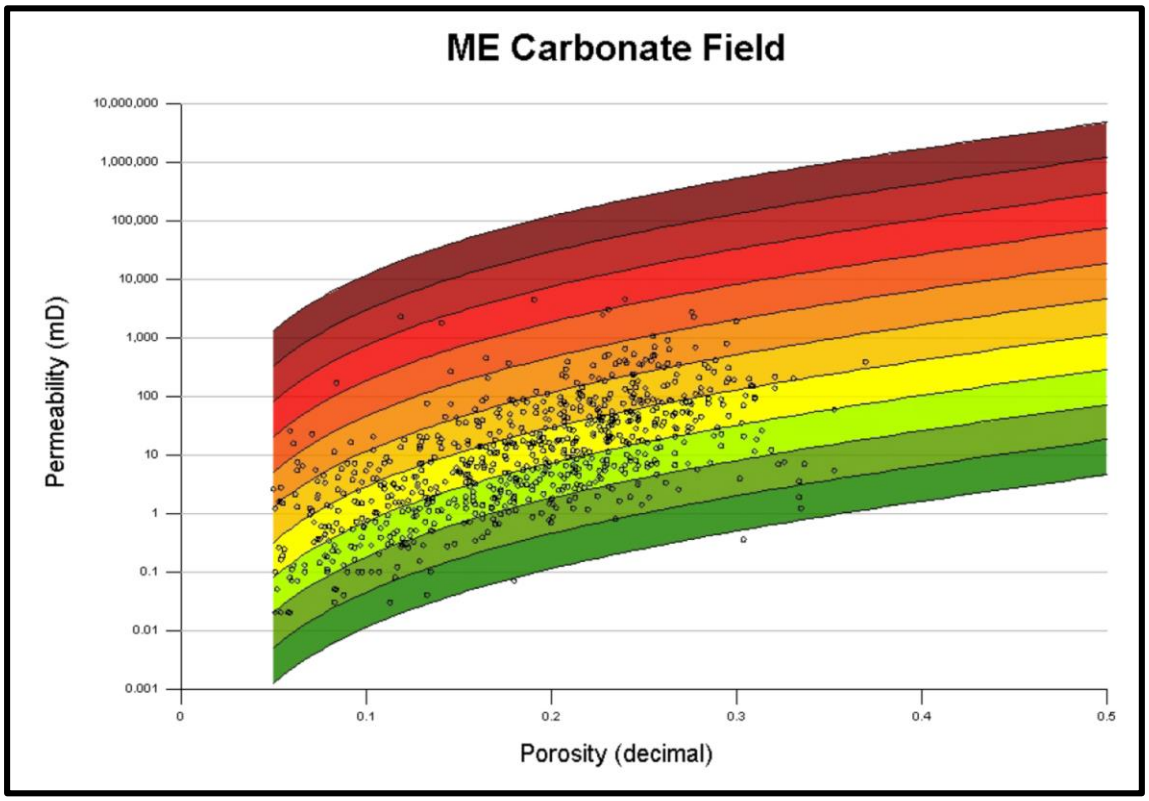


Figure 2.15: An example of a multi-petrotype reservoir in carbonate reservoirs of the Middle East. The plot encompassing several Global Hydraulic Elements (GHEs) (Corbett and Potter, 2004).

Table 2.2: Showing the proposed lower boundaries of the Hydraulic units (illustrated as FZI) and their assigned values of ten Global Hydraulic Elements (GHEs) (Corbett and Potter, 2004).

| FZI | GHE | FZI | GHE |
|---|---|---|---|
| 48 | 10 | 1.5 | 5 |
| 24 | 9 | 0.75 | 4 |
| 12 | 8 | 0.375 | 3 |
| 6 | 7 | 0.1875 | 2 |
| 3 | 6 | 0.0938 | 1 |

## 2.8 Geostatistical Modeling

Most of the classical statistic techniques do not take into account the relationship within the studied geological phenomena (Isaaks and Srivastava, 1989). However, the 3D geostatistical numerical models of the Earth have progressively played an essential role in the engineering and oil industry. There are various techniques to generate 3D reservoir modeling depending on the available data and modeling objectives. In each of these techniques, there are different approaches to model the reservoir properties based on geology, mathematics, and statistics, and software capabilities (Soleimani et al., 2008). For example, the spatial distribution of petrophysical properties such as porosity and water saturation can be represented or illustrated by utilizing the 3D geostatistical models (Dubrule, 1998). Eltom et al. (2013) generated high-resolution models for both lithofacies and porosity for the upper Jurassic Arab-D carbonate reservoir in central Saudi Arabia

using 14 outcrop sections with 15 meters spacing to capture the geological details. In this study, authors corresponded the lithofacies of sub surface with that of outcrop analog. Furthermore, they utilized the porosity values that were obtained from published porosity values of different oil fields in Saudi Arabia. In order to investigate the continuity of the lithofacies and porosity, semivariograms have been computed for lithofacies and porosity dataset. Three-dimensional model for lithofacies was generated using sequential indicator Simulation technique (SIS) (Figure 2.16). Porosity model was established by utilizing the subsurface-equivalent porosity values using sequential gaussian simulation algorithm (SGS). The results showed that the potential reservoir units are related to three lithofacies: grainstone, packstone, and some wackestone.

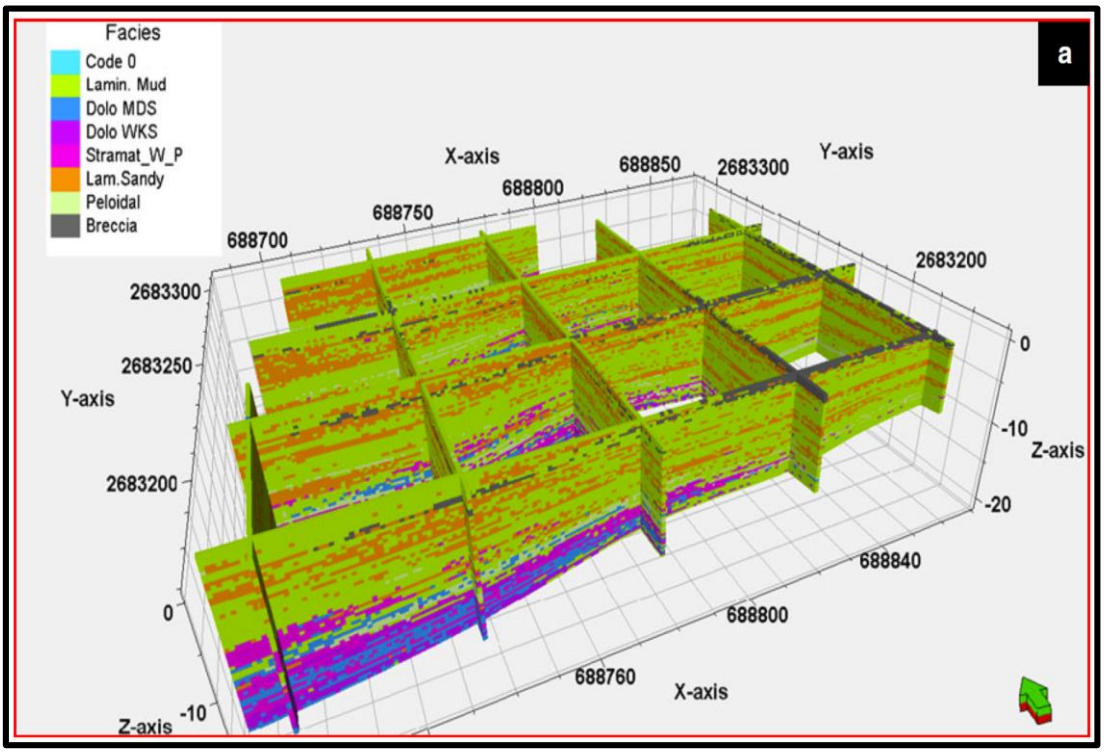


Figure 2.16: Three-dimensional (3D) geostatistical facies model of Arab-D reservoir using outcrop data from central Saudi Arabia (Eltom et al., 2013).

# CHAPTER 3

# METHODOLOGY

## 3.1 Introduction

The present study includes five main tasks in order to fulfill the research objectives: geological field investigations, sedimentological analysis, petrophysical measurements, statistical analysis and 3D geostatistical modeling for the lithofacies and reservoir properties. The interpretation of the depositional environments was depended on both field and laboratory observations. Individual tasks and methods that used are illustrated in the flow chart (Figure 3.1) and they have been discussed briefly in the following paragraphs.

## 3.2 Sedimentological and Stratigraphical Analysis

The geological field investigations were carried out on accessible and well-exposed outcrops of Dhruma Formation around Riyadh area in central Saudi Arabia. The studied sections are exposed along a road cut to Saudi White Cement Factory.

The study investigates the detailed sedimentological and stratigraphical aspects. The established and drawn vertical and lateral profiles (photo mosaic) have been used to get significant data, which will help to characterize the lithofacies and interpretation of their depositional environments. The documentation of architectural elements of Dhruma outcrops was used in facies analysis and in the classification of lithofacies into reservoir (grainy layers) and non-reservoirs rocks (muddy layers). The reservoir units have been

traced laterally (length) and vertically (thickness). The description of the facies includes color, lithology, fossils, bed boundaries and thickness, sedimentary structures, cyclicity, lateral continuity, etc. The Dunham classification system (1962) were used for facies description and analysis. Throughout the course of fieldwork, representative samples for each bed have been taken from established vertical and lateral profiles for further laboratory examination and petrophysical measurements.

The sampling strategy was relayed on the thickness of the bed itself, which may range from (10-30) cm and from (60-100) cm for thinner and thicker beds respectively. One representative sample has been taken from beds less than 30 cm thick, while for thicker beds (> 30 cm), samples were collected at 30 cm intervals. This sampling plan will ensure covering the entire facies types in established outcrop profiles. The collected Samples have been processed for sedimentological analysis (Thin section petrography, XRF, XRD and SEM analysis) and petrophysical measurements (porosity and permeability). More than 130 representative hand samples were collected from the field reconnaissance.

## 3.3 Laboratory Analysis

The laboratory analysis was two parts: sedimentological and petrophysical analysis of the collected samples from the field. The sedimentological analysis includes slabbing and petrographic analysis of the Thin-sections, XRF, X-ray diffraction (XRD) and Scanning Electron Microscopy (SEM). The analysis was used to evaluate the potential reservoir units through detailed depositional and diagenetic analysis. The laboratory techniques that being used are described briefly as follows:

### 3.3.1 Slabbing and thin-section petrography

Slabbed samples were made in the laboratory facilities of College of Petroleum Engineering and Geosciences (CPG) using Target "Masonry Saw" and HP Machines. Then the slabbed samples being studied by binocular microscope to capture any features that were difficult to observe from the outcrop such as color, lithology, sedimentary structures, fossils, etc. Thin-sections were made for the possible field samples. Valuable information was obtained from petrographyical analysis such as rock fabric, mineralogical composition, cementation, matrix, dissolution and pores types and their distribution The preparation process was carried out using the standard thin-section preparation techniques from cutting to impregnating to polishing. Different machines were used in thin-sections preparation which include: Instagram, Buehuler, Geoform, and Logitech. The samples first have been cut and impregnated by blue-dyed epoxy resin to help in differentiation of pore space. Then the samples were submerged in Alizarin Red stain to help in differentiation between calcite and dolomite. The polarized OLYMPIC Microscope was used in microfacies and diagenetic analysis.

### 3.3.2 Powder X-ray Fluorescence (XRF)

All collected samples were crushed and powdered. Five to eight grams were processed for XRF analysis to measure and analyze the elements and oxides ratios and quantities for each sample. JSX-1000S Element Eye™ Machine was utilized in this analysis.

### 3.3.3 Powder X-ray Diffraction (XRD)

The same powder samples were also used in this analysis. Ten samples were selected for mineralogical composition for each facies and to assess the diagenetic analysis. The analysis was performed in the Research Institute (RI) facilities at KFUPM.

### 3.3.4 Scanning Electron Microscopy (SEM)

Thirty samples were selected to perform this analysis to identify mineralogy, cement type, authigenic clay minerals, matrix, texture and dissolution of grains within the rocks and its impact on porosity. The analysis was carried on the fresh and small part of selected samples. The samples were coated with gold first to avoid sample charging. This analysis was carried out in CPG laboratory facilities by using GEOL JSM.5900LV Machine.

### 3.3.5 Porosity and Permeability Measurement (Petrophysical Analysis)

Complete porosity (Φ) and permeability (k) measurements were conducted on representative core plugs collected from the field investigation. The measurements have been used in petrophysical analysis and heterogeneity assessment. Around seventy core plugs were prepared and measured. For quality control (QC), the measurement was repeated three times for each core plug. The core plugs were drilled and prepared by using Core Miling Machine (MSC) at CPG laboratory facilities. The core plugs have 1” diameter with 2” length. Then the porosity measurements were carried out for individual plug using

Core Test RPI-219 Helium Porosimeter, whereas permeability measurements were achieved using Hassler holder assembly permeameter (Nitrogen gas permeability).

## 3.4 Statistical Analysis

The statistical analysis encompasses a sequence of well-defined steps. The first step is displaying of petrophysical data (porosity and permeability) which derived from the measurements of core plugs, then have been statistically analyzed for univariate parameters such as mean, median, mode, minimum, maximum, lower and upper quartiles, variance, standard deviation, coefficient of variation, skewness, and kurtosis. Such analysis will give significant information about the data sets and the variability within it. The histograms, cross plots, (normal and log) probability plots were generated to give a general visual summary of porosity and permeability data and their distribution.

## 3.5 Geostatistical Modeling

Geostatistical modeling has been achieved using open source (Petrel) software from Schlumberger to simulate facies and petrophysical properties ($\phi$ and k). Before conducting geostatistics modeling, the dataset was examined for normality. The variograms have been computed to delineate the trend and spatial variability. Then, kriging and simulation have been utilized to develop the models.

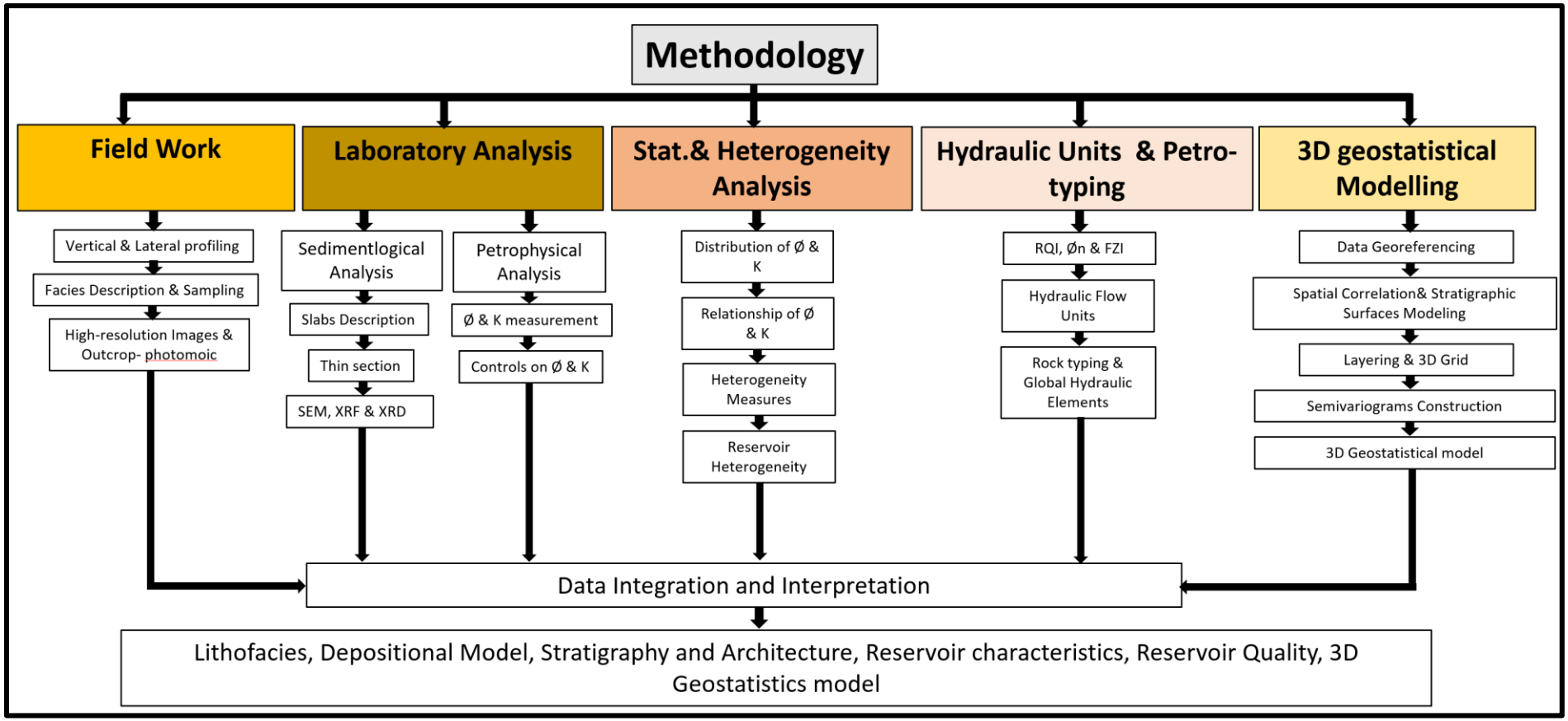


Figure 3.1: Flowchart shows tasks and methods that were followed in the study.

# CHAPTER 4

# LITHOFACIES AND STRATIGRAPHIC ANALYSIS

## 4.1 Introduction

This chapter presents the identified lithofacies types and the detailed description and assigned depositional environments of Middle Jurassic Dhruma Formation outcrops in central Saudi Arabia. The identified lithofacies have been compared and interpreted based on the standard microfacies types (SMF) of carbonate ramp which introduced by Flügel (2004) (Figure 4.1). The paleoenvironmental model of Middle to Upper Jurassic carbonate reservoirs in Saudi Arabia which proposed by Hughes, (2004) was also used to interpret the depositional environment. The model was based on benthic foraminifera and associated bio components that captured from the thin-section analysis (Figure 4.2). The Dunham (1962) carbonate rocks classification system was followed to classify and describe the carbonate lithofacies of Dhruma Formation in term of depositional texture, color, components (Skeletal and non-skeletal) and sedimentary structures. The Dunham classification was modified by Embry & Klovan in 1971 to encompass deposits that were originally bounded during deposition (Figure 4.3). Three scales of observations which derived from outcrops, slabbed samples, and thin section petrography were utilized in the lithofacies analysis and their interpreted paleoenvironments (Figure 4.4). The high-resolution stratigraphic and architectural analysis also performed based on outcrop photo mosaic, defined microfacies, and stratal pattern.

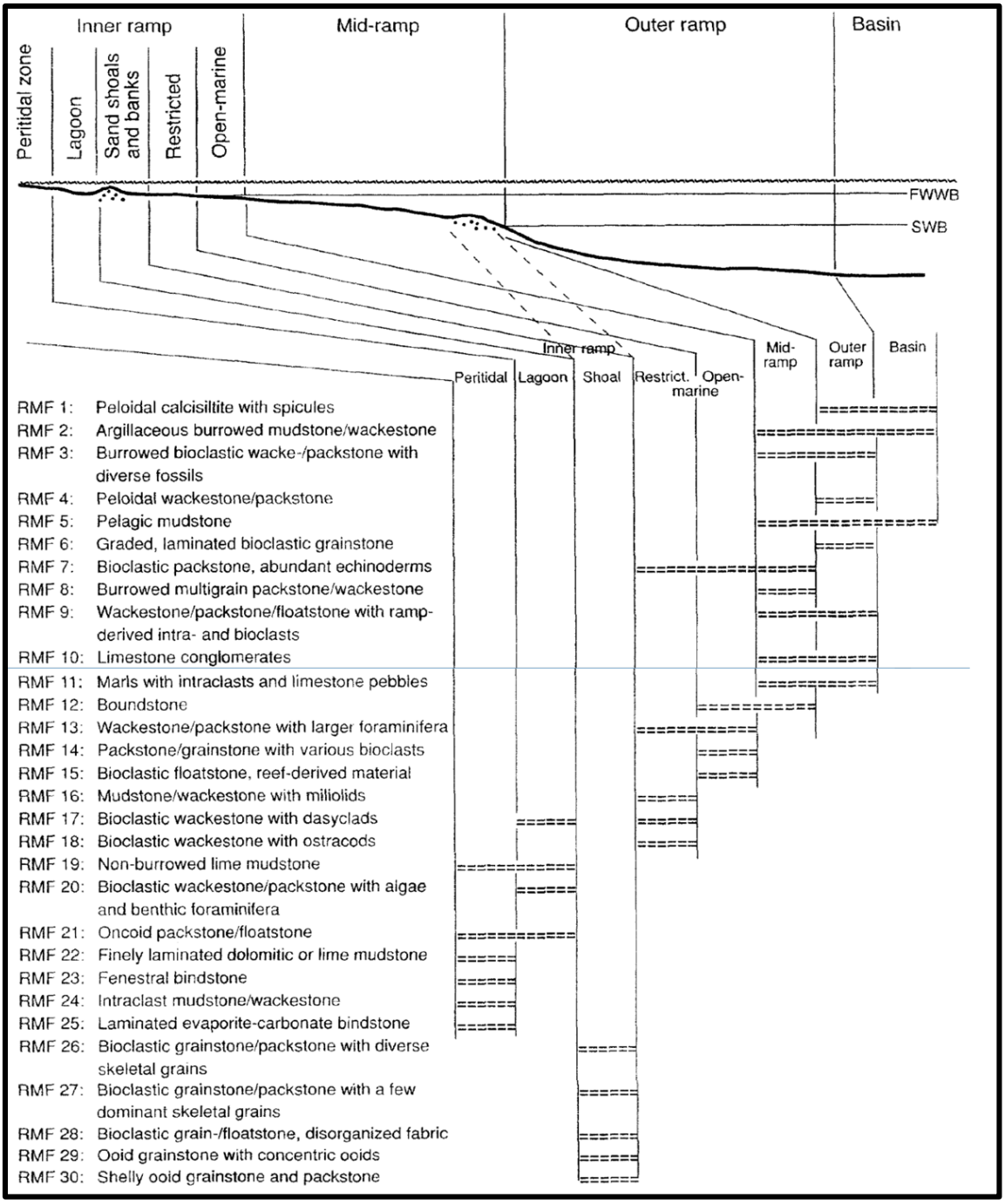


Figure 4.1: Strongly established common microfacies types showing their distribution over a homoclinal carbonate ramp (Flügel, 2004). The diagram shows some of the common microfacies types that have been described from different studies dealt with the Paleozoic and Mesozoic carbonate ramps.

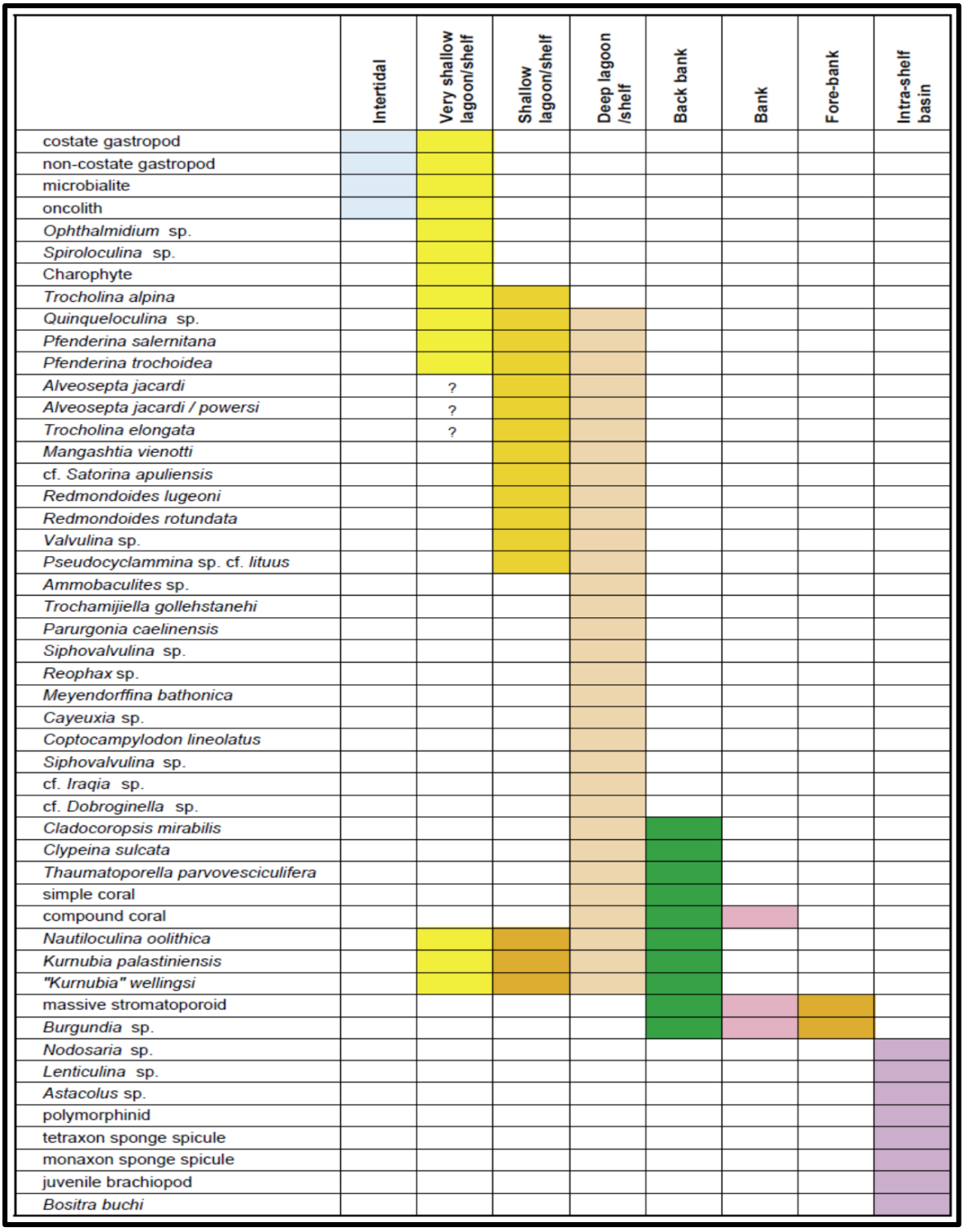


Figure 4.2: Proposed paleoenvironmental model of the Middle to Late Jurassic based on the bio components (Hughes, 2004). Different bio components can be found in various environments.

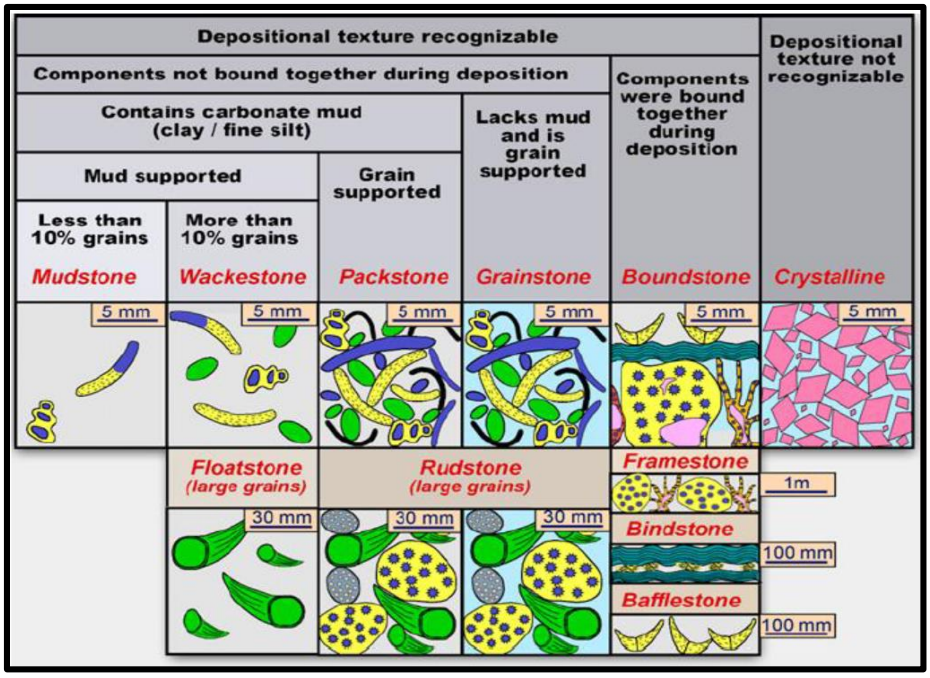


Figure 4.3: Dunham classification scheme of carbonate rocks (modified from Dunham, 1962).

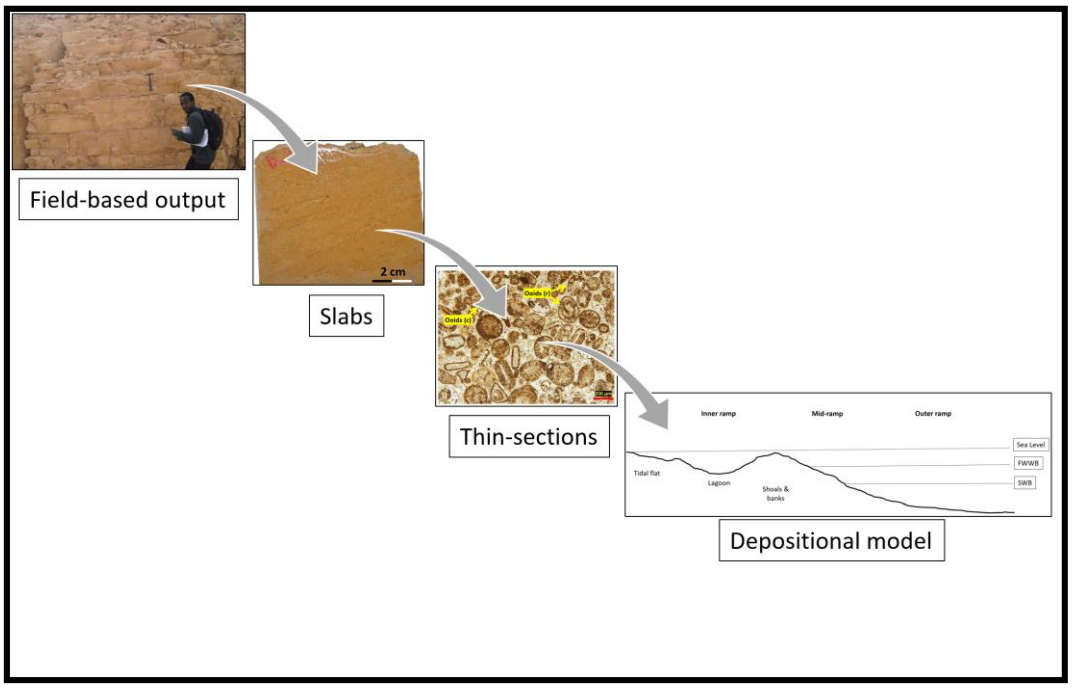


Figure 4.4: Different scale of observations being used in lithofacies analysis and interpretation of their depositional environment of the D5 and D6 Members.

## 4.2 Identified Lithofacies

Previous work on lithofacies analysis of carbonates Dhruma Formation was conducted mainly by Powers et al. (1966), Vaslet et al. (1983, 1985), Vaslet et al. (1983) and EL-Sorogy et al. (2017) to cover the entire members of Dhruma Formation. The high heterogeneity of carbonates facies makes them complicated to predict their reservoir architecture and quality. In the current study, a detailed lithofacies analysis were carried out on Dhruma Formation in order to update the previously lithofacies types and interpret their depositional environment. Different bio components were used in microfacies analysis and paleoenvironment interpretation (Figure 4.5 and Figure 4.6). However, some of these bio components were also used to confirm the stratigraphic equivalent of the reservoir intervals within the D5 and D6 Members. Furthermore, the high-resolution lithofacies and stratigraphic analysis are needed in order to enhance the static reservoir description and architecture. Therefore, nine lithofacies types (LFTs) were established which ranged from outer ramp to deep lagoon environment (Table 4.1). Each lithofacies was described in term of color, texture, lithology, sedimentary structures, components and thickness (Table 4.2). The most abundant lithofacies types of the studied interval of D5 and D6 Members include fissile shale (36%), peloidal echinoderm packstone (19%), skeletal peletal spiculitic wackestone (15%) and skeletal foraminiferal peloidal packstone (12%). The rest of the lithofacies types have abundance range from (<1% to 7%) (Figure 4.7), however, the muddy lithofacies are dominated the grainy ones.

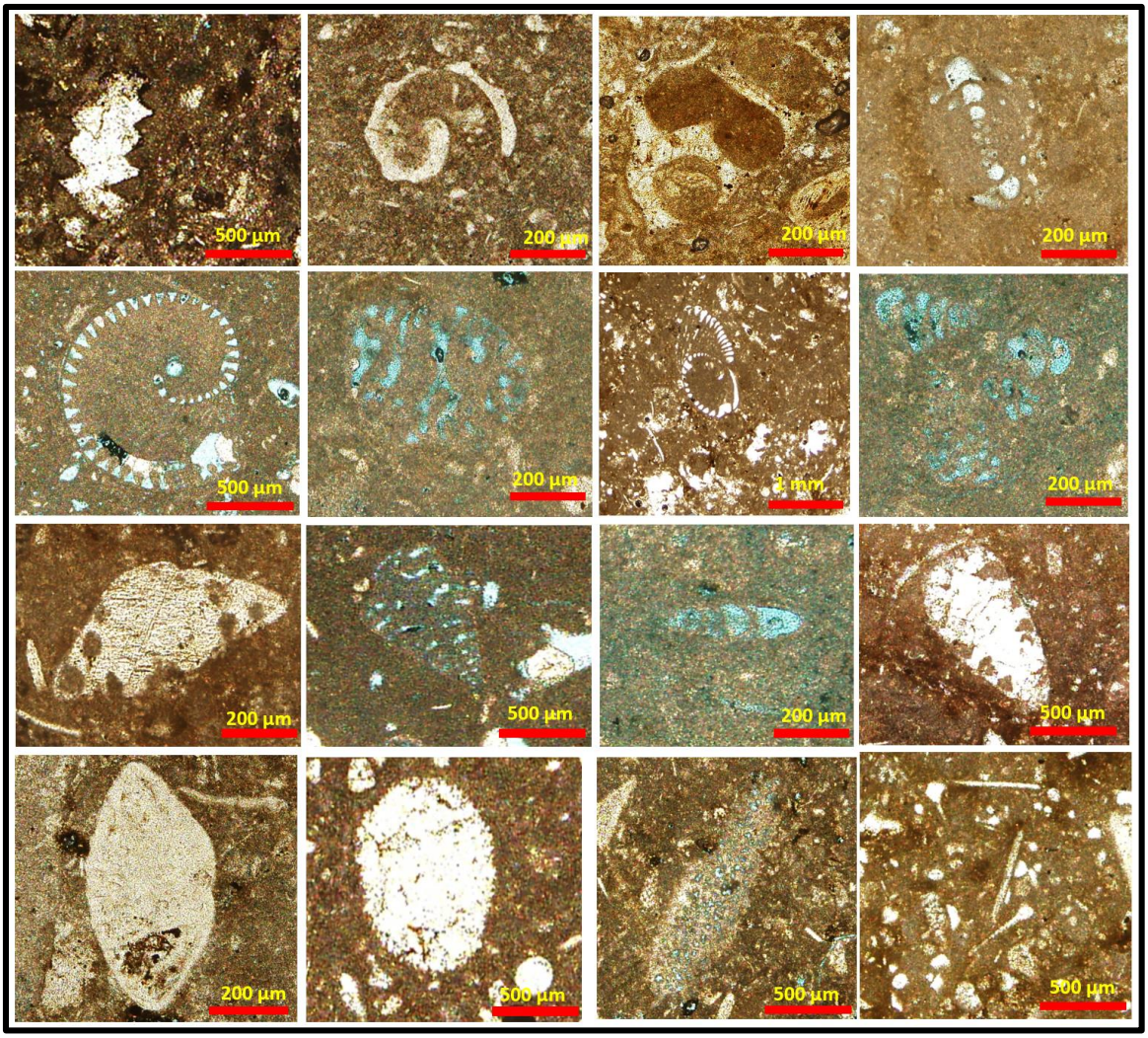


Figure 4.5: Thin-section photographs showing different bio components that captured and being used in lithofacies and paleoenvironmental analysis. Some of these bio components were used to confirm the stratigraphic equivalent of the reservoir intervals within the D5 and D6 Members as defined by Hughes (2004).

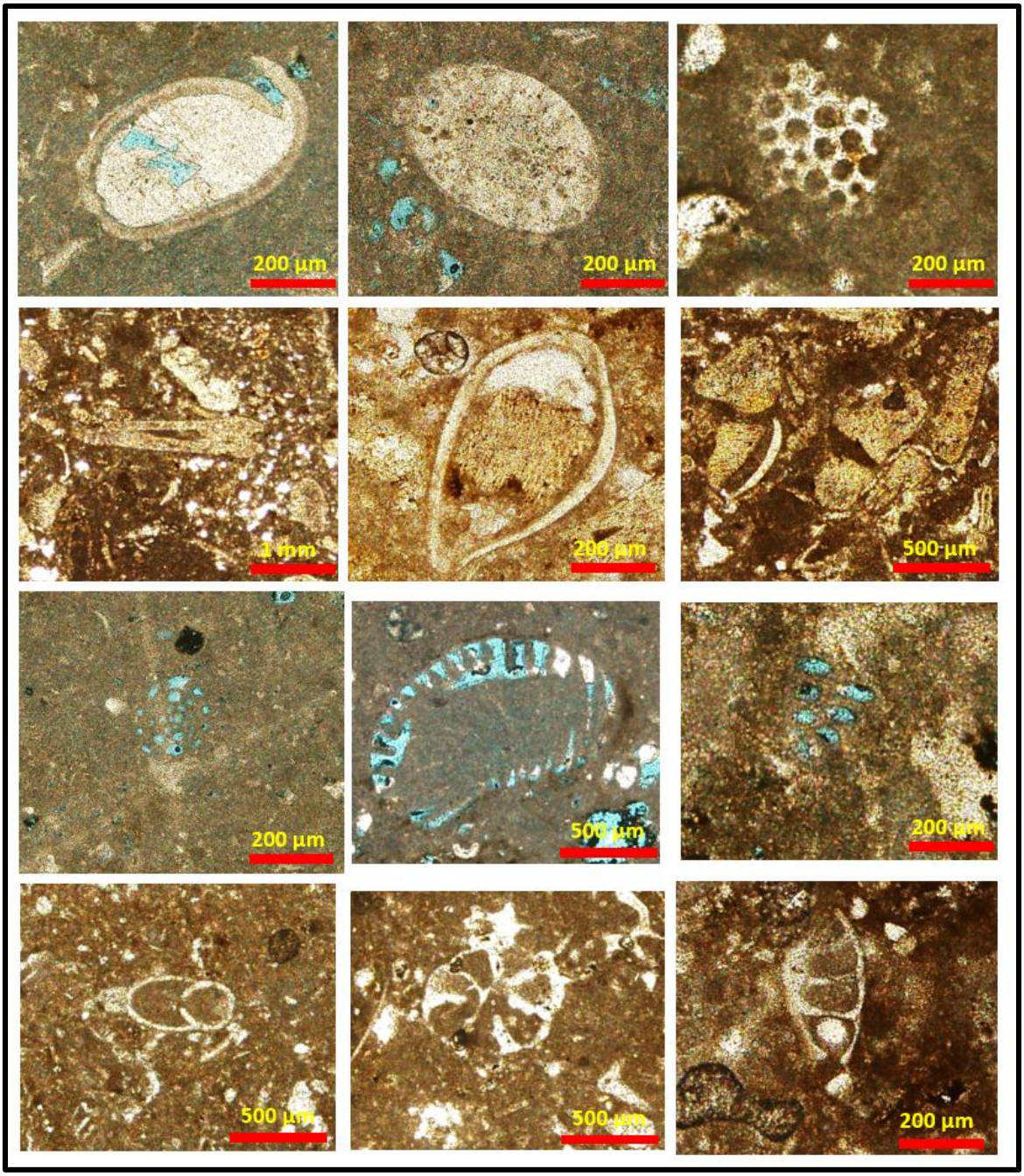


Figure 4.6: Thin-section photographs showing different bio components that captured and being used in lithofacies and paleoenvironmental analysis. Some of these bio components were used to confirm the stratigraphic equivalent of the reservoir intervals within the D5 and D6 Members as defined by Hughes (2004).

Table 4.1: Identified lithofacies types and their assigned depositional environments of the D5 and D6 Members of Dhruma Formation.

| Lithofacies (LFTs) | Depositional Environment |
|---|---|
| Fissile shale (LFT3) | Outer ramp |
| Skeletal peletal spiculitic wackestone (LFT1) | |
| Intraformational rudstone (LFT7) | Mid-ramp |
| Peloidal echinoderm packstone (LFT2) | Mid- inner ramp |
| Cross-bedded peloidal spiculitic echinoderm pack-grainstone (LFT4) | |
| Cross-bedded peloidal skeletal oolitic grainstone (LFT5) | Shoal |
| Oolitic grainstone (LFT6) | |
| Skeletal peloidal foraminiferal packstone (LFT8) | Shallow-deep lagoon |
| Skeletal foraminiferal wackestone (LFT9) | Deep-lagoon |

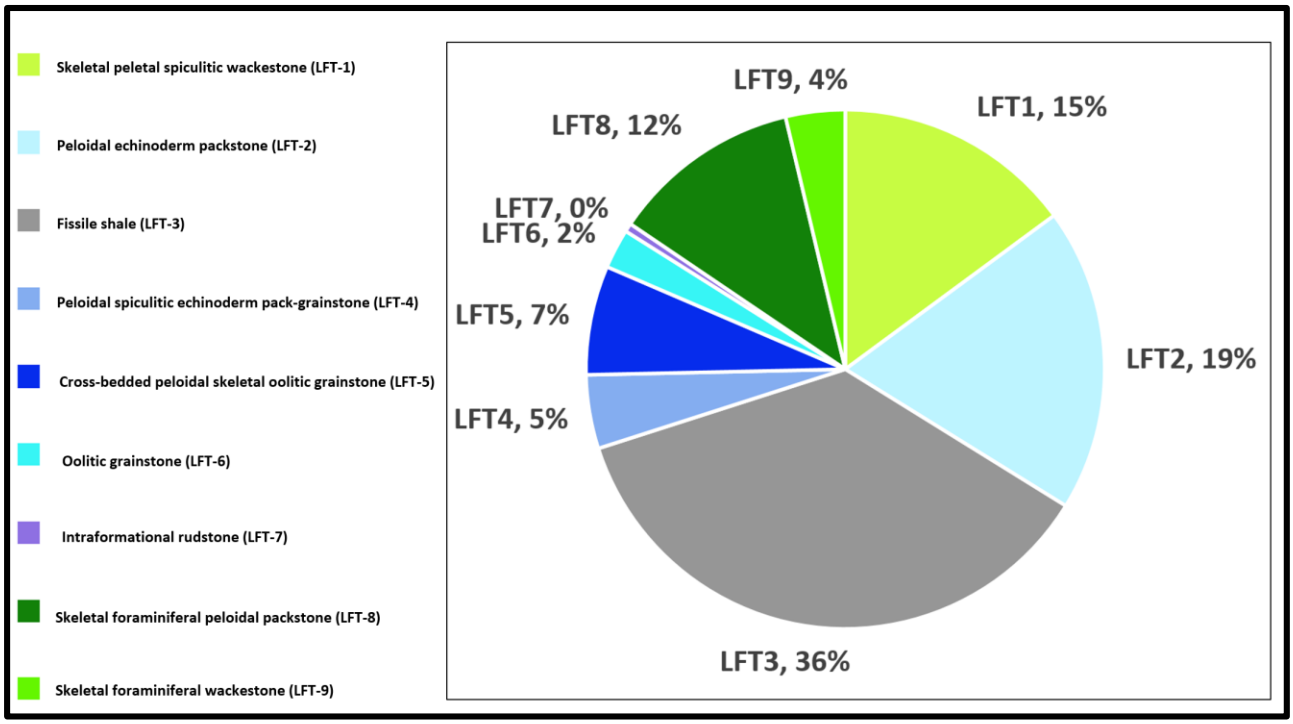


Figure 4.7: Lithofacies abundance (%) in studied sections of the D5 and D6 Members of Dhruma Formation. The fissle shale (LFT3) represents the dominant among the lithofacies types.

### 4.2.1 Skeletal peletal spiculitic wackestone (LFT1)

Light brown massive and very fine-grained, intensively bioturbated (mico-boring) muddy to wackestone texture. This lithofacies varies in thickness from 8 to 120 cm and mostly interbedded with fissile shale, peloidal echinoderm packstone, and peloidal spiculitic echinoderm pack-grainstone (Figure 4.8). It found also in the lower part of the vertical stratigraphic section. Petrographically it contains high percentage of sponge spicules in addition common to rare fecal pellets and peloids (Figure 4.9). Other rare components include shell fragments (bivalve shells), foraminifera and echinoderm fragments. Open and filled fractures exist. This lithofacies was interpreted to be equivalent to RMF1 of Flügel, (2004) peloidal calcitic with spicules.

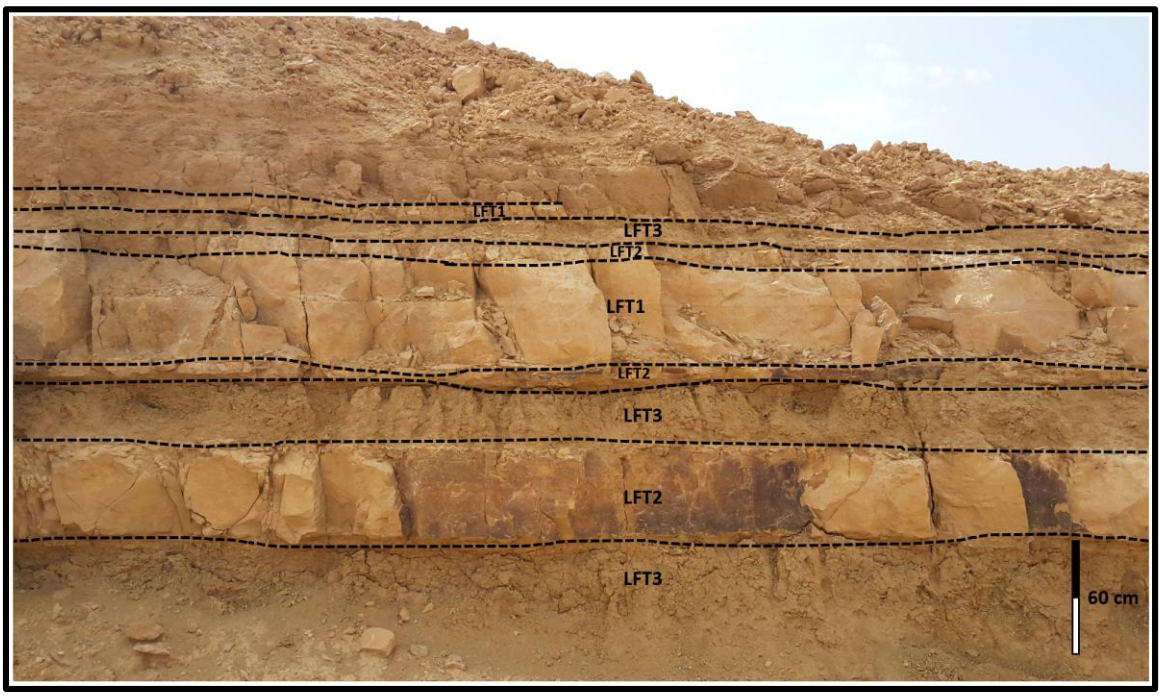


Figure 4.8: Outcrop photograph showing the interbedding between fissile shale (LFT3), peloidal echinoderm packstone (LFT2), and skeletal peletal spiculitic wackestone (LFT1). The individual lithofacies varies in thickness and generally reflects a shallowing upward trend.

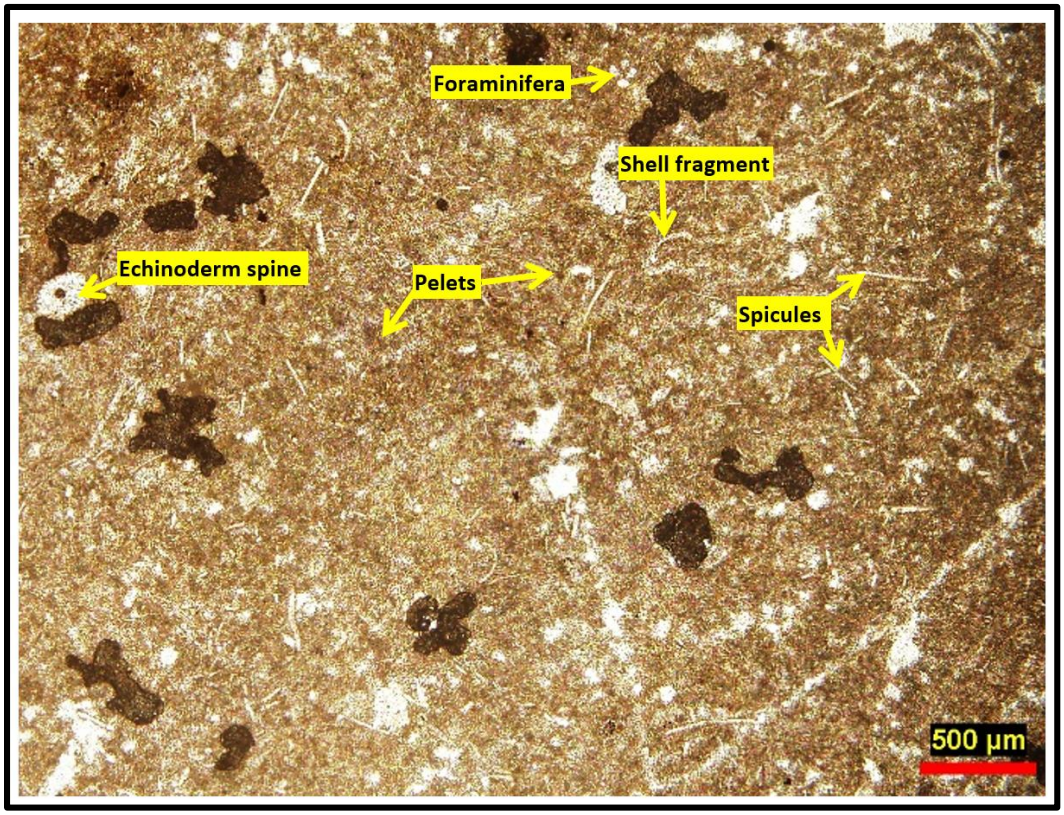


Figure 4.9: Thin-section photograph of the skeletal peletal spiculitic wackestone (LFT1), it has been intensively bioturbated and contains a high percentage of spicules.

### 4.2.2 Peloidal echinoderm packstone (LFT2)

Beige to yellowish brown massive (Figure 4.11A) with thickness range from 5 to 210 cm. In outcrop, the zoophycus ichnofacies were observed within this lithofacies which indicates a position above storm wave base (SWB) (Figure 4.10). Petrographically, the skeletal grains get coarser and dominated by echinoderm fragments (plates and spines) and form a coarse texture of common peloids and pellets (Figure 4.11B). These components are poorly sorted and poorly rounded. The other rare skeletal grains found in this facies include spicules, bivalve shells, foraminifera (miliolids and others) and gastropod with intensive bioturbation. Generally, the percentage of skeletal fragments are greater than 60% and

peloids and pellets constitute about (30-40%). This facies contains a high percentage of the matrix. The skeletal and non-skeletal grains were intensively micritized and some intervals show partial calcite cement overgrowth. This lithofacies was interpreted to be equivalent to RMF7 of Flügel, (2004), bioclastic packstone, abundant echinoderms.

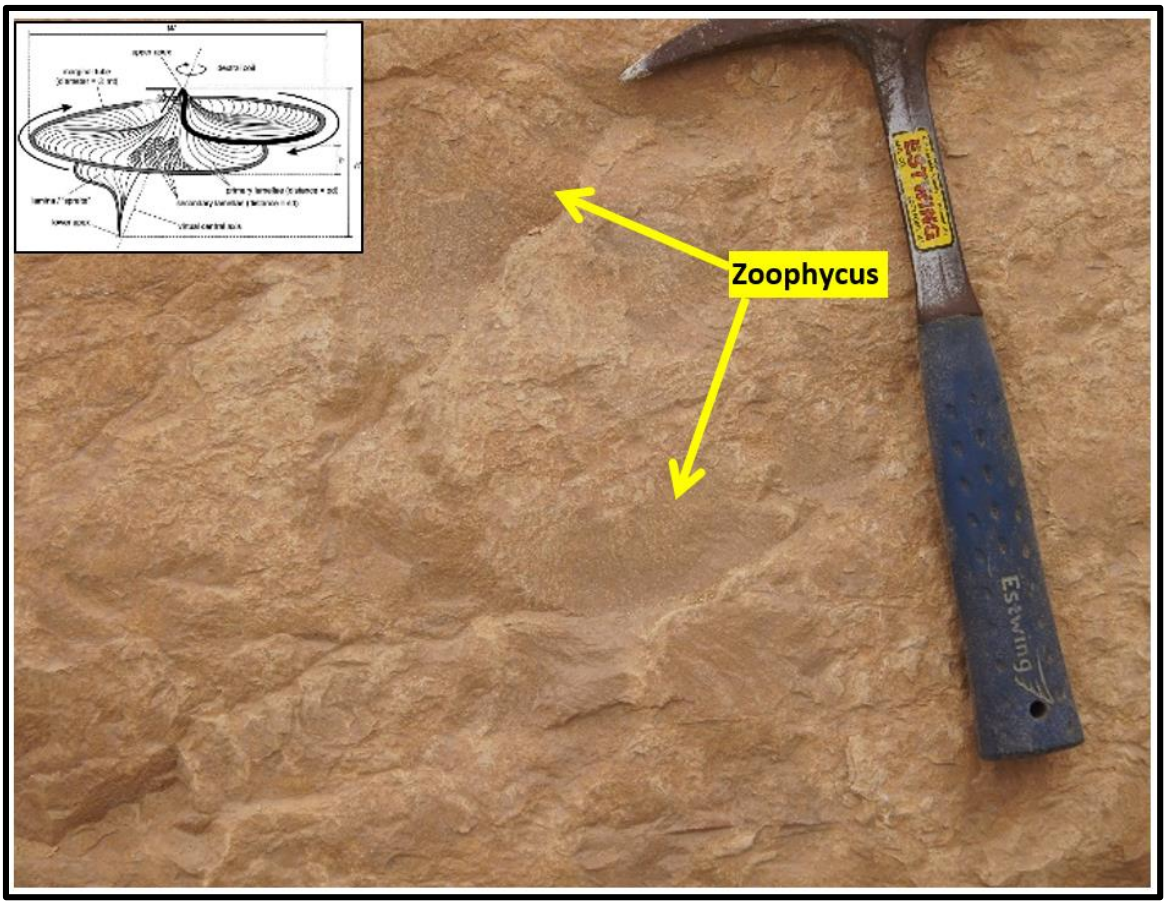


Figure 4.10: Outcrop photograph shows Zoophycus ichnofacies (LFT2) which indicate a position below fair weather wave base (FWWB).

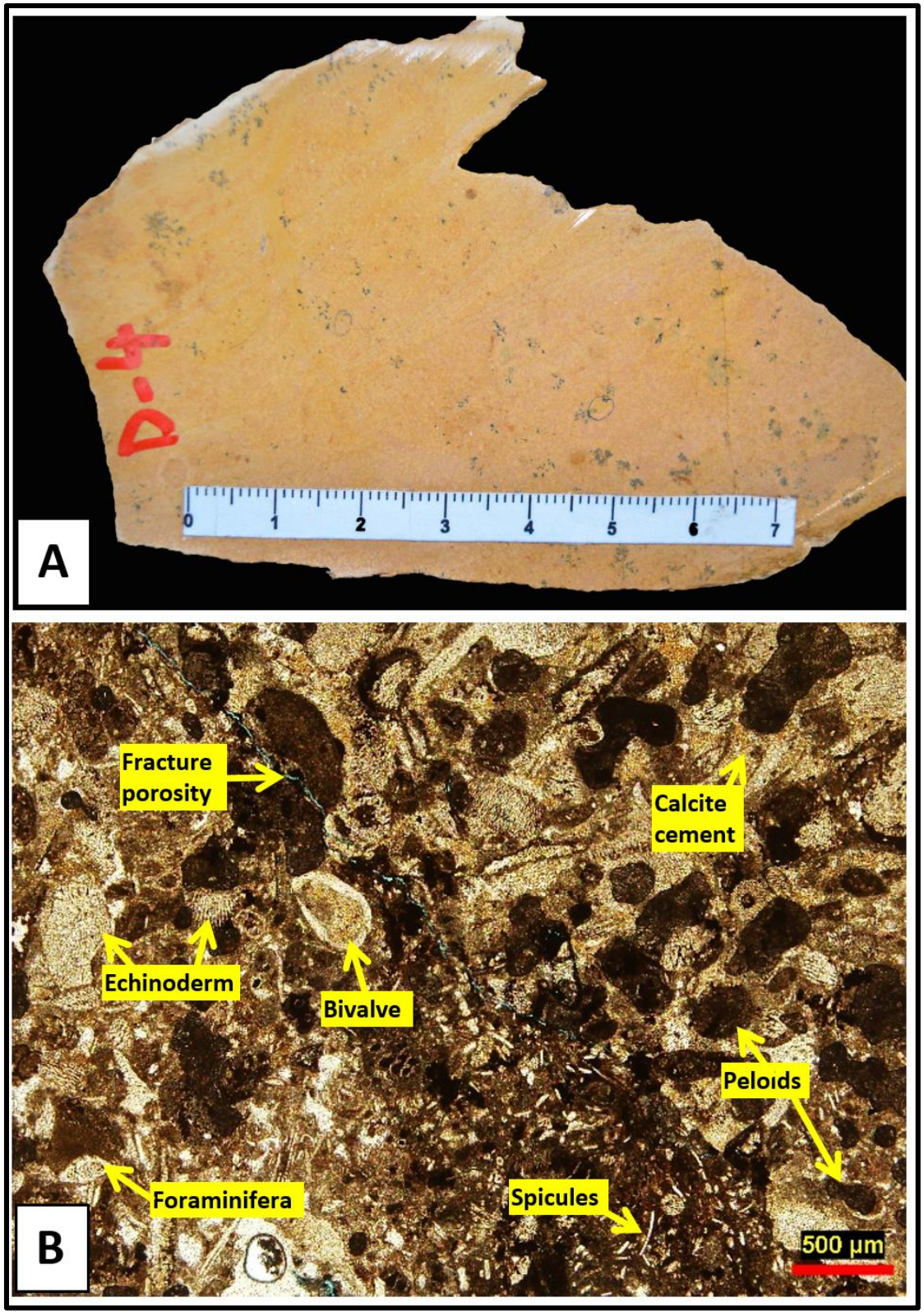


Figure 4.11: (A) Slabbed sample photograph showing the massive structure and (B) Thin-section photograph of peloidal echinoderm packstone lithofacies (LFT2).

### 4.2.3 Fissile shale (LFT3)

The most abundant lithofacies type in studied sections. Light yellowish brown to dark brown (Firebrick), friable and calcareous fissile shale (Figure 4.12 .(This lithofacies is very thick and it has a thickness range from 5 cm to 6 m. Some intervals are massive, and show intensive bioturbation and contain rare and small shell fragments in addition to undefined skeletal grains. Thin-section was difficult to be made for this lithofacies since it is friable.This lithofacies was interpreted to be equivalent to RMF2 of Flügel, (2004), argillaceous burrowed mudstone.

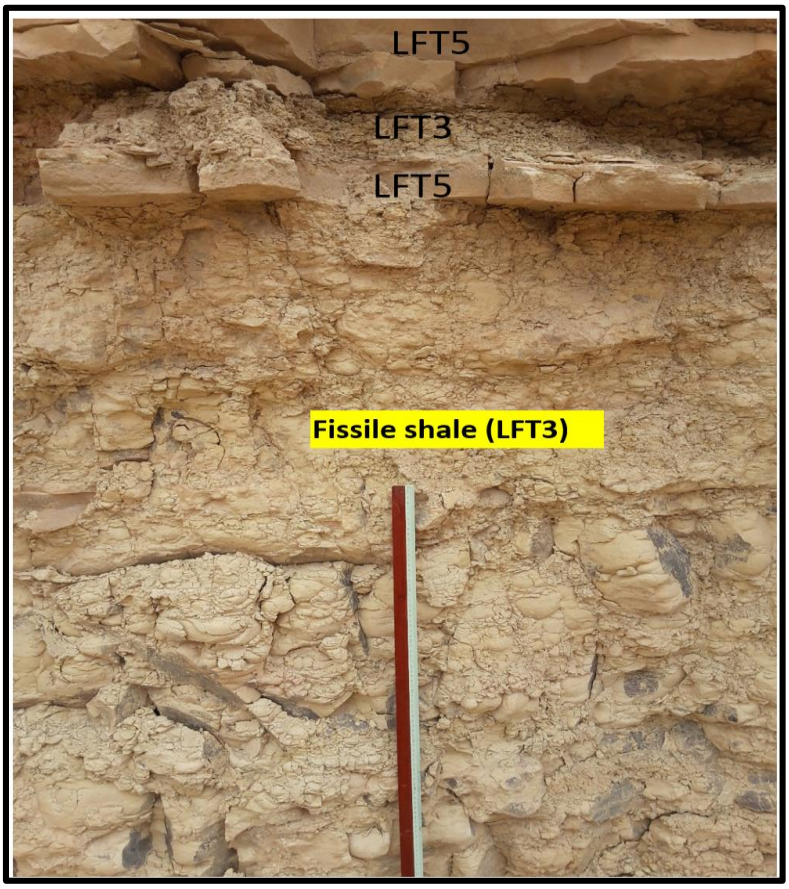


Figure 4.12: Outcrop photograph showing fissile shale lithofacies (LFT3) and cross-bedded peloidal oolitic grainstone (LFT5). The fissile shale lithofacies are the dominant one in studied sections and it has been found mostly interbedded with other lithofacies (LFT1, LFT2 & LFT4).

### 4.2.4 Peloidal spiculitic echinoderm pack-grainstone (LFT4)

Yellowish brown to dark brown trough-x bedded coarse-grained and intensively bioturbated with thickness range from 10 to 60 cm (Figure 4.13A). The dominant components are skeletal grains mostly echinoderm fragments (plates and spines) (Figure 4.13B). Common skeletal grains include foraminifera and shell fragments with rare gastropods and brachiopods. Non-skeletal grains include poorly sorted and poorly rounded peloids. Generally, the percentage of the skeletal component is (>80%), while peloids constitute about (10%). This lithofacies contains high matrix materials with partial calcite cement overgrowth and rare open and filled fractures. All features of trough-x bedding, textures, and components indicate open marine condition above the fair weather wave base (FWWB). This lithofacies was interpreted to be equivalent to RMF7 of Flügel, (2004), bioclastic packstone with abundant echinoderms.

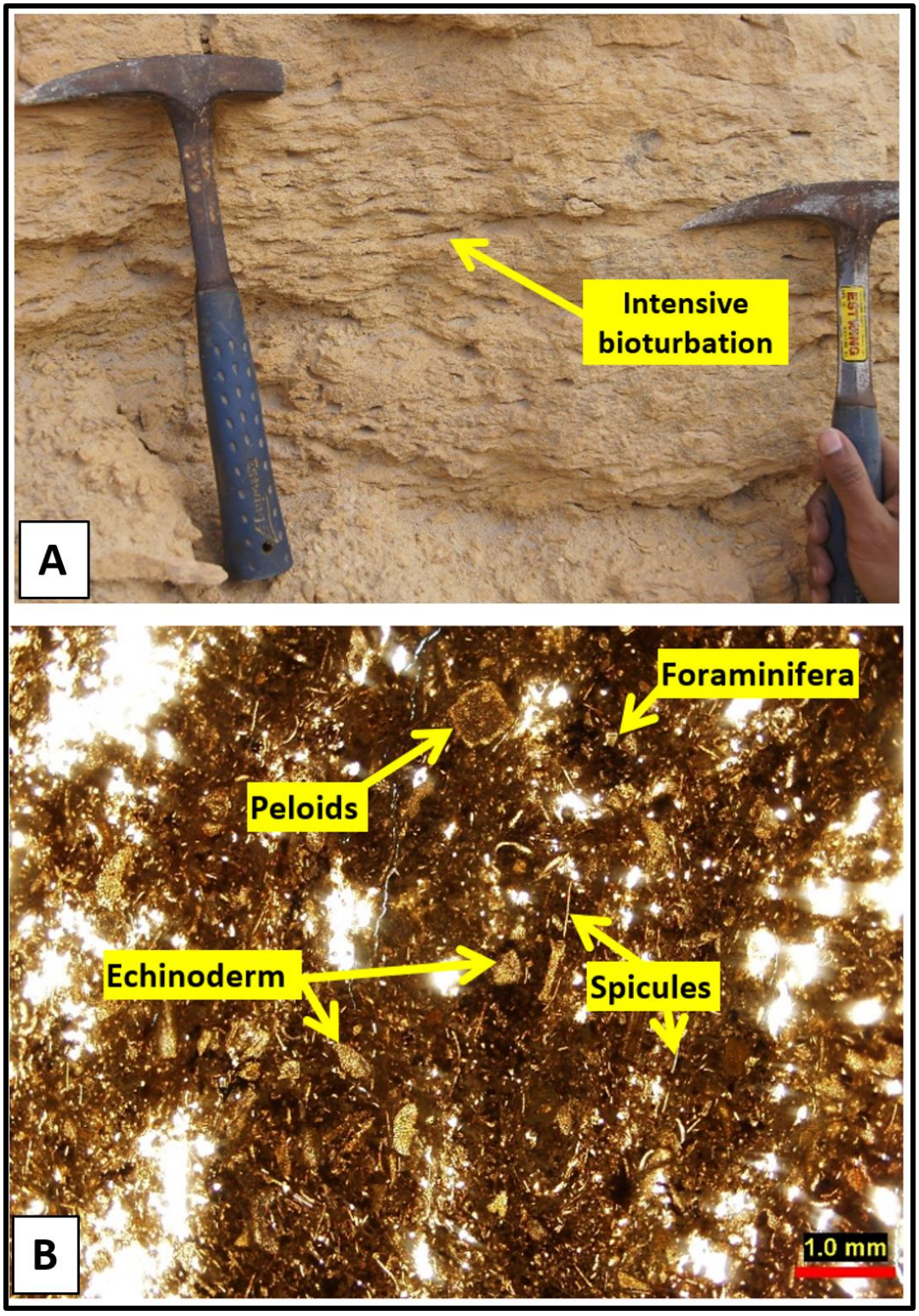


Figure 4.13: (A) Outcrop photograph showing intensive bioturbation (LFT4) and (B) Thin-section photograph of peloidal spiculitic echinoderm pack-grainstone (LFT4)

### 4.2.5 Cross-bedded peloidal skeletal oolitic grainstone (LFT5)

Light yellowish orange x-bedded fine to medium grained with thickness range from 5 to 170 cm. In the outcrop, common macro brachiopods and shell fragments were observed as well as in the slabbed samples(Figure 4.14A and Figure 4.14B) . Thin-section petrographyical analysis shows that the dominant components are ooids, with the radial micro fabric of the cortex (Figure 4.14C). Ooids are moderate to well sorted and moderately rounded. The skeletal grains are dominated by shell fragments and brachiopods with rare gastropods, foraminifera and echinoderm fragments. Peloids and lithoclast are rare. Generally, the percentage of ooids is around (60%), whereas the skeletal grains constitute around (40%). It seems that there is an intercalation between the ooids and skeletal grains. This lithofacies type indicates a high-energy condition in the depositional environment which indicated by the presence of the herringbone x-bedding (Figure 4.15). The entire ground and grains have been intensively cemented by calcite.

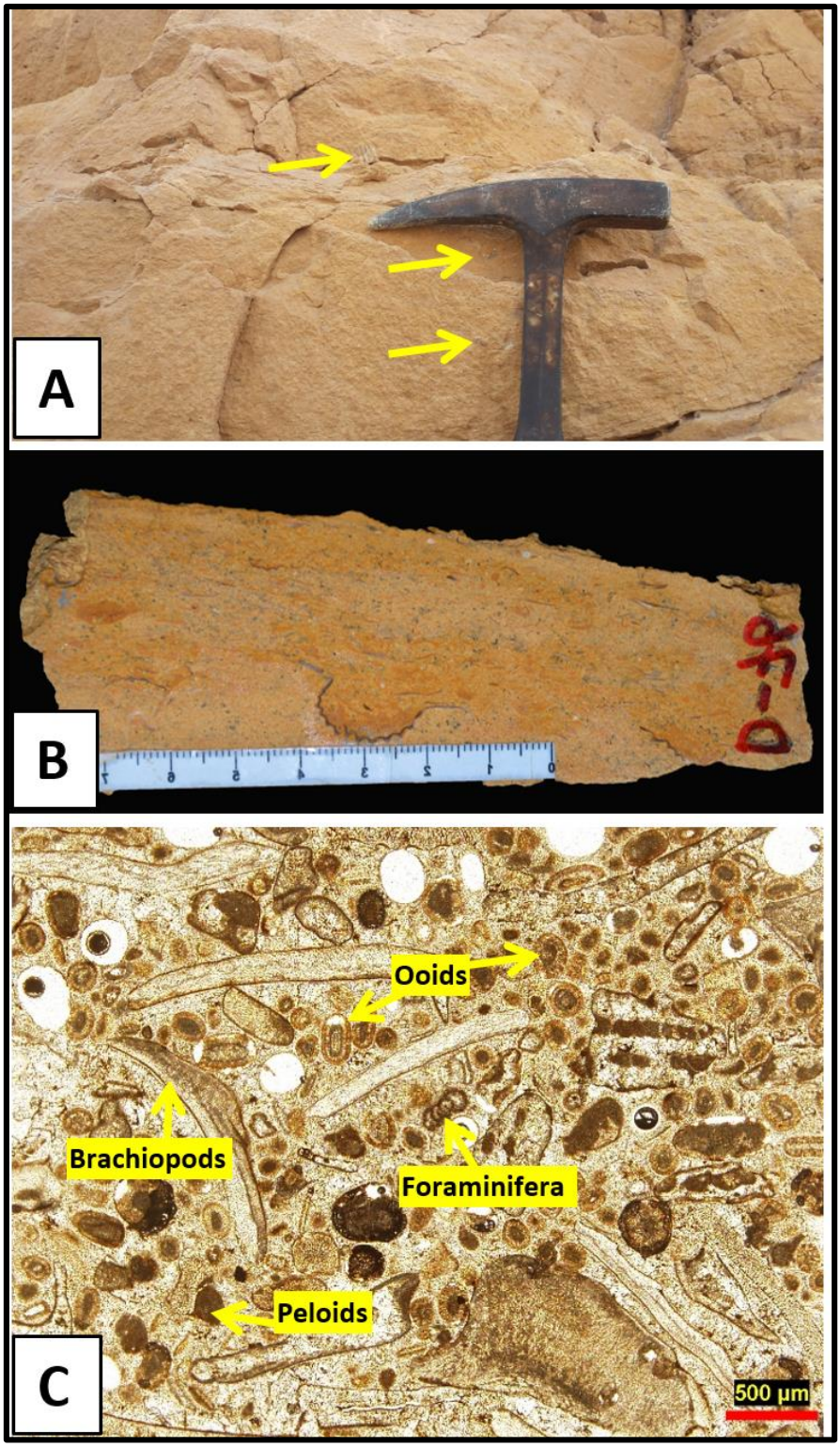


Figure 4.14: (A) Outcrop photograph shows macro brachiopods, (B) Slabbed sample photograph of cross-bedded peloidal skeletal oolitic grainstone showing the macro brachiopods (LFT5) and (C) Thin-section photograph showing the dominant of ooids with radial micro fabric (LFT5).

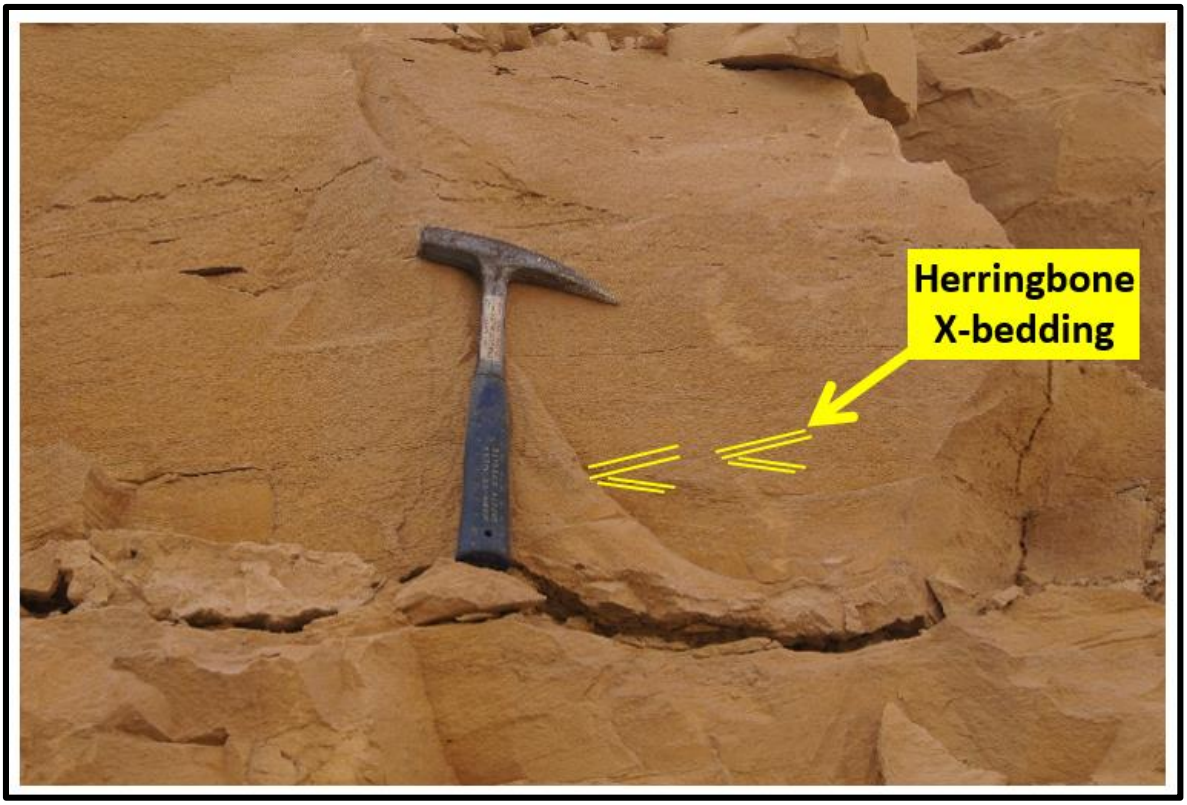


Figure 4.15: Outcrop photograph showing the herringbone x-bedding in cross-bedded peloidal skeletal oolitic grainstone (LFT5).

### 4.2.6 Oolitic grainstone (LFT6)

Light yellowish orange, x-bedded and coarse to medium grained with thickness ranges from 10 to 60 cm (Figure 4.16A). The dominant component is ooids. The ooids show both radial and minor concentric or tangential micro fabric of the cortex (Figure 4.16B). Some of the ooids start with radial and end with concentric cortex.

The percentage of ooids is about (95%). The skeletal grains are rare (5-10%) compare to that in the LFT5. The skeletal grains include shell fragments, foraminifera, gastropods, and echinoderms. Rare mud clasts were observed in the slabbed sample (Figure 4.16A). This lithofacies type also indicates a high-energy condition in the depositional environment. All components are well cemented by calcite cement. This lithofacies was interpreted to be equivalent to RMF29 of Flügel, (2004), ooids grainstone with concentric ooids.

These two lithofacies (LFT5 and LFT6) were found in a thick amalgamated succession with a decrease in thickness upward and erosion surfaces between them (Figure 4.17C). The amalgamated interval shows layers are cutting through each other, and pinching out and they are channelized with stylolites. These amalgamated units contain different types of cross-bedding which include planner (Figure 4.17A), trough and herringbone cross-bedding (Figure 4.15). This lithofacies was also found interbedded with spiculitic echinoderm pack-grainstone lithofacies (LFT4) with almost similar bed thickness for both lithofacies (Figure 4.17B).

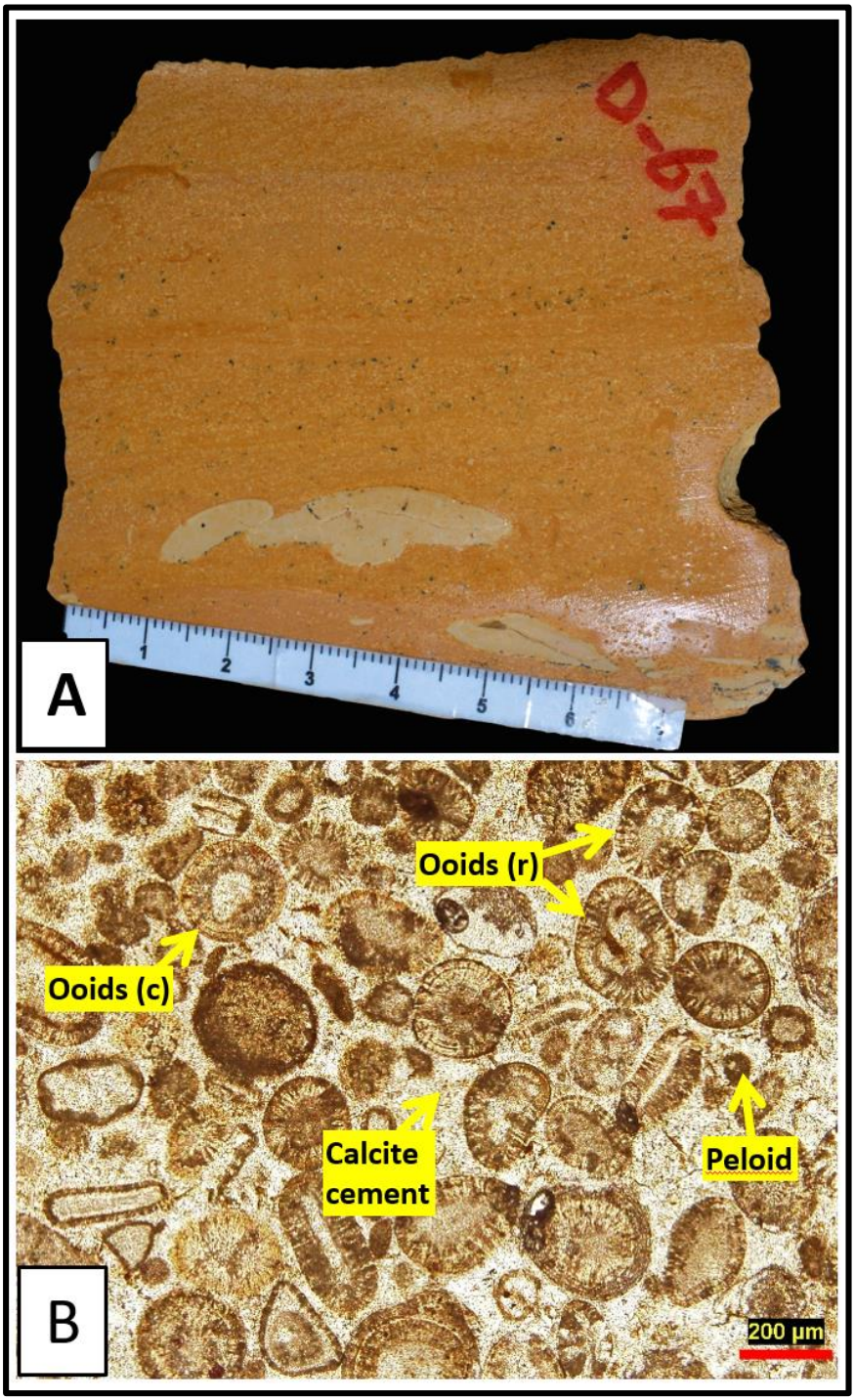


Figure 4.16: (A) Slabbed sample photograph shows mud clasts and x-bedding (LFT6) and (B) Thin-section photograph of oolitic grainstone (LFT6) with both ooids micro fabric: ooids with radial cortex (r), and ooids with concentric cortex (c).

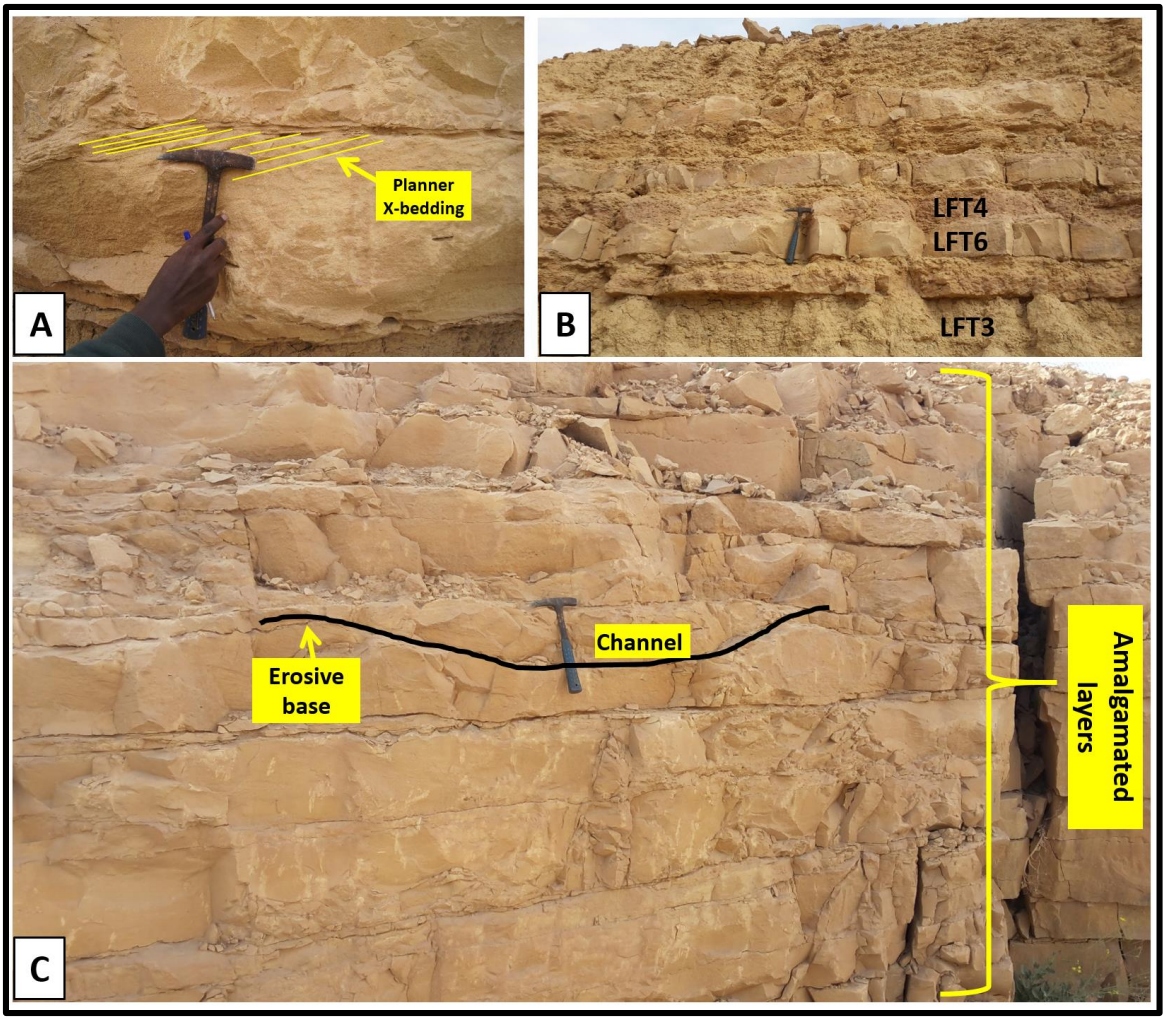


Figure 4.17: (A) Outcrop photograph of planner x-bedding (LFT6), (B) Outcrop photograph showing the interbedded between peloidal spiculitic echinoderm pack-grainstone (LFT4) and oolitic grainstone (LFT6) which reflect a shallowing upward trend, (C) channelized oolitic grainstone with erosive bases (LFT6) within a thick amalgamated unit of oolitic grainstone and cross-bedded peloidal skeletal oolitic grainstone (LFT5).

### 4.2.7 Intraformational rudstone (LFT7)

Gray to brownish color thin layer with scoured features. This lithofacies is the least abundant among the other eight lithofacies types and it has a thickness of 30 cm. It consists of pebbles and conglomerate size of rock fragments greater than 2 mm. it has very poorly sorted and very poorly rounded with grain size decrease upward (Figure 4.18). On the top of this unit, there is a high abundance of large brachiopods and oysters. This lithofacies was interpreted as a tempestite and indicates a depositional setting above storm wave base (SWB). The lithofacies can be considered to be equivalent to RMF12 of Flügel, (2004)**,** boundstone.


Figure 4.18: Outcrop photograph of intraformational rudstone lithofacies (LFT7) shows poorly sorted conglomerate and pebbles with a decrease in size upward. On the top of this lithofacies dominant oysters bearing was observed.

### 4.2.8 Skeletal foraminiferal peloidal packstone (LFT8)

Beige to yellowish brown (Figure 4.21A) with thick beds of massive and medium grained packstone (Figure 4.19). The thickness ranges from 35 to 160 cm. Slabbed samples show abundant foraminifera which is possible to observe using a binocular microscope (Figure 4.21A). The dominant component is peloids. Peloids are poorly sorted and poorly rounded (Figure 4.21B). Common skeletal grains are foraminifera. Rare components include spicules, shell fragments, gastropods, brachiopods and echinoderm fragments. The environmental interpretation of the benthic foraminiferal assemblages indicates mainly shallow to deep lagoon condition. The benthic foraminifera assemblages include Trocholina elongata, Pfenderina salernitana, Clypeina sulcate, Redmondoides lugeoni and Valvulina. The hard ground was observed within this lithofacies which acts as a barrier for fluids movement (Figure 4.20).

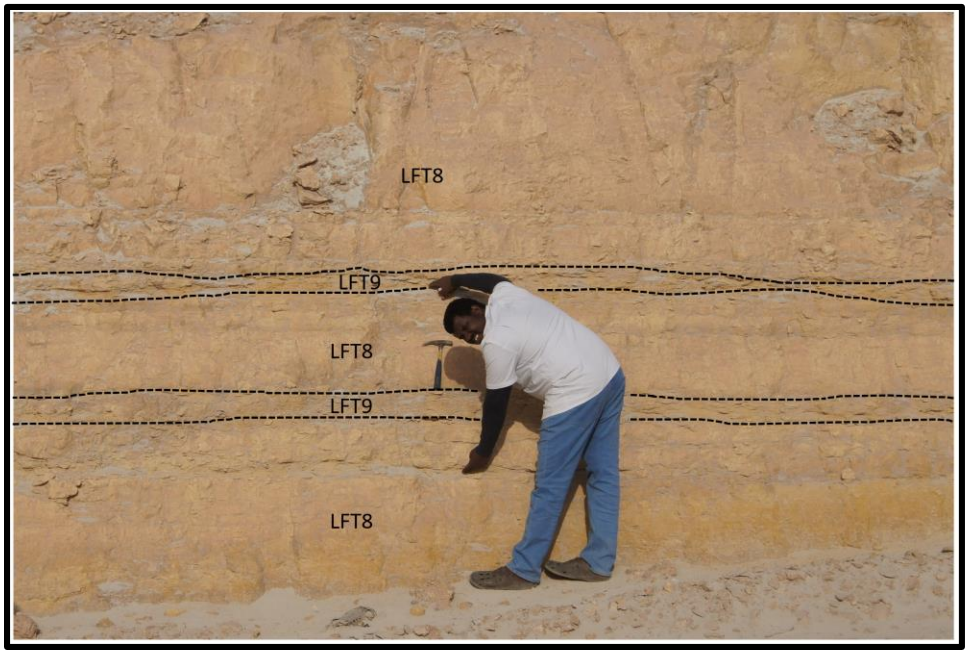


Figure 4.19: Outcrop photograph showing the interbedding between the two lagoonal lithofacies: skeletal foraminiferal peloidal packstone (LFT8) and skeletal foraminiferal wackestone (LFT9). Both lithofacies have massive structure.

Figure 4.20: Outcrop photograph showing the hard ground. It considered as a reservoir barrier for fluids movement.

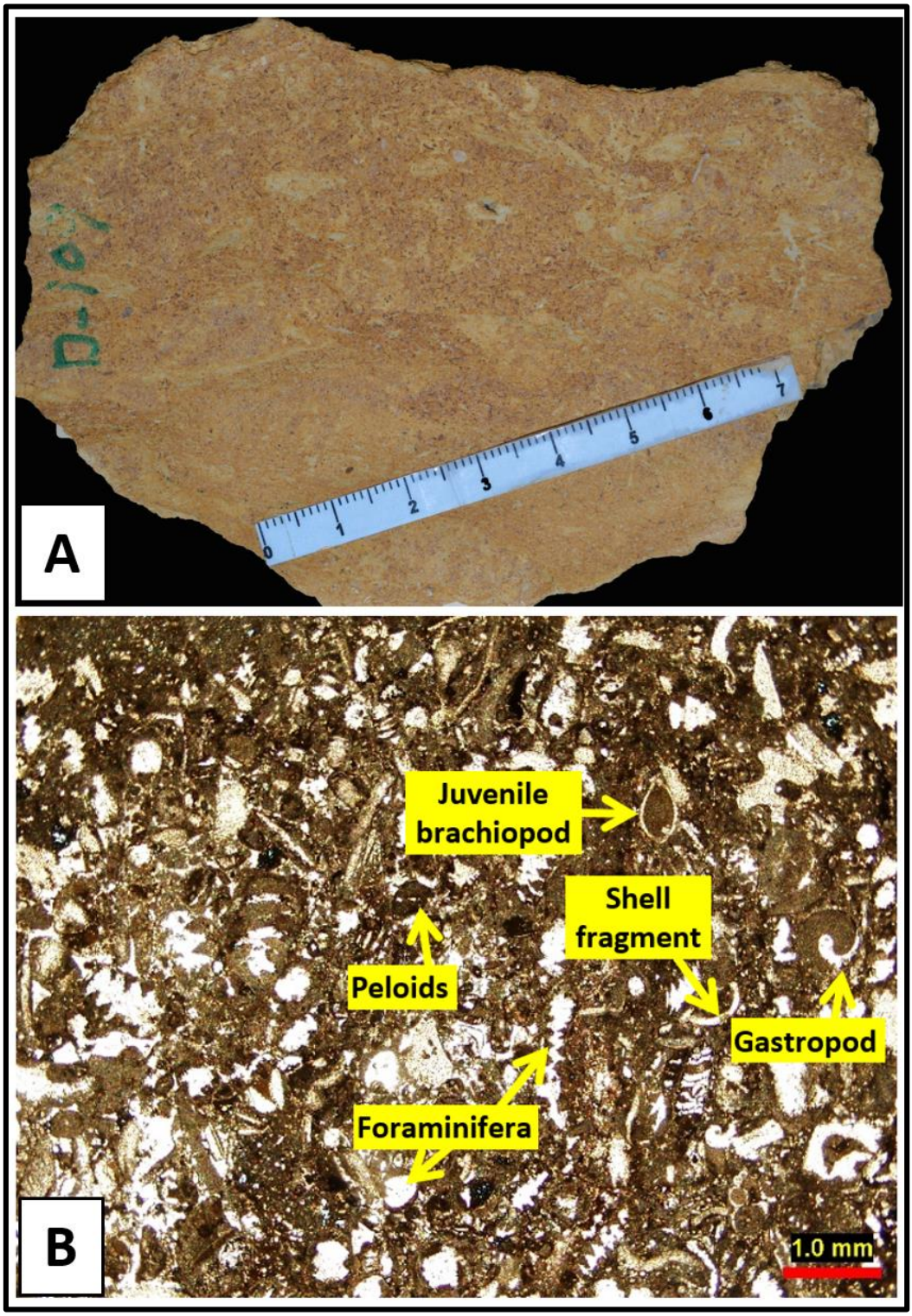


Figure 4.21: (A) Slabbed sample photograph showing abundance foraminifera (LFT8) and (B) Thin-section photograph of skeletal peloidal foraminiferal packstone (LFT8).

### 4.2.9 Skeletal foraminiferal wackestone (LFT9)

Beige to yellowish (Figure 4.22A) thinly beds massive and medium to fine grained (Figure 4.19). The thickness ranges from 5 to 55 cm. The benthic foraminiferal assemblages are the dominant component with less abundant of sponge spicules (Figure 4.22B). Other rare skeletal grains include shell fragments and echinoderms. The non-skeletal grains include rare peloids. The environmental interpretation of the depositional environment was supported by benthic foraminiferal assemblages, which indicate deep lagoon condition. Benthic foraminifera includes Pfenderina trochoidea, Redmondoides lugeoni, Parurgonia caelinensis, Alveosepta jacardi / powersi, Pfenderina salernitana, Trocholina alpine, Valvulina sp. and Pfenderina trochoidea.

These two lagoonal lithofacies (LFT8 and LFT9) were found interbedded with each other, and they reflect shallowing upward trend (Figure 4.19). Different benthic foraminiferal bio component which previously defined by Hughes (2004) was used to determine the paleoenvironment. The depositional environment was interpreted as shallow to deep lagoon. These two lithofacies were interpreted to be equivalent to RMF20 of Flügel, (2004), bioclastic wackestone/packstone with algae and benthic foraminifera.

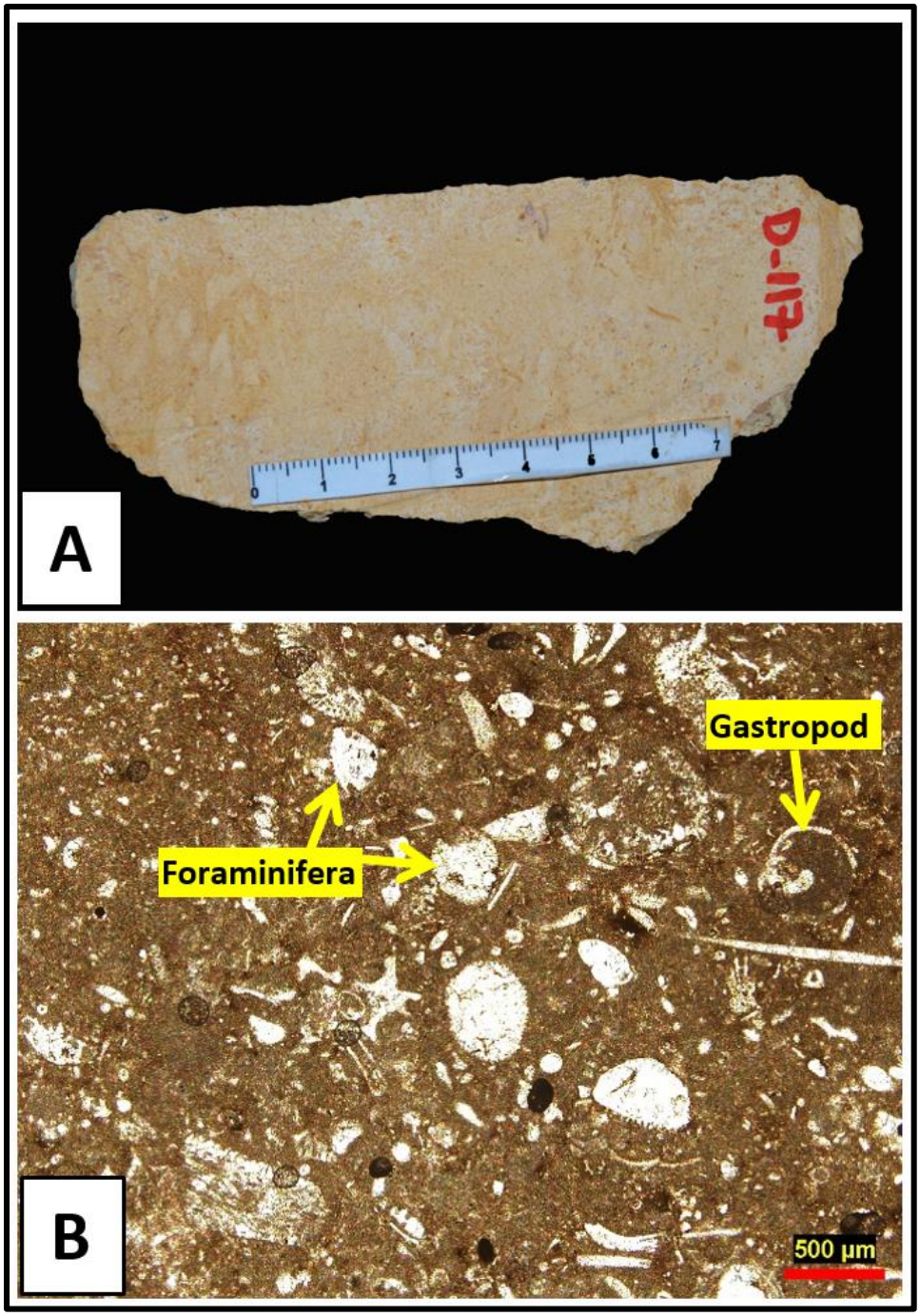


Figure 4.22: (A) Slabbed sample photograph (LFT9) and (B) Thin-section photograph of skeletal foraminiferal wackestone lithofacies (LFT9).

Table 4.2: Summary of the identified lithofacies types of the D5 and D6 Members of Middle Jurassic carbonates Dhruma Formation. Nine lithofacies types were recognized with their interpreted dispositional environment.

| Lithofacies type (LFTs) | Facies code | Lithology, texture & color | Sedimentary structure | Components | Thickness | Interpretation |
|---|---|---|---|---|---|---|
| **LFT1:** Skeletal peletal spiculitic wackestone | | Light brown wackestone | massive | sponge spicules (a), pellets (c), shell fragments (r), foraminifera (r), echinoderms (r) | 8 to 120 cm | Outer ramp |
| **LFT2:** Peloidal echinoderm packstone | | Beige to yellowish brown packstone | massive | echinoderms (a), peloids (c), spicules (r), bivalve shells (r), foraminifera (r), gastropods (r) | 5 to 210 cm | Open marine to mid ramp |
| **LFT3:** Fissile shale | | Light yellowish brown to dark brown fissile shale | massive | shell debris (r), undefined skeletal debris (r) | 5 to 590 cm | Outer ramp |
| **LFT4**: Peloidal spiculitic echinoderm pack-grainstone | | Yellowish brown to dark brown pack-grainstone | Trough-x bedding | Echinoderm (a), shell fragments (c), foraminifera (c), gastropods (r), brachiopods (r), spicules (r), peloids (r) | 10 to 60 cm | Open marine to mid ramp |
| **LFT5:** Cross-bedded peloidal skeletal oolitic grainstone | | Light yellowish orange grainstone | Trough x-bedding, planner x-bedding, herringbone x-bedding | ooids (a), shell fragments (c), brachiopods (c), gastropods (r), foraminifera (r), peloids (r) | 5 to 170 cm | Sand shoals |
| **LFT6:** Oolitic grainstone | | Light yellowish orange grainstone | Planner x-lamination, trough x-bedding | ooids (a), shell fragments (r), foraminifera (r), gastropods (r) | 10 to 60 cm | Sand shoals |
| **LFT7:** Intraformational rudstone | | Gray to brownish rudstone | scoured | Pebbles & conglomerate (a). brachiopods (c) | 30 cm | Mid-ramp |
| **LFT8:** Skeletal peloidal foraminiferal packstone | | Beige to yellowish brown packstone | massive | peloids (a), foraminifera (c), shell fragment (r), gastropods (r), brachiopods (r), spicules (r) | 35 to 160 cm | Shallow to deep lagoon |
| **LFT9:** Skeletal foraminiferal wackestone | | Beige to yellowish wackestone | massive | foraminifera (a), shell fragment (r), spicules (r) | 5 to 55 cm | deep lagoon |

## 4.3 Depositional Model of the D5 and D6 Members of Dhruma Formation

The detailed lithofacies analysis indicates five major carbonate ramp environment, including outer ramp, mid-ramp, open marine to mid-ramp, shoals and banks, and lagoon environments (Figure 4.23). Diverse bio components have been captured from thin-section analysis and been used in paleoenvironmental analysis (Figure 4.5 and Figure 4.6). However, some of these bio components were used to confirm the stratigraphic equivalent of the reservoir intervals within the D5 and D6 Members as defined by Hughes (2004).

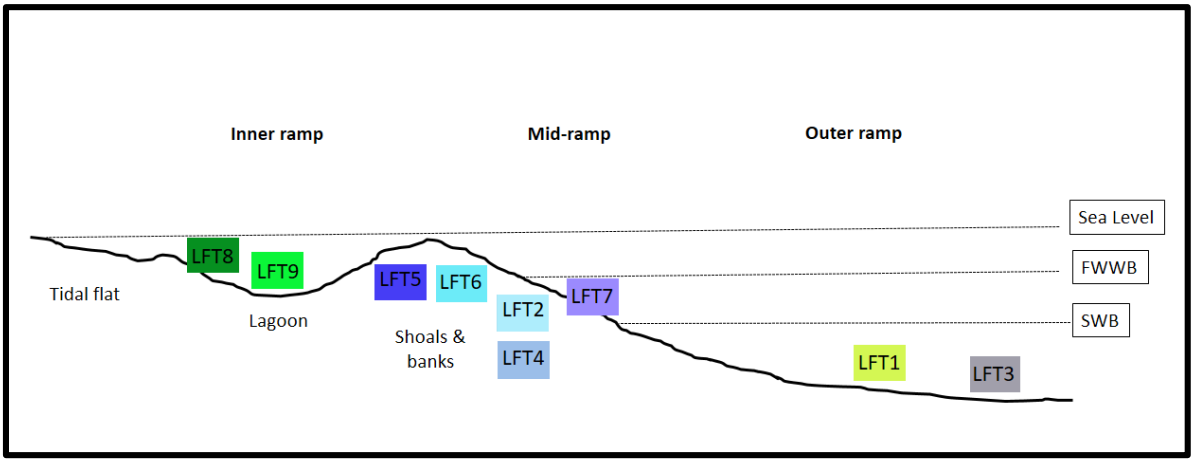


Figure 4.23: A simplified conceptual depositional model of the D5 and D6 Members showing the position of different lithofacies types on a carbonate ramp from outer to inner ramp.

## 4.4 Stratigraphic Analysis and Architecture

The stratigraphic analysis was based on identified lithofacies and been used along field observations to generate a high-resolution stratigraphic model of Dhruma carbonates in outcrops. The high-resolution outcrop photo mosaic (Figure 4.24) and colored 2D outcrop panel (Figure 4.25) was also established to assess the detailed analysis and capturing of the small cyclicity. However, the stratigraphic cycles of the lithofacies with different scales were documented to understand the architecture of the reservoir within the real inter-well spacing. The recognized cyclicity of the D5 and D6 Members ranges from small-scale to large-scale cycles (Figure 4.26 and Figure 4.28). The high-resolution outcrop photo mosaic shows the lateral continuity of strata for a distance of more than 600 meters without significant lateral facies change, and this represents a high resolution for the real inter- well spacing (Figure 4.24).

The detailed vertical stratigraphic analysis based on photo mosaic and identified lithofacies revealed around 53 cycle and cycle sets ($5^{th}$ to $6^{th}$ order) (Figure 4.26). The identified parasequences range in thickness from centimeters to six meters with an average of 1.5 meter. These parasequences are stacked to form four high-frequency sequences (HFSs) and generally show increase in thickness and overall shallowing upward $4^{th}$ to $5^{th}$ order high-resolution sequences. The high-frequency sequences range in thickness from one meter up to fourteen meters. The latter were grouped into a single depositional sequence of $3^{rd}$ order magnitude. The Jurassic maximum flooding surface 30 (MFS J30) was also captured, and it is located within the D5 Member, and it is compatible with that previously defined MFS J30 by Sharland et al. (2001) and Enay et al. (2009). It placed within a thick transgressive shale/ mudstone. The reservoir architecture shows that the muddy units were intensively

affected the vertical reservoir continuity of the reservoir units. The lower part of the vertical stratigraphic section assumed to be equivalent to the upper part of the D5 Member, while the upper part of studied section considered to be equivalent to the D6 Member. The latter contains the reservoir equivalent to Lower Fadhili reservoir. The stable isotope patterns of carbon and oxygen along the composite stratigraphic section are relatively depleted in transgressive dominated compared with that in regressive dominated part (Figure 5.6).

The lower Fadhili reservoir was studied by Al-Mojel, (2010) from the subsurface cores in Khurais field, Saudi Arabia. The average distance between these wells is 19.8 km. Detailed sedimentology and stratigraphic analysis were carried out to assess the reservoir continuity characterization and modeling. Five lithofacies types have been defined range from lower shoreface to lagoonal deposits in addition to other two lithofacies that do not genetically belongs to the Lower Fadhili reservoir. These are marginal marine shales and mud and oolitic-intraclast grainstone beach facies. The stratigraphic analysis revealed two composite sequences (LFC-1 and LFC-2), and both of them are composed of four high-frequency sequences. In the current study, the defined lithofacies of the D6 Member from the outcrop shows relatively similar component to that of the subsurface equivalent with different given names of the lithofacies. From lithofacies comparison between the outcrop analog and the subsurface, and it can be concluded that the studied outcrop section just includes lower part of the subsurface Lower Fadhili reservoir with two high-frequency sequences (HFS-3 and HFS-4). The other two high frequency (HFS-1 and HFS-2) sequences belong to the D5 Member (Figure 4.26). However, the highly cemented oolitic grainstone lithofacies which contains phreatic meteoric calcite cement are similar to that

of the subsurface, where the base of the Lower Fadhili reservoir composite sequence-1 overlies the subaerial exposure surface above this lithofacies.

In studied outcrop sections, the same oolitic grainstone lithofacies was found highly cemented by blocky calcite cement, which indicates meteoric phreatic diagenetic zone. The same zone also has unique characteristics $\delta^{18}O$ and $\delta^{13}C$ isotope patterns (Figure 5.6). An abrupt shift in $\delta^{18}O$ values with slight shift in $\delta^{13}C$ values were also observed within the thick amalgamated unit of oolitic grainstone. Both values have heavier composition and show enrichment above and along the shift level compared with that in the underlying intervals below the shift level (Figure 5.6), where lighter isotope composition could be noted. The abrupt shift in $\delta^{18}O$ values seem to be an indication of a subaerial exposure surface. Both features of meteoric phreatic blocky calcite cement with shift in $\delta^{18}O$ values indicate subaerial exposure surface just above the thick amalgamated unit of oolitic grainstone lithofacies. Similar isotope patterns were observed in Barbados diagenetic environment by (Allan and Matthews, 1982). However, porosity log along composite stratigraphic section of the D5 and D6 Members shows generally a positive correlation with $\delta^{18}O$ and $\delta^{13}C$ values. Moreover, porosity and permeability values are relatively high above the exposure surface. To sum up, along the 680 m lateral distance, there is no lateral lithofacies change been noted from the photomosaic and detailed field investigation from the outcrop sections.

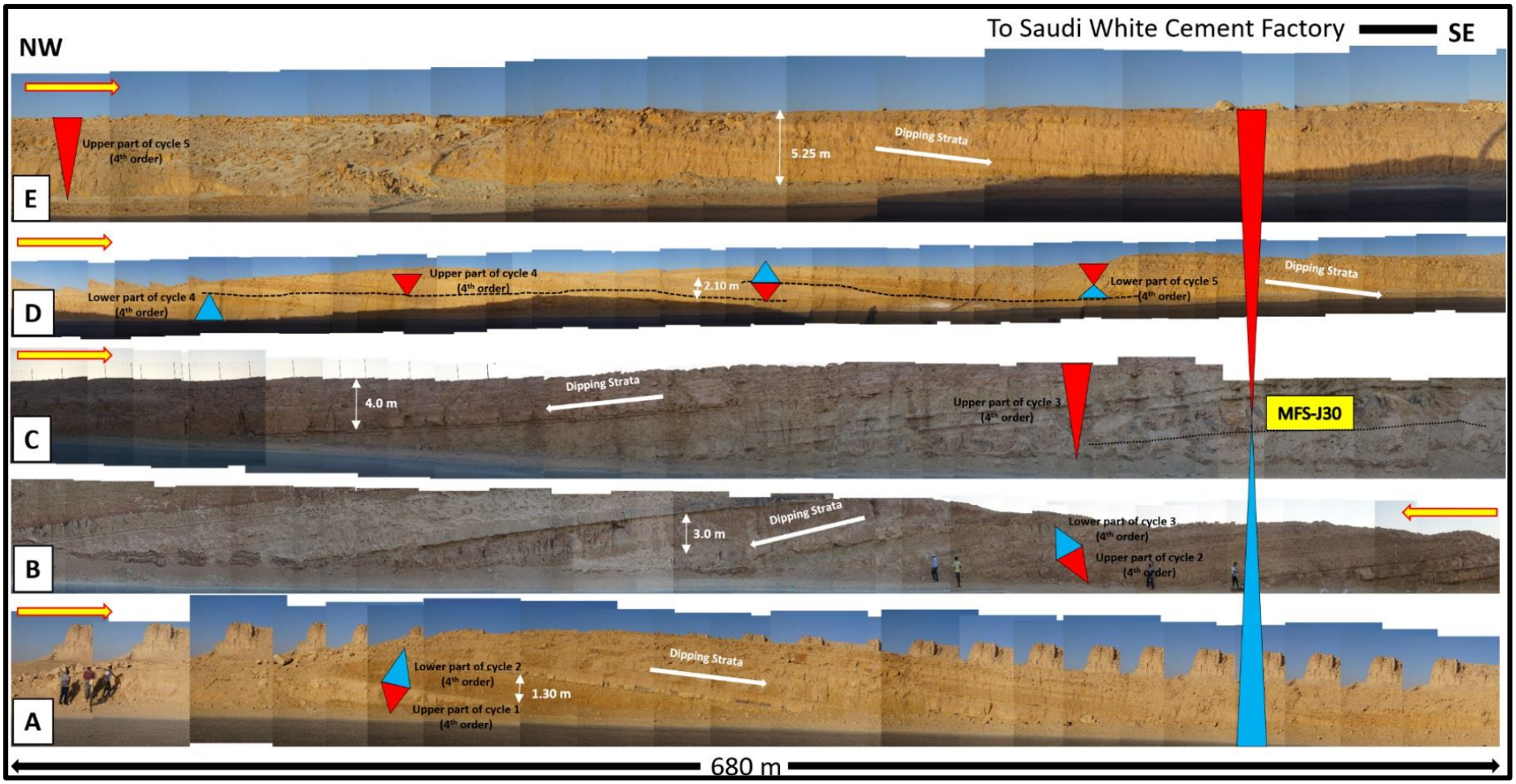


Figure 4.24: Outcrop photomosaic of the Middle Jurassic carbonates Dhruma Formation captured in a road-cut to Saudi White Cement Factory southwest of Riyadh city near Khashm Mi'dad area in central Saudi Arabia. Note that the different studied sections are dipping. From the nature of cyclicity and literatures, the studied sections belong to the D5 and D6 Members of Dhruma Formation. The lower Fadhili reservoir is located within the D6 Member.

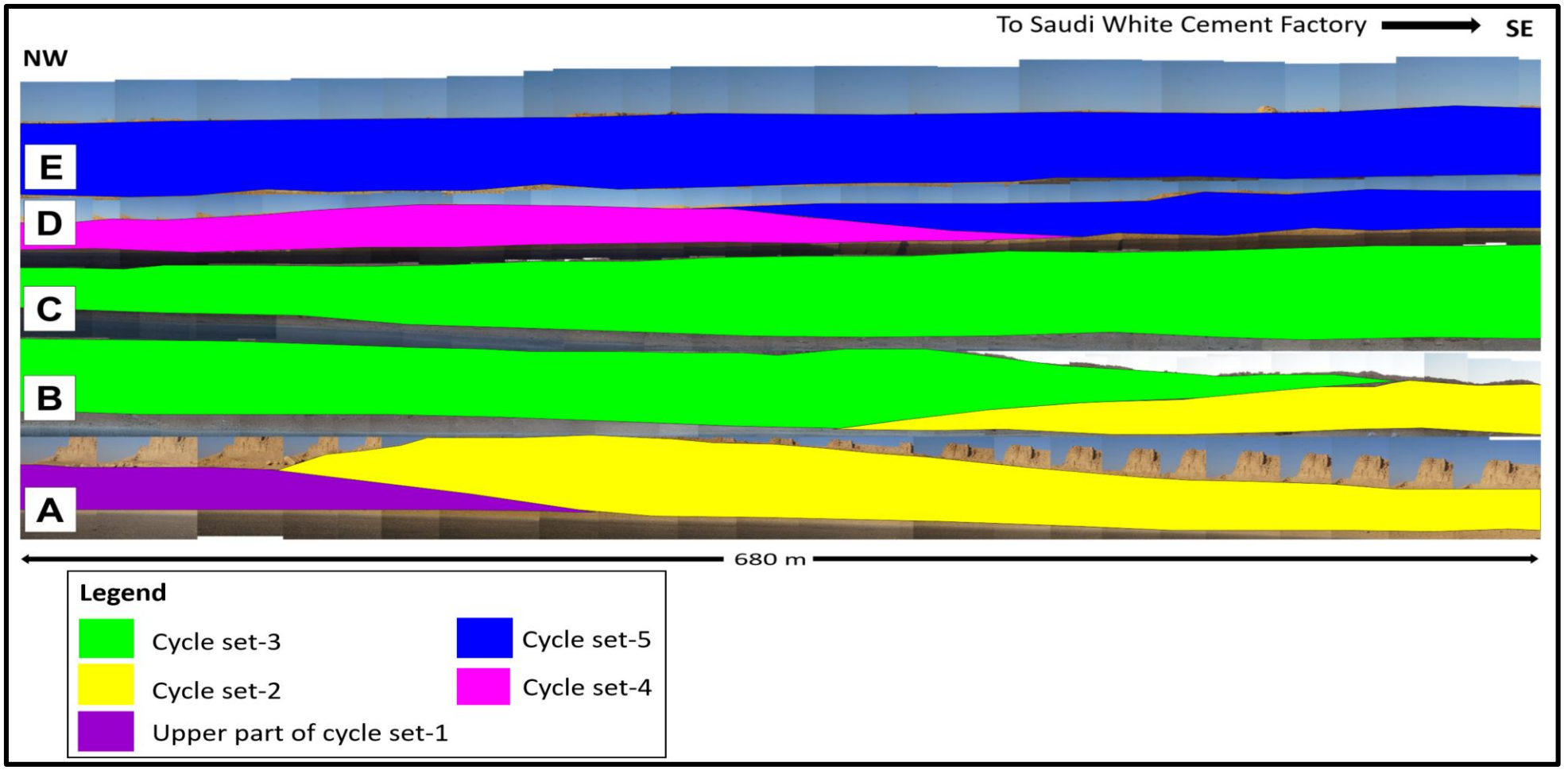


Figure 4.25: Colored 2D outcrop architectural panel of the D5 and D6 Members shows the stacking pattern of cycles set ($4^{th}$ order sequences) (A), (B), (C), (D) and (E) from north west to south east direction.

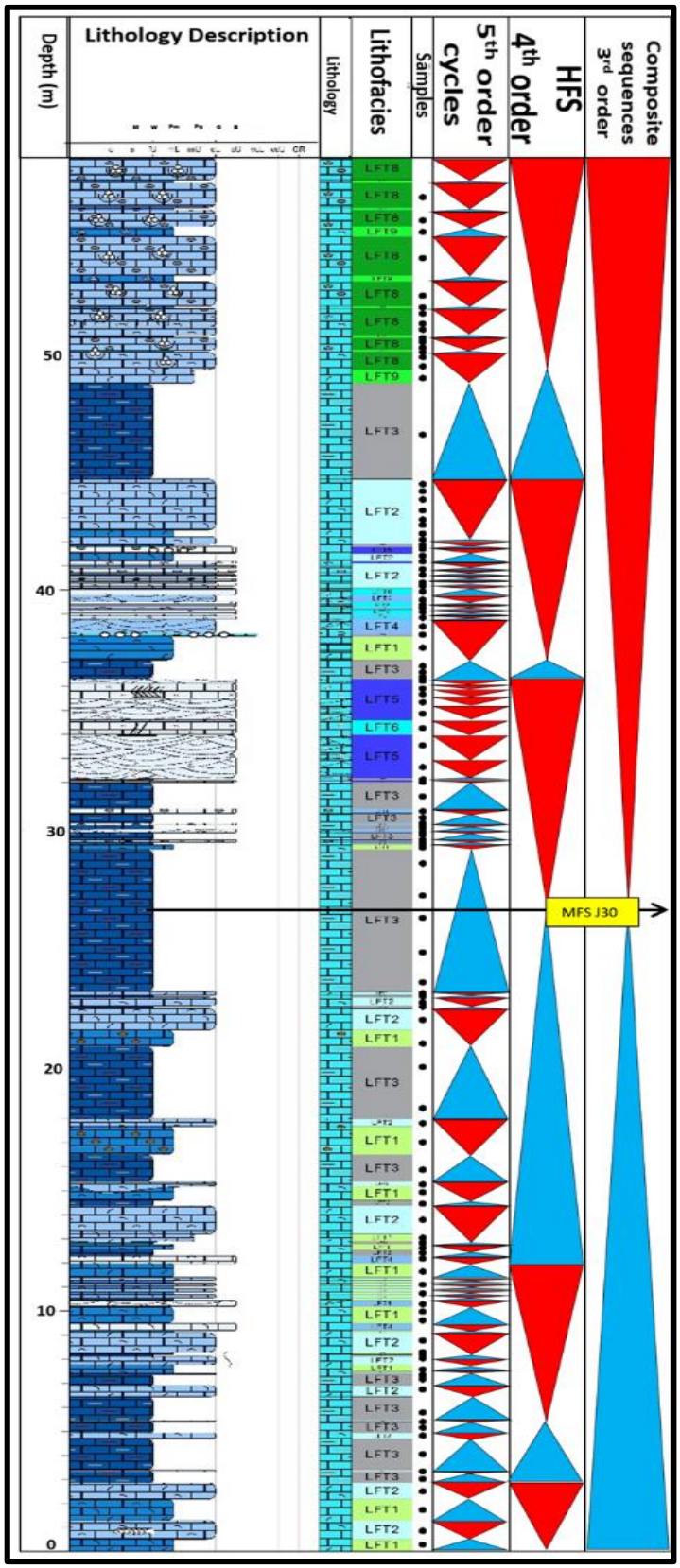


Figure 4.26: Composite lithostratigraphic section of the D5 and D6 Members of Jurassic carbonate Dhruma Formation southwest of Riyadh city near Khashm Mi'dad area in central Saudi Arabia. The defined lithofacies types and codes were indicated in the vertical stratigraphic section. For legend and terminologies see (Figure 4.27).

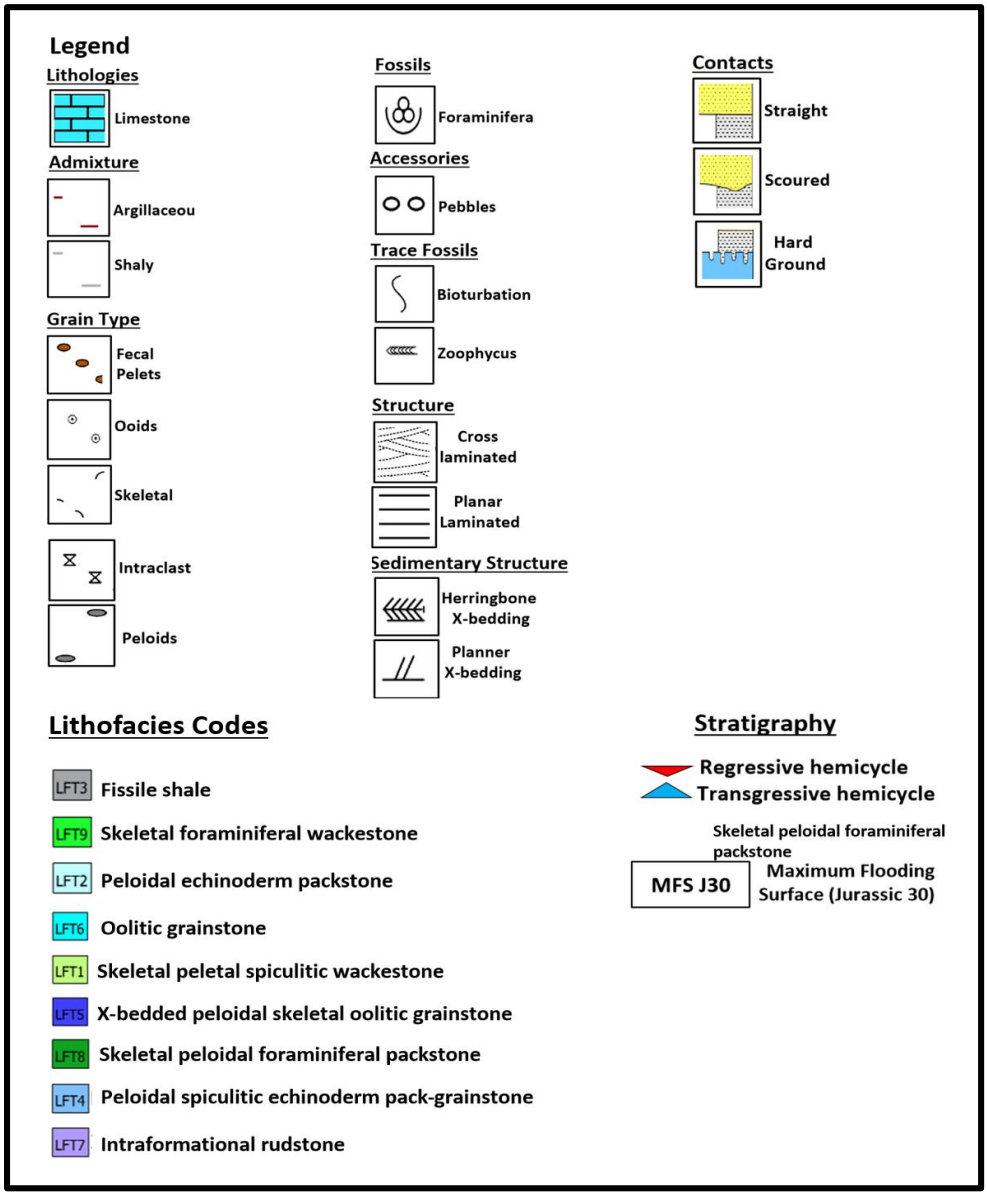


Figure 4.27: Legend shows the terminologies and symbols that were used in the composite vertical stratigraphic section of the D5 and D6 Members of carbonates Dhruma Formation in (Figure 4.26).

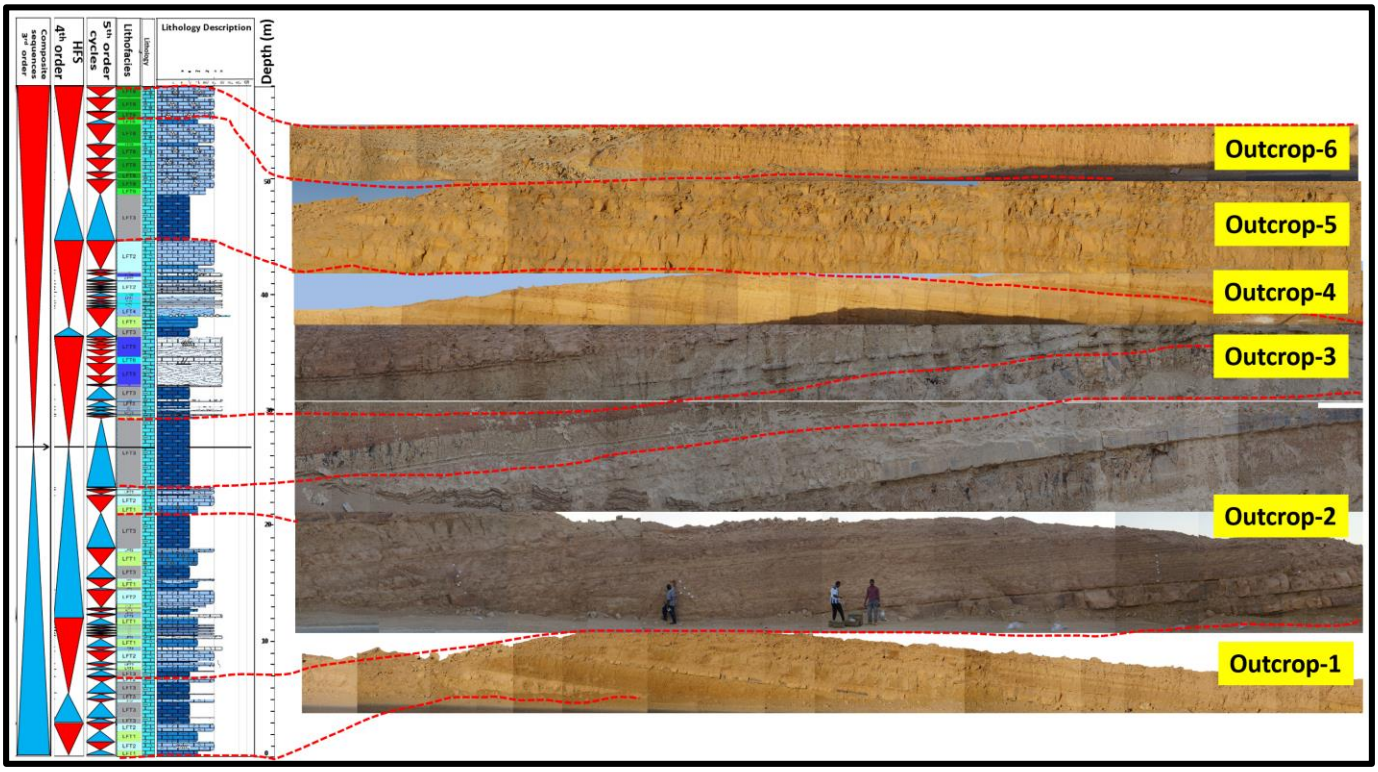


Figure 4.28: Outcrop photo mosaic and composite vertical stratigraphic section of the D5 and D6 Members of Jurassic carbonates Dhruma Formation in a road-cut to Saudi White Cement Factory southwest of Riyadh city near Khashm Mi'dad area in central Saudi Arabia. The lower portion of the succession has transgressive dominated nature, while the upper part is characterized by regressive dominated nature.

# CHAPTER 5

# RESERVOIR CHARACTERISTICS AND QUALITY

## 5.1 Introduction

The reservoir quality is an important part that must be studied in order to understand the storage, property distribution and fluid conduits within the reservoir. Porosity and permeability are the two main parameters utilized to assess the quality of the reservoir. Both parameters were obtained from cores or well logs. The quality of the reservoir is affected by primary depositional texture and later diagenetic alterations. The latter controls the pore geometry, packing and the orientation of the grain as well as the type and degree of cement that occupied the pore space. These subsurface heterogeneities can be traced and mapped using the 3D geostatistical modeling. The modeling of reservoir units has limitation related to insufficient data that are used to build the model. This limitation will not allow capturing small variations in reservoir properties (Eltom et al., 2013).

Diagenesis encompasses all processes that occurred naturally and cause changes in sediments. The process starts from the time of deposition, and they continue throughout compaction, lithification or consolidation and beyond and before the limit of metamorphism. The carbonate rocks are highly susceptible and affected by diagenesis compared to siliciclastic rocks, because of two major factors which are: their biological origin and high reactivity of carbonate minerals (Wilson, 1975; Moore and Wade, 2013).

The major diagenetic processes that influence the carbonates are; dissolution, cementation, compaction, micritization, neomorphism and dolomitization (Flügel, 2010). Here we are going to briefly discuss some of them related to the current study.

**Dissolution**: This process takes place by dissolution of two components: the grains and cement by fluids in under saturation condition. The process can be easily noticed in two main environments: meteoric and in deep burial environments (Longman, 1980; Moore and Wade, 2013). The mineral composition and chemistry of pore fluids control the dissolution intensity of carbonates either to be partially or complete dissolution.

**Cementation**: The mechanism of cementation encompasses all processes that lead to cement to be precipitated by over-saturated pore fluids. The cement occupied the primary and secondary pores. The volume of the pore fluids is also an important factor. However, with more pore fluids we are going to get intensive cementation (Longman, 1980; Moore and Wade, 2013). The cementation process can be noticed in the three diagenetic environments: meteoric, marine and deep burial environments and it has different types of cement as well as textures.

**Compaction:** The mechanism comprises both mechanical and/or chemical processes that take place as a result of the weight of the overburden deposits that causes a stress affect the underlain sediments. The distinctive features of this process can be observed by grain-to-grain contact since the compaction makes them closer to each other. The compaction can be noticed in shallow and deep burial diagenetic environments (Flügel, 2010).

**Micritization:** This process affects the carbonate grains either skeletal and non-skeletal grains, and the grains will be converted into fine-grained calcite. The micritization usually remove the internal grain structure. The micritization may be caused by the activity of

organism such as endolithic and fungi which drill inside the bioclasts. The micritic envelope developed during the early stage of the micritization, usually with the irregularity of internal surface. The internal structure of the bioclast can be completely micritized and lost by intensive micritization (Reid and Macintyre, 2000).

**Dolomitization:** This process takes place by the replacement of the original calcium carbonate ($CaCO_3$) by magnesium carbonate, and it can be partially or completely dolomitized by the action of Mg- carrying water (Flügel, 2010).

There are three different diagenetic environments that affect the petrophysical properties of the carbonate reservoirs which include: marine, meteoric, and burial diagenetic environments (Flügel, 2010). Each one of these environments has it is own distinctive features and processes.

The reservoir quality of the D5 and D6 Members of Dhruma Formation will be investigated from different aspects including the effect of primary depositional texture and later diagenetic alterations. The diagenetic features and environments will be highlighted and discussed briefly with their impacts on reservoir quality. Different techniques will be utilized in this study which include: Thin-section petrography, X-ray diffraction (XRD), scanning electron microscopy and stable isotope results of carbon and oxygen.

## 5.2 Impact on Reservoir Quality Evolution

The carbonate rocks are highly affected by post-depositional cementation and dissolution compared to siliciclastic rocks. These processes control the porosity evolution and permeability values of the reservoir. In this subsection, we are going to characterize the pore types of each lithofacies and the factors controlling the reservoir quality in carbonate Dhruma Formation in outcrops in central Saudi Arabia.

### 5.2.1 Pore-types

The carbonate rocks show a wide spectrum of different pore types Choquette and Pray (1970). The authors defined 15 basic types of porosity that can be found in the carbonate facies. Seven out of fifteen of these pore types are very common and they have significant volume, which include: interparticle, intraparticle, intercrystal, moldic, fenestral, fracture and vuggy porosities. The remaining types seem to be less abundant. The pore size and shape in carbonate rocks are affected by the skeletal grains of various organism assemblages. However, it is important in hydrocarbon exploration to characterize the pore types and what factors control the development of porosity. The well-known Choquette and Pray (1970) classification of porosity (Figure 5.1) will be followed to classify and identify different porosity types in the analyzed samples of Dhruma Formation carbonates. The Thin-section petrography and SEM images were used to achieve this purpose. The porosity types identified in studied samples include: fracture, intraparticle, moldic, intercrystalline porosities (Figure 5.2). The dominant pore types are fractures and intraparticle porosity. Furthermore, microporosity was also observed (Figure 5.2). The

moldic porosity and intraparticle porosity are the dominant ones in the uppermost part of the vertical composite stratigraphic section which is equivalent to Lower Fadhili reservoir in the subsurface.

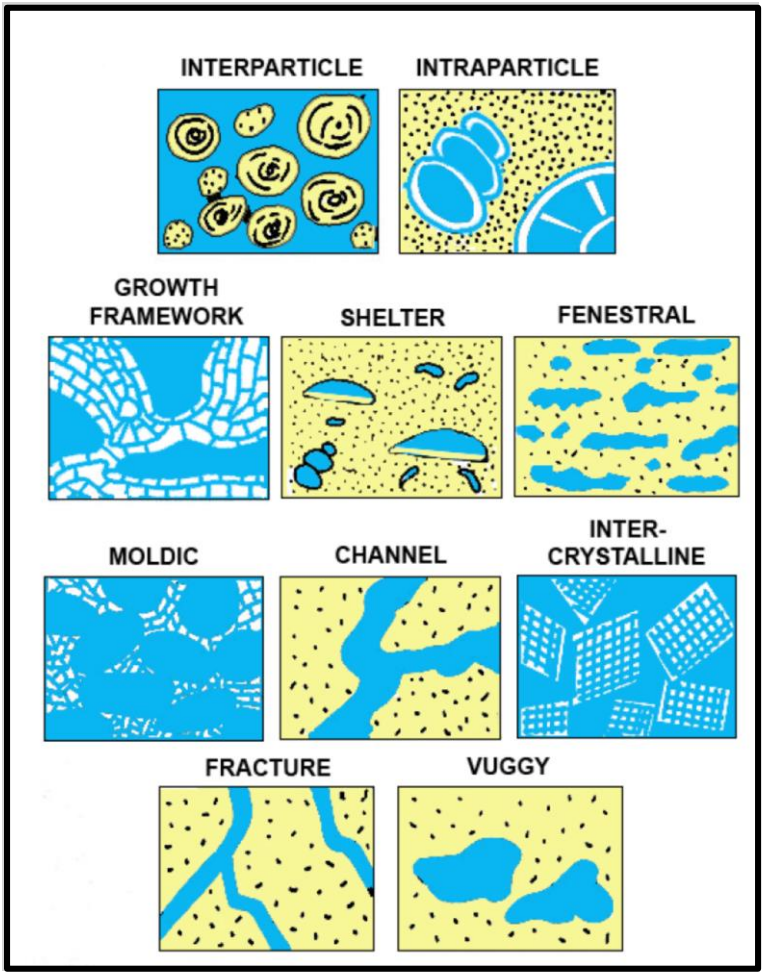


Figure 5.1: Carbonate pores classification. After Choquette & Pray (1970).

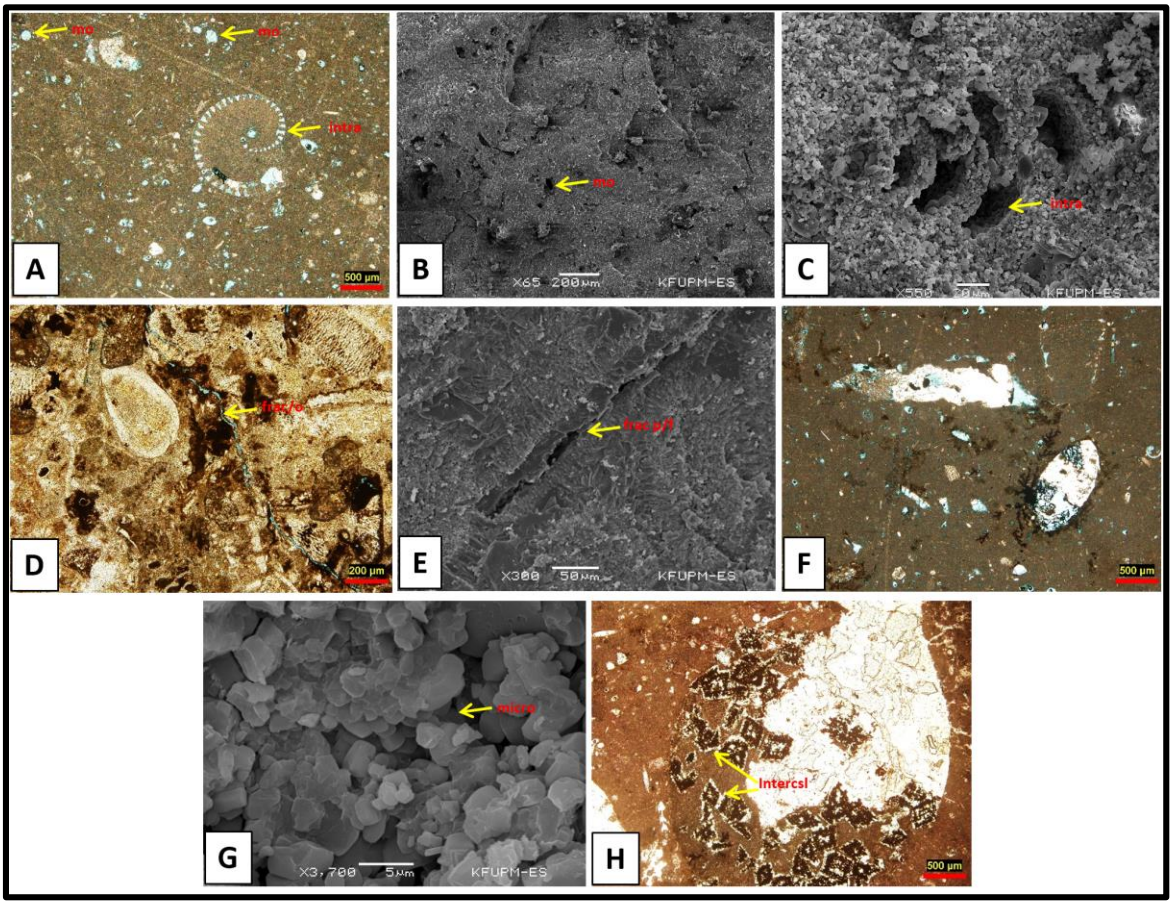


Figure 5.2: Different pore types were captured in identified lithofacies: (A) Thin-section photograph shows moldic (mo) and intraparticle porosity (intra), (B) SEM photograph shows abundant moldic porosity (mo), (C) SEM photograph shows the primary intraparticle porosity in biserial foraminifera, (D) Thin-section photograph shows the open fracture porosity (frac), (E) SEM photograph shows partially filled fracture porosity (frac p/f), (F) Thin-section photograph shows abundant moldic porosity, intraparticle, and microporosity. The microporosity appears in hazy blue color, (G) SEM photograph shows the microporosity which found in the upper most part of the studied section which equivalent to the Lower Fadhili reservoir in the subsurface, and (H) Thin-section photograph shows intercrystal porosity (intercsl) between the dolomite crystals. After dolomitization, dedolomitization took place and it has been observed in two intervals.

### 5.2.2 Diagenesis and its impacts on reservoir quality evolution

Different diagenetic features have been observed in the carbonate Dhruma Formation from thin-sections, scanning electron microscope, XRF and XRD analysis. The diagenetic processes influenced the reservoir quality in different ways either by enhancing or destroying the pore space. In this subsection, we are going briefly to discuss the effect of diagenetic alterations on porosity evolution. The carbon and oxygen isotope signatures were also used to understand the porosity evolution within the stratigraphic framework and to indicate stratigraphic surfaces (Figure 5.6).

**Micritization**

Micritization happens in the marine environment on the sea floor or just below it by the effect of an organism such as endolithic algae, fungi, and bacteria (Figure 5.3). These organisms are boring the grains, and then the grains been filled by fine grain sediments or cement and this leads to the formation of the micritic envelope. The micritic envelope will save the grain shape even if the grain is completely dissolved. Micritization is common in Dhruma Formation lithofacies (Figure 5.4).

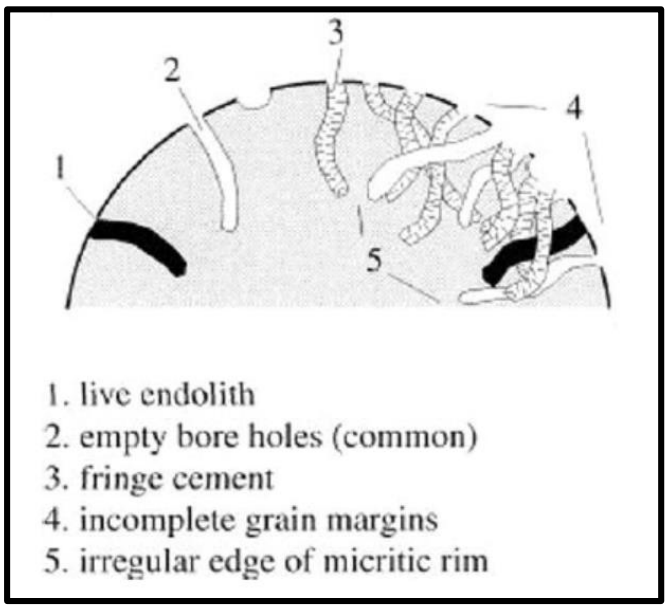


Figure 5.3: Micritization mechanism by endolithic organism which digging within the grain (modified from Reid & Macintyre, 2000).

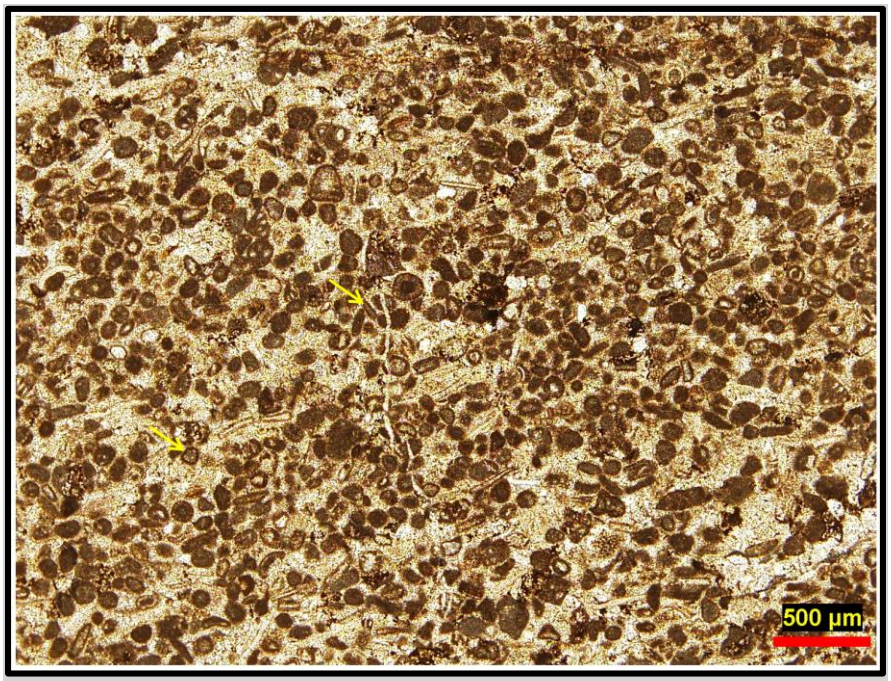


Figure 5.4: Thin section photograph showing a micritic envelope (yellow arrows) in the oolitic grainstone lithofacies (LFT5).

**Cementation**

The cementation defined as filling of the open pore either primary or secondary minerals by the precipitation of the new materials. This process can destroy or save the porosity from compaction due to burial by cementation in the earlier stages, then the dissolution of the cement allows the development of secondary porosity. In some intervals, the blocky calcite or complete pore filling equant calcite fabric was observed. It has finer texture near the grains and become coarser between the grains themselves. This blocky calcite is low magnesium calcite and characterizes the meteoric phreatic diagenetic zone (Figure 5.5 A and B). The porosity log of the thick amalgamated unit of oolitic grainstone and peloidal skeletal oolitic grainstone show significant negative deflection of $\delta\,^{18}O$ and $\delta\,^{13}C$ isotope patterns (Figure 5.6). This zone is highly calcite cemented. However, it can be observed that in the upper most part of this unit relatively high porosity values been recorded and become low with increasing depth.

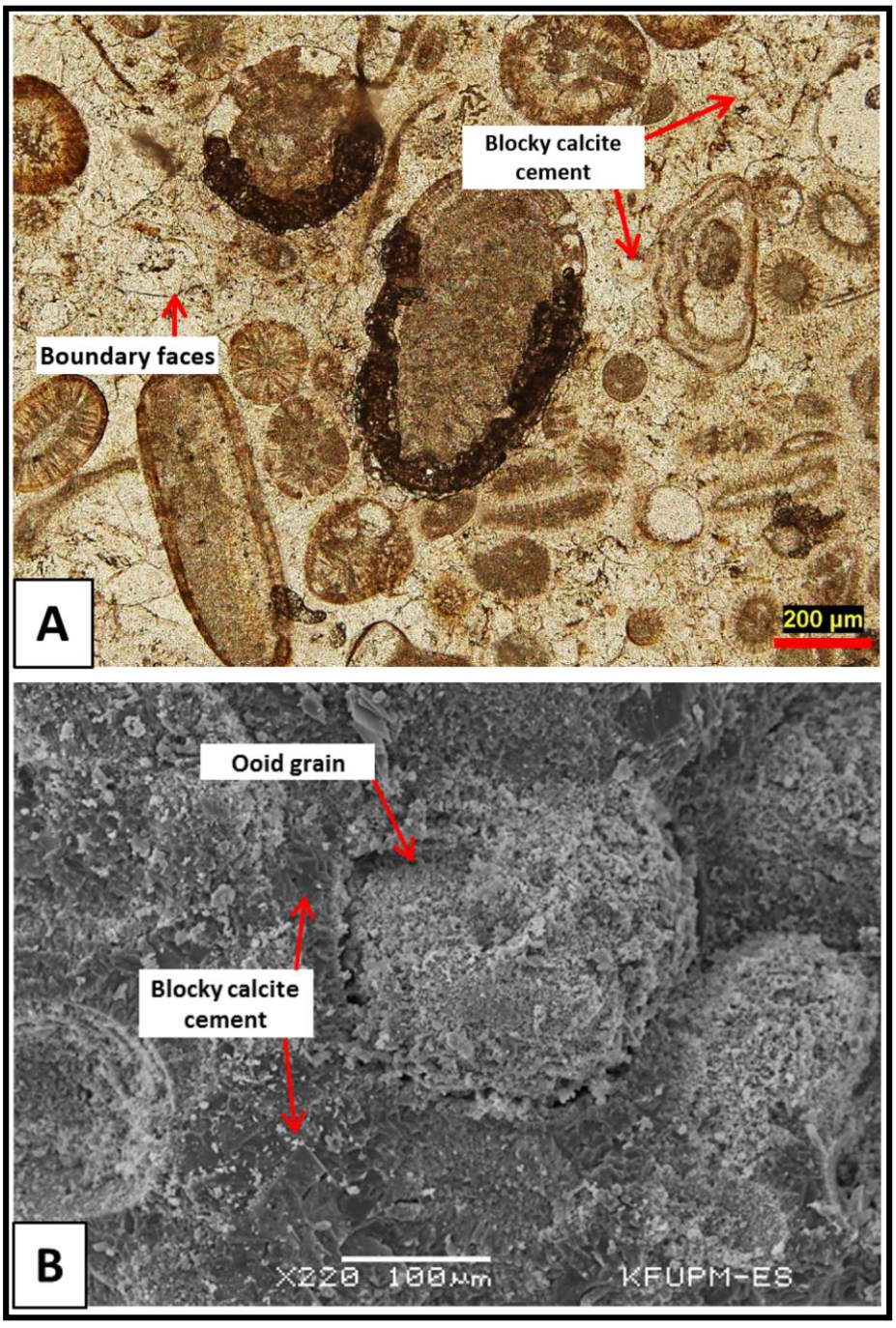


Figure 5.5: (A) Thin section photograph showing the meteoric phreatic blocky calcite with distinctive boundary faces between the crystals and (B) SEM photograph for the same cement fabric. It is totally filled and block the interparticle pores.

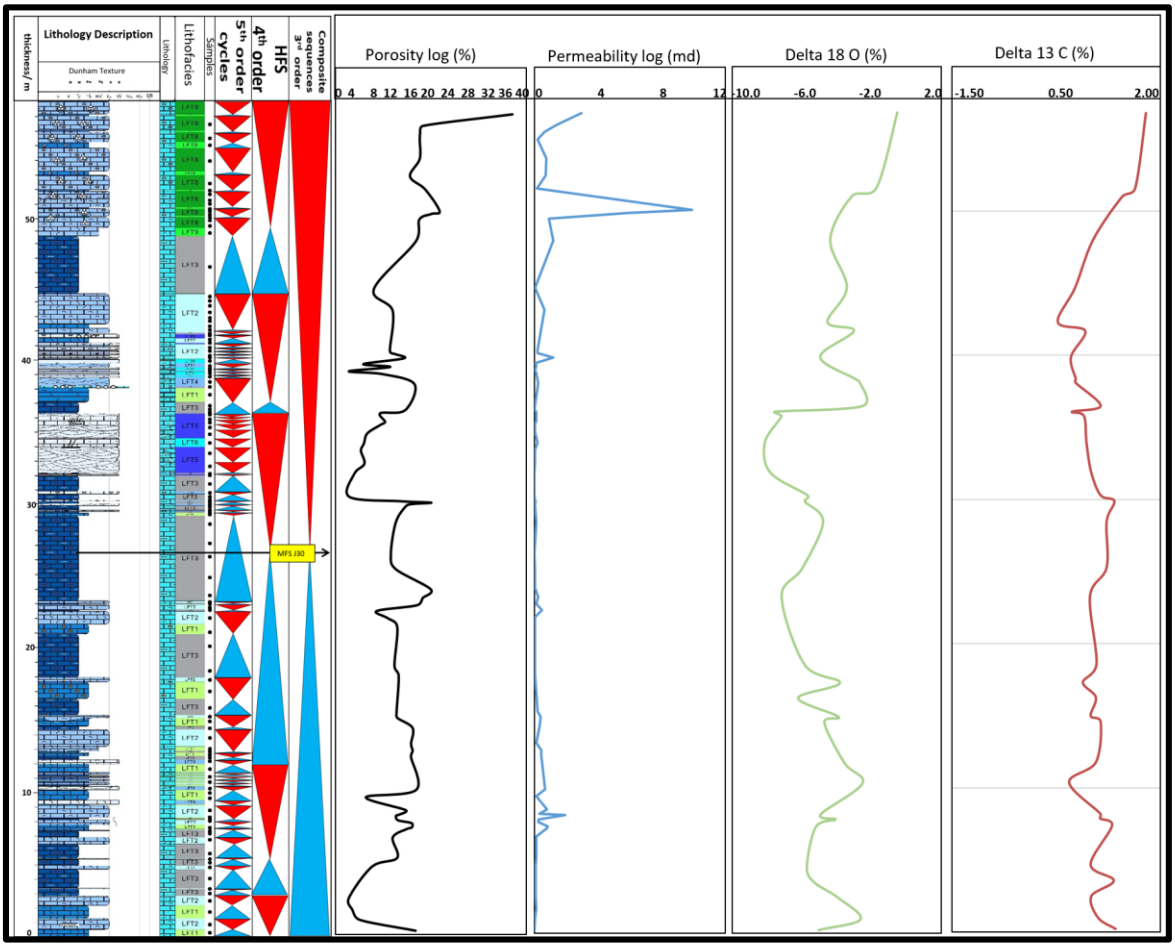


Figure 5.6: Porosity and permeability logs of the D5 and D6 Members and related carbon and oxygen isotope patterns. It can be clearly noticed that the variability in porosity profile along vertical stratigraphic section generally shows a positive correlation with carbon and oxygen ratios. However, the transgressive part is dominated by heavier isotope composition compared with regresive dominated part.

**Dissolution**

The dissolution occurs by under-saturated water with respect to carbonate grains. The dissolution will dissolve the unstable carbonate minerals. In Dhruma Formation in some intervals it can be observed that intensive dissolution by meteoric water leads to the formation of abundant moldic porosity (Figure 5.7). Here the porosity was significantly enhanced, and porosity and permeability readings are relatively higher in these intervals. This zone of meteoric dissolution also showed enrichment in carbon and oxygen isotope ratios (Figure 5.6).


Figure 5.7: Abundant moldic porosity developed as result of intensive meteoric dissolution.

**Dolomitization/ Dedolomitization**

Dolomitization is the process that converts limestone or calcium carbonate either partially or completely into dolomite by solution contains magnesium carbonate (Flügel, 2010). The opposite process is known as dedolomitization (Evamy, 1967). Dedolomitization is the partial or complete transformation of dolomite rocks to limestones or dolomite to calcite which involves each crystal. This transformation process includes two main stages; neomorphic replacement of dolomite by calcite, then the dolomite will be dissolved and followed by calcite cementation (Middleton, 2003). Evamy, 1967 proposed a model of the dedolomitization followed dolomitization. The model shows that dolomitization followed by dedolomitization and then by selective leaching takes place and the later end with calcite cementation (Figure 5.8). The variability in porosity related to dedolomitization is changeable and it is difficult to interpret. A similar pattern has been observed and documented in this study of the D5 and D6 Members of carbonate Dhruma Formation in certain intervals (Figure 5.9 A and B), and the dolomite rhombohedron and rhombohedral pores are very clear. As result of replacement of iron by calcium, iron oxides/ iron hydroxides have been formed and covered the dolomite crystals which converted into calcite by dedolomitization process. We proposed that two types of dolomite are exist before dedolomitization took place. XRD analysis showed no dolomite at all with dominant calcite and little quartz content (Figure 5.10). However, the XRF analysis shows little Magnesium (Figure 5.11). Traces of quartz in XRD result may suggest possible siliciclastic input. Just above this zone of the dolomitization/ dedolomitization, anhydrite mineral was observed in thin-sections (Figure 5.12), and this may suggest the sabkha-evaporative dolomitization model of the D5 and D6 Members of Dhruma Formation (Figure 5.13).

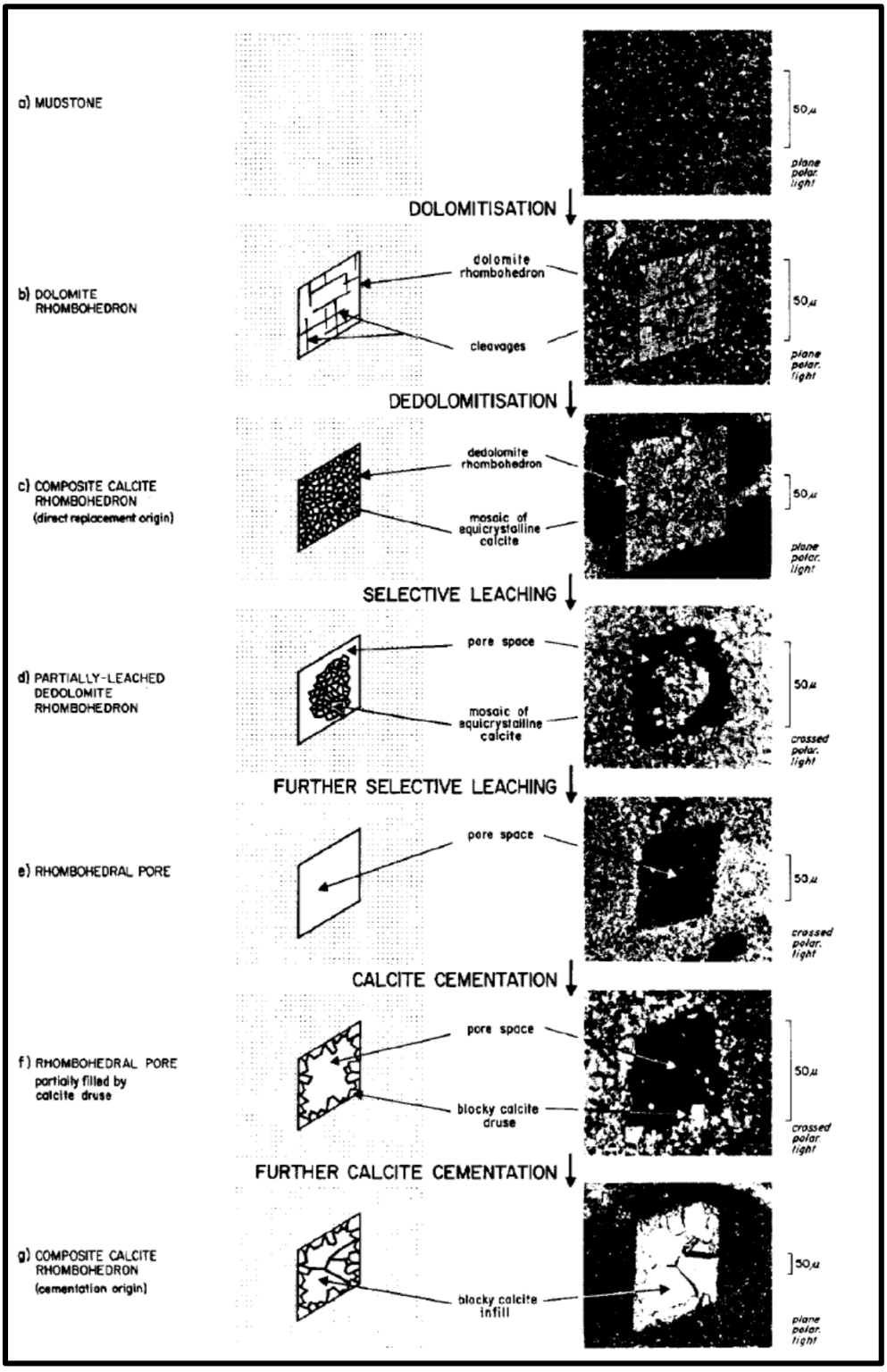


Figure 5.8: A proposed schematic diagenetic history of particular limestone been subjected to dedolomitization (Evamy, 1967).

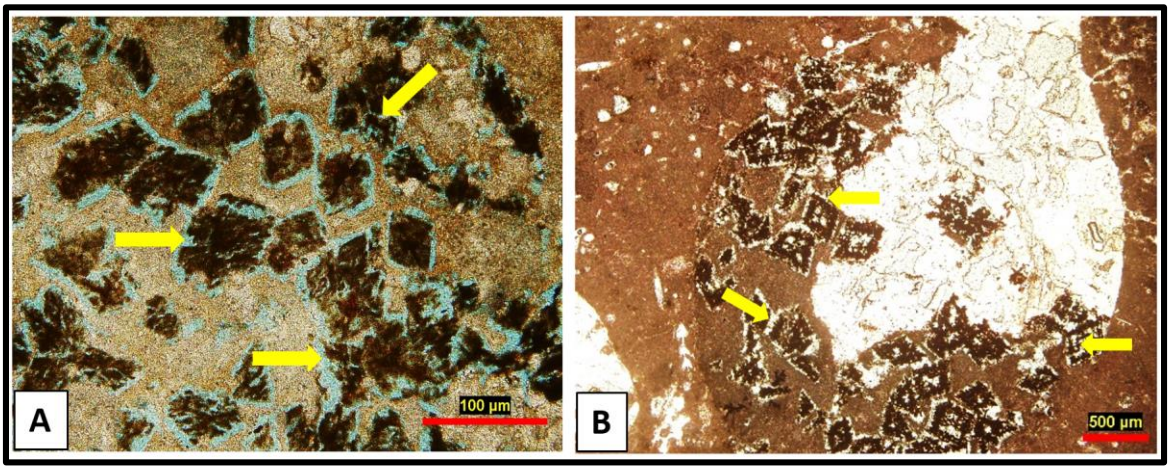


Figure 5.9: (A) and (B) Dolomitization followed by dedolomitization in certain intervals of D5 and D6 Members of Middle Jurassic Dhruma Formation in central Saudi Arabia.

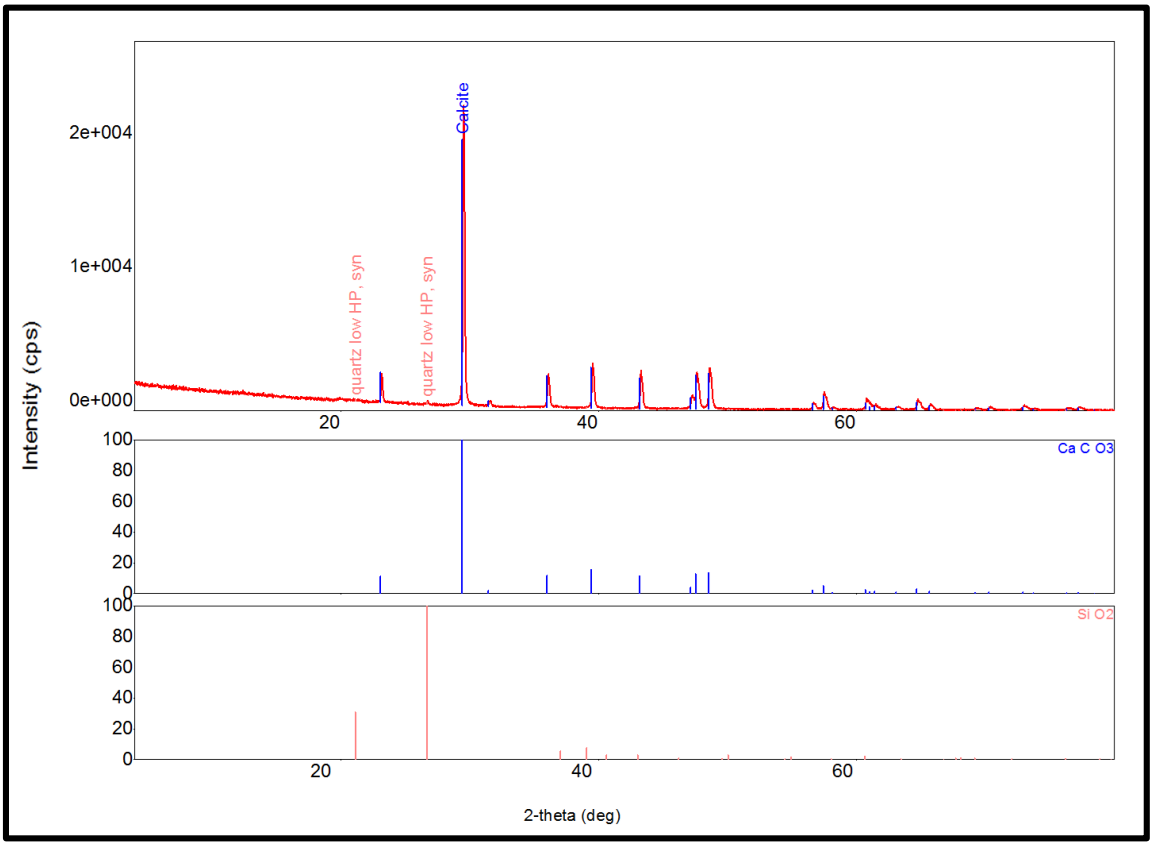


Figure 5.10: XRD data shows the dominant calcite minerals and minor quartz. No dolomite was found. Traces of quartz may suggest possible siliclastic input.

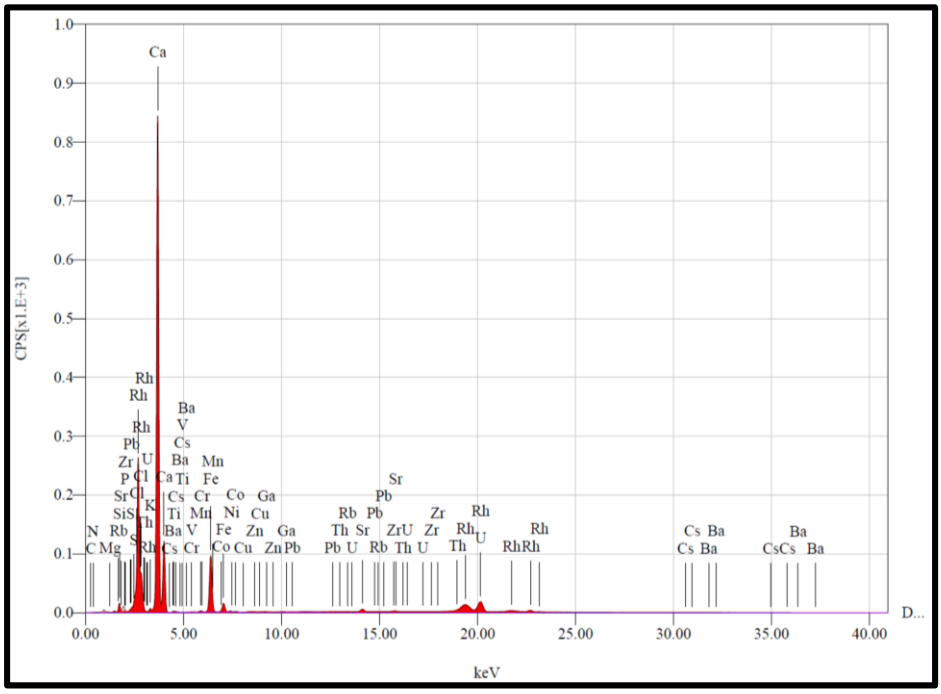


Figure 5.11: XRF data showing the distribution of elements with traces of Magnesium.

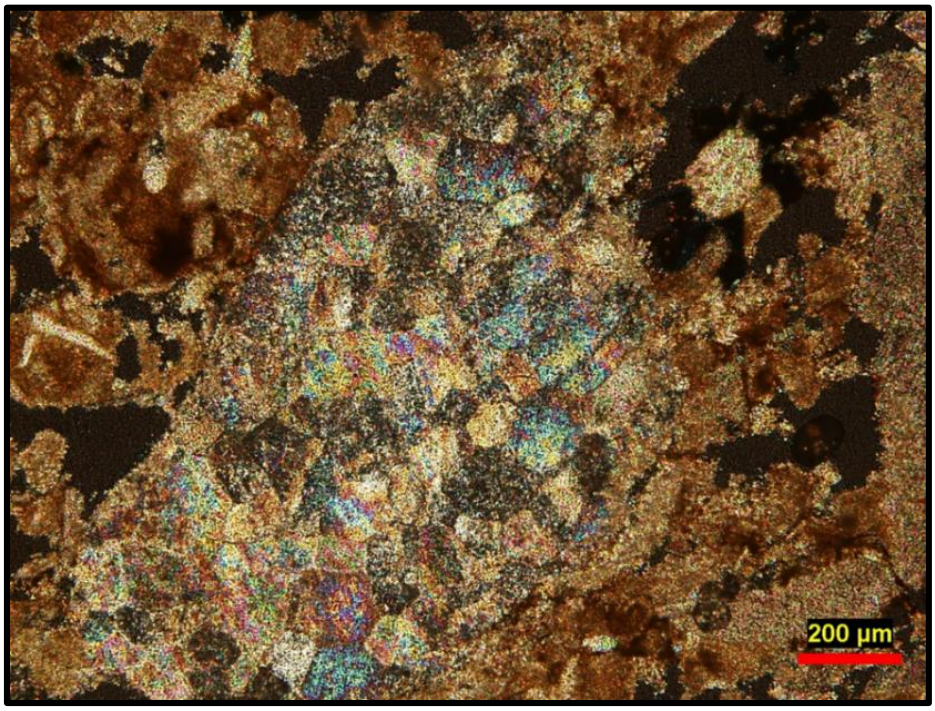


Figure 5.12: Anhydrite mineral with high interference color captured just above the zone of dolomitization/ dedolomitization.

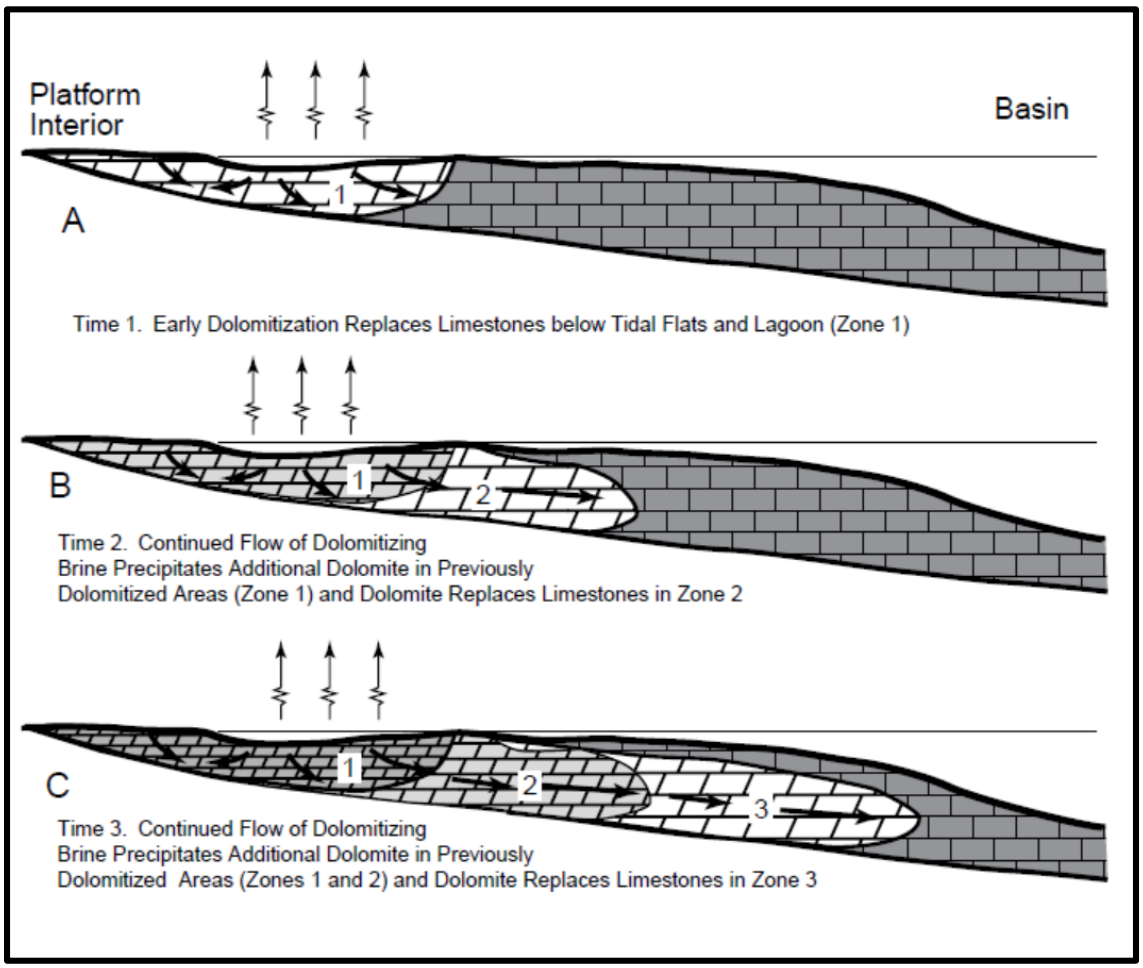


Figure 5.13: A proposed dolomitization model (sabkha-evaporative model) for the D5 and D6 Members of Dhruma Formation (from Saller and Henderson, 2001). The dolomitization was followed by dedolomitization.

**Burial diagenesis**

The burial diagenesis includes many processes: cementation, compaction, pressure dissolution as well as fracturing. In studied intervals of carbonate Jurassic Dhruma Formation different burial diagenesis features were observed which includes (Figure 5.14):

- Fracturing of the grains itself
- Grains with concavo-convex contacts
- Pressure dissolution which indicated by stylolite in the outcrop.

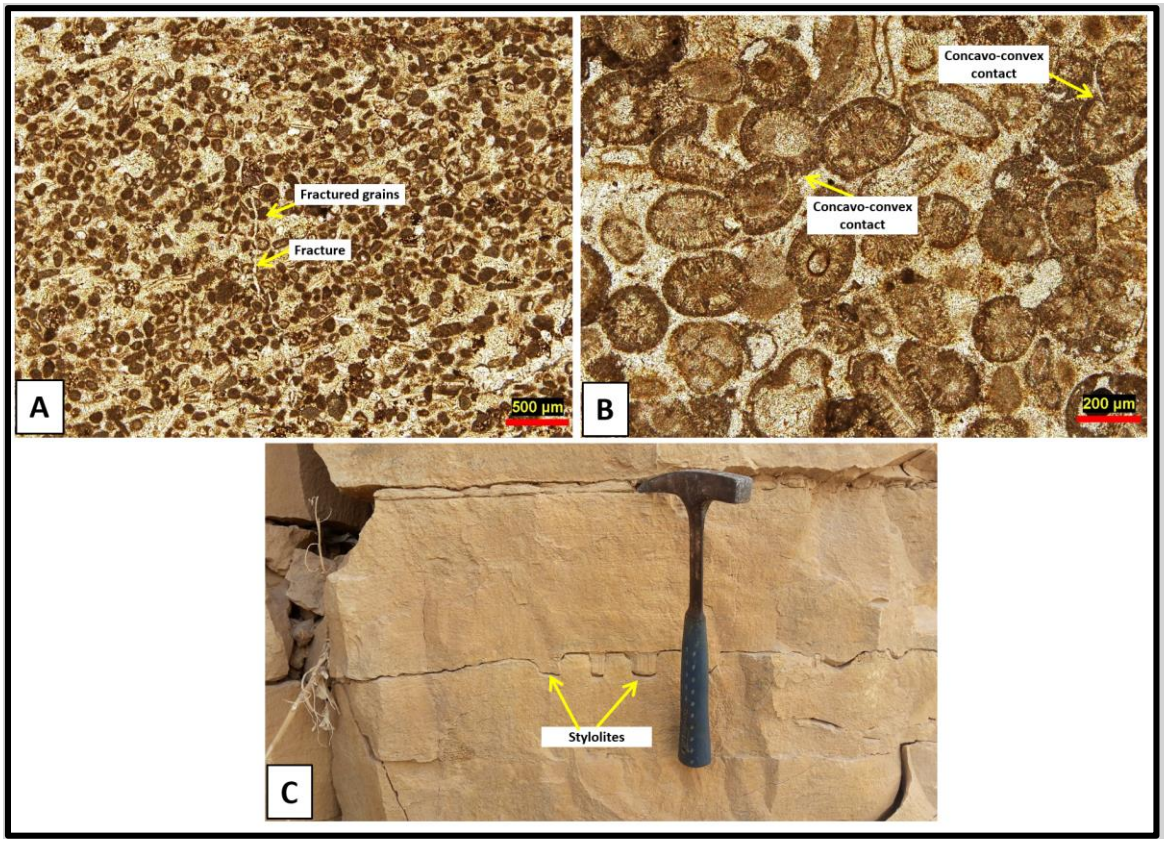


Figure 5.14: Burial diagentic features: (A) Thin section photograph shows the fracturing of the grains, (B) Thin-section photograph shows the concavo-convex contact between the grains and (C) outcrop photograph shows well-developed stylolite with different amgnitude.

## 5.3 Petrophysical characteristics and reservoir heterogeneity of Dhruma Formation (D5 and D6 Members)

Before analyzing and determining the different factors affect the reservoir quality it is important to characterize the petrophysical attributes. The univariate and bivariate statistics were utilized with considerations of many geological aspects such as rock texture, lithofacies types, diagenesis and sequence stratigraphic framework. The porosity and permeability were analyzed from core plugs that obtained from outcrop samples of the carbonates D5 and D6 Members of Dhruma Formation. Generally, porosity has non-normal distribution and negatively skewed (Figure 5.15) with mean of 13.0, and standard deviation of 5.6 (Table 5.1). The permeability also has non-normal distribution and positively skewed (Figure 5.16) with mean value of 0.54 and standard deviation of 1.4.

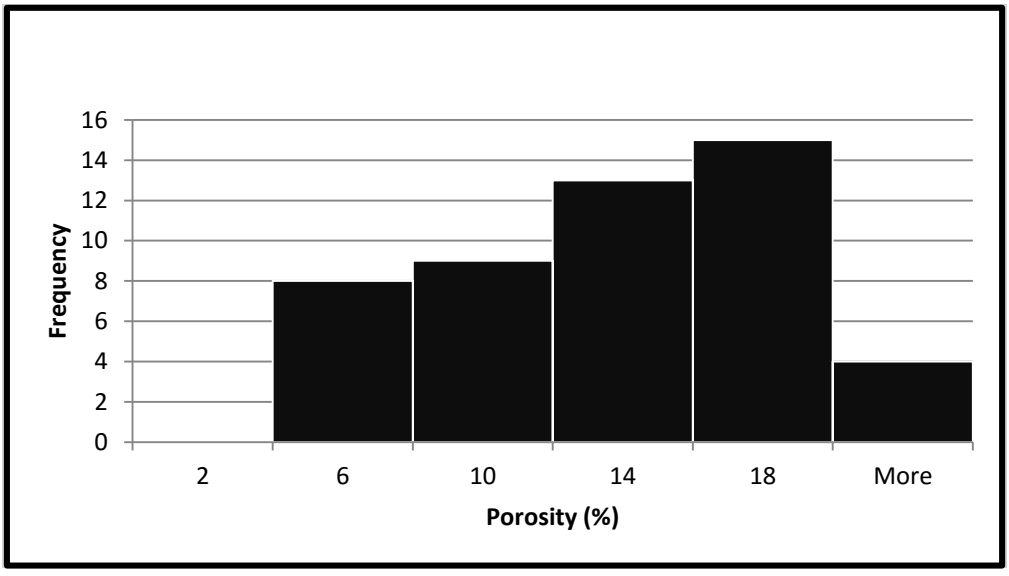


Figure 5.15: Histogram of porosity distribution. It is clearly negatively skewed.

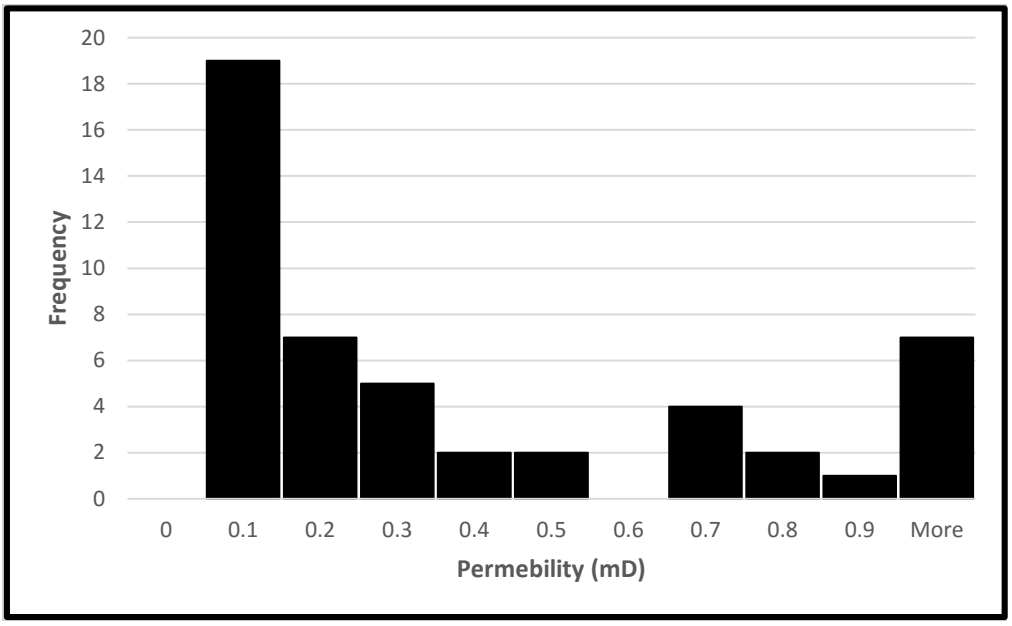


Figure 5.16: Histogram of permeability distribution. It is clearly positively skewed.

Table 5.1: Selected univariate statistics of porosity and permeability measurements.

| **Univariate Statistics** | **Porosity (%)** | **Permeability (mD)** |
|---|---|---|
| Mean | 13.05189121 | 0.546464706 |
| Median | 13.00480853 | 0.1159 |
| Mode | 12.59683978 | 0.0005 |
| Standard Deviation | 5.594085829 | 1.420806886 |
| Kurtosis | 3.84161179 | 30.66522362 |
| Skewness | 0.783028085 | 5.239594773 |
| Minimum | 2.786083252 | 0.0005 |
| Maximum | 37.04028195 | 9.8817 |

The statistical analysis of different lithofacies of the D5 and D6 Members show that the relatively high porosity and permeability readings are associated with two lithofacies: skeletal peloidal foraminiferal packstone (LFT8) and skeletal foraminiferal wackestone (LFT9) (Table 5.2 and Table 5.3). Both lithofacies are lagoonal with muddy-grainy and mud-dominated textures respectively. The reason of that is due to intensive meteoric dissolution which creates abundant moldic porosity. The peloidal echinoderm packstone (LFT2) shows scattered pattern of these two variables, because of the effect of calcite cementation and primary depositional texture (Figure 5.17). However, porosity and permeability values in the oolitic grainy lithofacies (LFT5 and LFT6) are significantly low due to intensive meteoric calcite cementation, which blocked most of the original pore space, and this, in turn, destroyed porosity. The correlation between porosity and permeability is quite poor with a correlation coefficient ($R^2$) of 0.2176 and reflects the variabilities in reservoir rock units (Figure 5.18). These variabilities may have attributed to the combined effect of primary depositional texture and diagenetic over print. The comparison between Arab-D carbonates reservoir in Uthmaniyah field, Saudi Arabia, and Dhruma Formation in outcrops (D5 and D6 Members) shows different pattern of these two variables for different lithofacies textures (muddy, muddy-grainy and grainy). Generally, in Arab-D reservoir the pattern of distribution of porosity and permeability are consistent with a correlation coefficient of 0.837, while in Dhruma carbonates it shows different distribution. In Arab-D, the porosity ranges from almost 19% up to 30%. The granular lithofacies in Dhruma carbonates have very low porosity and permeability values compared with that in Arab-D reservoir, and this is due to intensive meteoric calcite cementation, which blocked most of the original pore spaces. The granular lithofacies of Dhruma are

located within the same field of muddy lithofacies, and the cause of that is intensive phreatic meteoric calcite cementation. However, all recognized lithofacies of Dhruma carbonates are located within the muddy field of Arab-D reservoir. In the Arab-D, high porosity and permeability distribution patterns are lithologically controlled. The muddy and muddy granular facies in both Arab-D and Dhruma show a wide range of distribution, and part of the muddy and muddy-granular lithofacies in Dhruma Formation show relatively good reservoir quality as a result of diagenetic effects such as dolomitization/ dedolomitization and intensive meteoric dissolution (Figure 5.19). Furthermore, the muddy and muddy-granular textures have low pore spaces which prevent to some extend the solutions contain calcite to be precipitated in pore spaces. The porosity distribution analysis of the Upper Khartam Member of Khuff Formation in outcrops in the central Saudi Arabia by Bukhari, 2016 shows that the grainy texture lithofacies relatively heterogeneous with a coefficient of variation of 0.66 compared with D5 and D6 Members, which have a coefficient of variation of 0.56. The muddy-grainy texture lithofacies in Upper Khartam Member shows high heterogeneous nature with Cv of 0.72 compared with D5 and D6 Members with Cv of 0.45. However, the reservoir quality of Khartam and Dhruma carbonates are both lithologically and diagenetically controlled.

Table 5.2: Statistical comparison for the identified lithofacies. The lagoonal lithofacies (LFT8 and LFT9) relatively have highest porosity values among the other lithofacies types.

| Lithofacies | Porosity (%) | | |
|---|---|---|---|
| | **Average** | **Max** | **Min** |
| **LFT1** | 13.9 | 16.88 | 3.55 |
| **LFT2** | 11.77 | 18.276 | 2.786 |
| **LFT3** | 14.1 | 19.933 | 11.5968 |
| **LFT4** | 11.49 | 20.05 | 2.933 |
| **LFT5** | 7.44 | 10.4 | 3.9567 |
| **LFT6** | 8.14 | 14.36 | 2.8141 |
| **LFT7** | 16.56 | 16.56 | 16.56 |
| **LFT8** | 20.739 | 37.04 | 15.59 |
| **LFT9** | 17.447 | 21.798 | 16.829 |

Table 5.3: Statistical comparison for the identified lithofacies. The lagoonal lithofacies (LFT8 and LFT9) relatively have highest permeability values among the other lithofacies types.

| Lithofacies | Permeability (mD) | | |
|---|---|---|---|
| | **Average** | **Max** | **Min** |
| **LFT1** | 0.226 | 0.647 | 0.0005 |
| **LFT2** | 0.3305 | 1.9046 | 0.0302 |
| **LFT3** | 0.1101 | 0.7909 | 0.0005 |
| **LFT4** | 0.039 | 0.0711 | 0.0084 |
| **LFT5** | 0.0499 | 0.1146 | 0.0081 |
| **LFT6** | 0.243 | 1.1823 | 0.0184 |
| **LFT7** | 0.2181 | 0.2181 | 0.2181 |
| **LFT8** | 1.7698 | 5.8719 | 0.1517 |
| **LFT9** | 3.0392 | 9.8817 | 0.2025 |

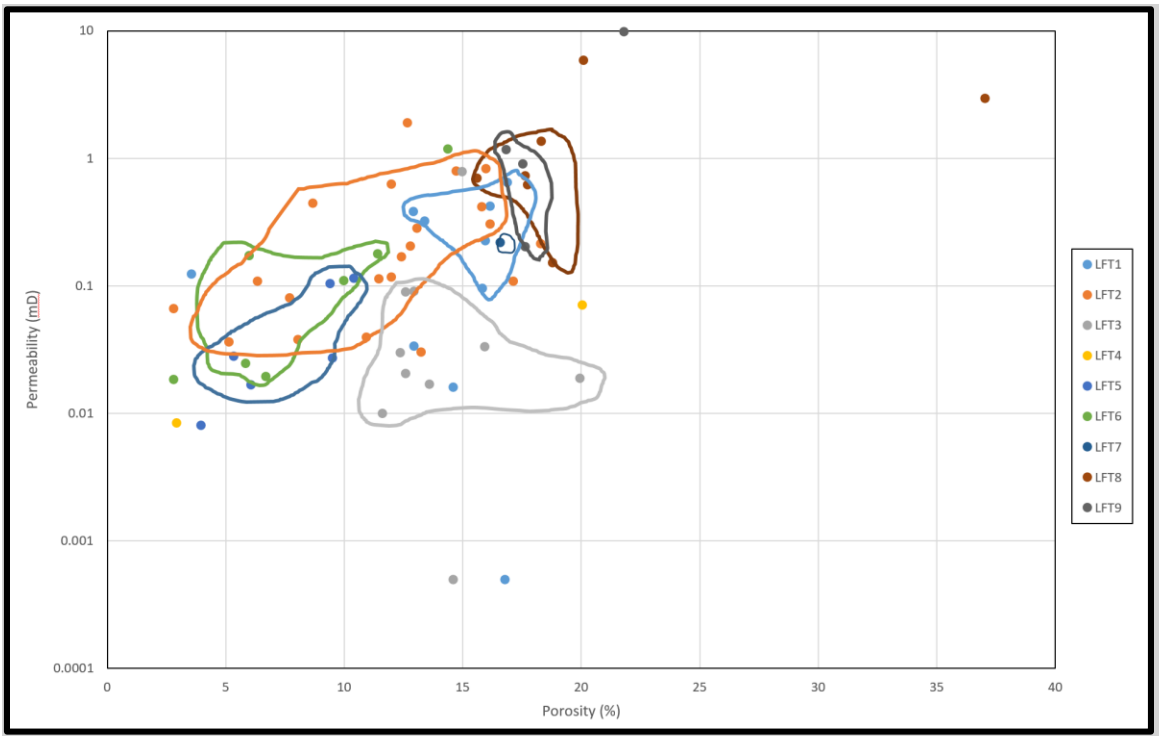


Figure 5.17: Cross –plot between porosity and permeability for the identified lithofacies of the D5 and D6 Members of Dhruma Formation. The plot showing that the lagoonal lithofacies of skeletal peloidal foraminiferal packstone and skeletal foraminiferal wackestone (LFT8 and LFT9) having higher porosity and permeability readings compared to that of shoals lithofacies types which include: cross-bedded peloidal skeletal oolitic grainstone and oolitic grainstone (LFT5 and LFT6).

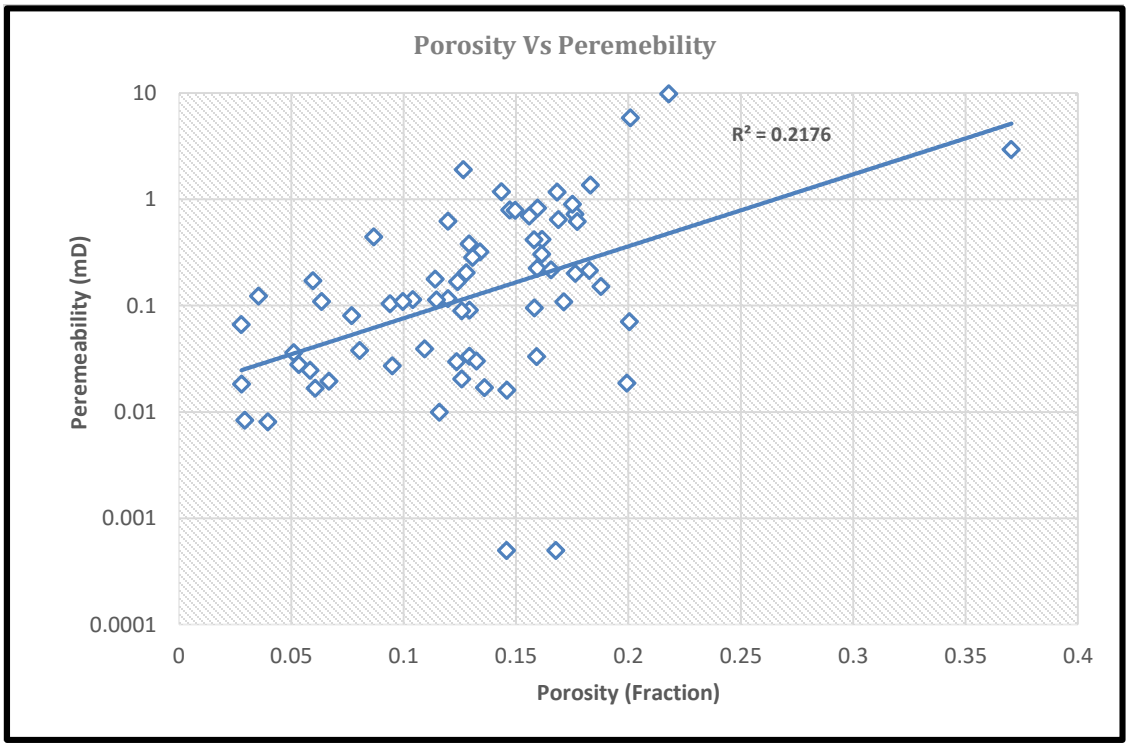


Figure 5.18: Cross- plot between porosity and permeability for the D5 and D6 Members of Dhruma carbonates in outcrop.

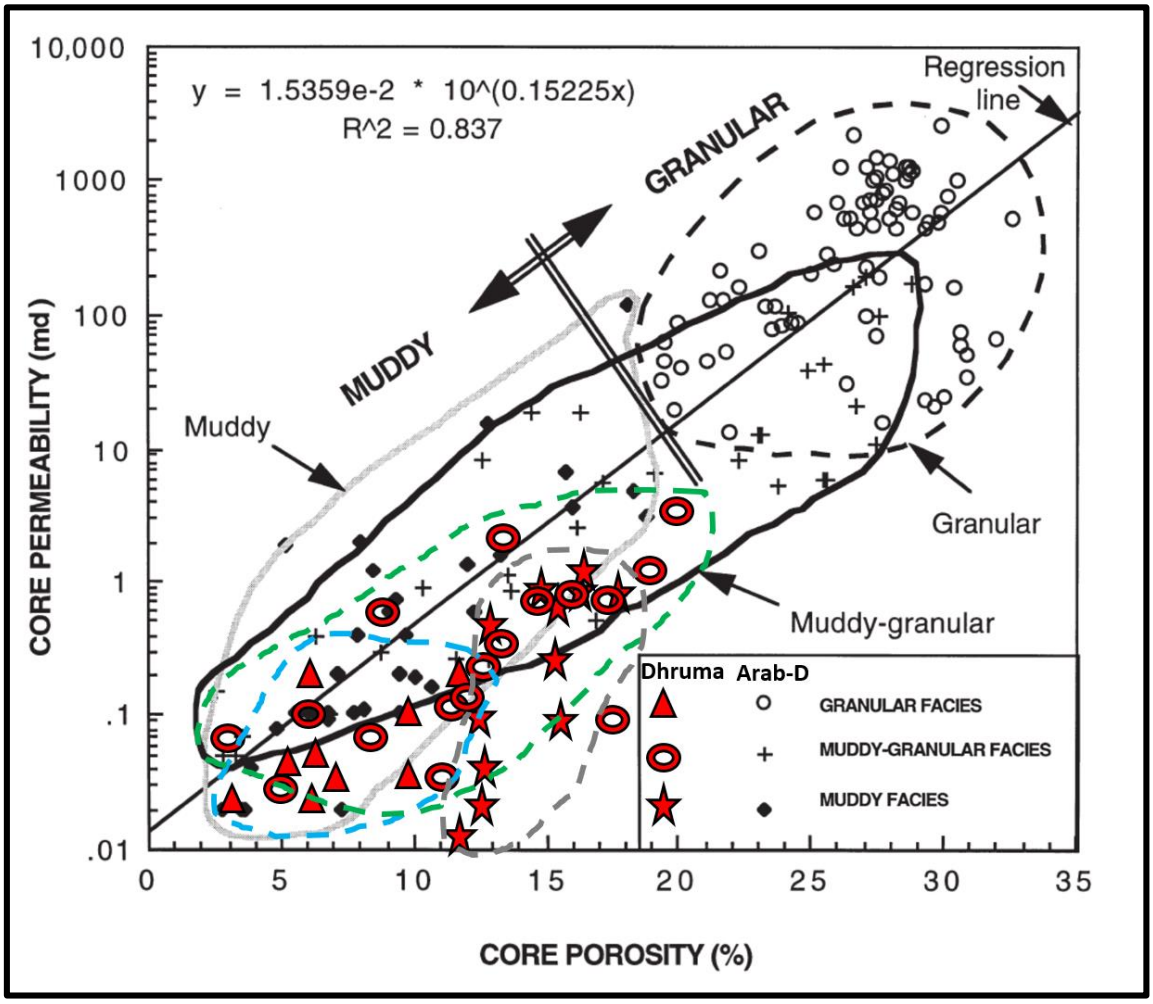


Figure 5.19: Porosity-permeability relationship in Arab-D reservoir in Uthmaniya field compared with the D5 and D6 Members of Dhruma Formation from outcrops in central Saudi Arabia ( modified from Saner and Sahin, 1999).

In order to introduce a quantitative assessment for the degree of heterogeneity of the reservoir units within the D5 and D6 Members in Dhruma Formation, three heterogeneity measures were utilized namely coefficient of variation, Lorenz coefficient, and Dykstra-parsons coefficient. The coefficient of variation for porosity is 0.41, which indicates homogeneous nature of the distribution. However, the Cv for permeability is much higher (2.51) which indicates very heterogeneous nature of the distribution. The Lorenz coefficient (Lc) for the entire data is about 0.76, which indicates very heterogeneous nature of the reservoir intervals (Figure 5.20). The Dykstra Parsons coefficient for permeability variation is about 0.84 which indicates also very heterogeneous nature of the studied intervals of the D5 and D6 Members (Figure 5.21). However, this heterogeneity reflects different depositional textures and the effects of diagenetic alterations. The vertical stratigraphic profile of porosity and permeability along the stratigraphic framework shows clearly these variabilities which attributed to the effects of original depositional texture and later diagenetic processes (Figure 5.22).

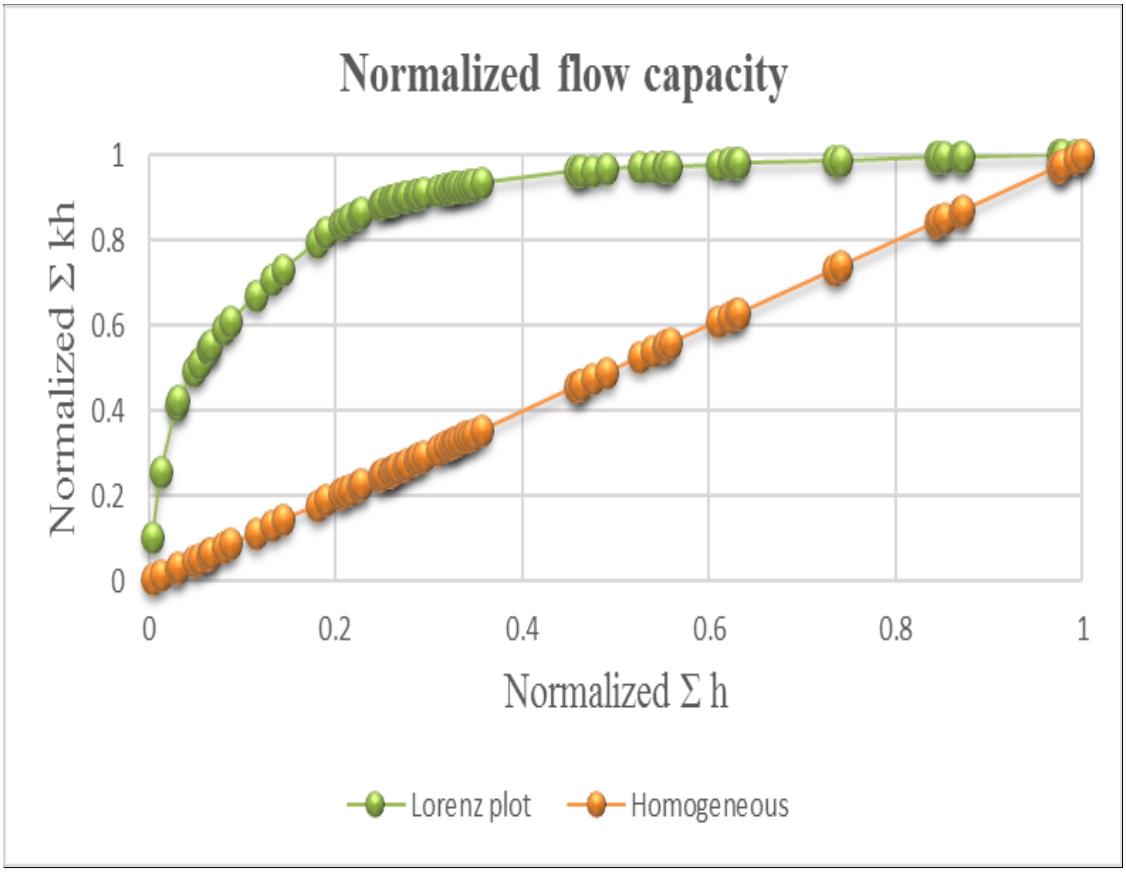


Figure 5.20: Lorenz plot to test the heterogeneity in permeability of the reservoir.

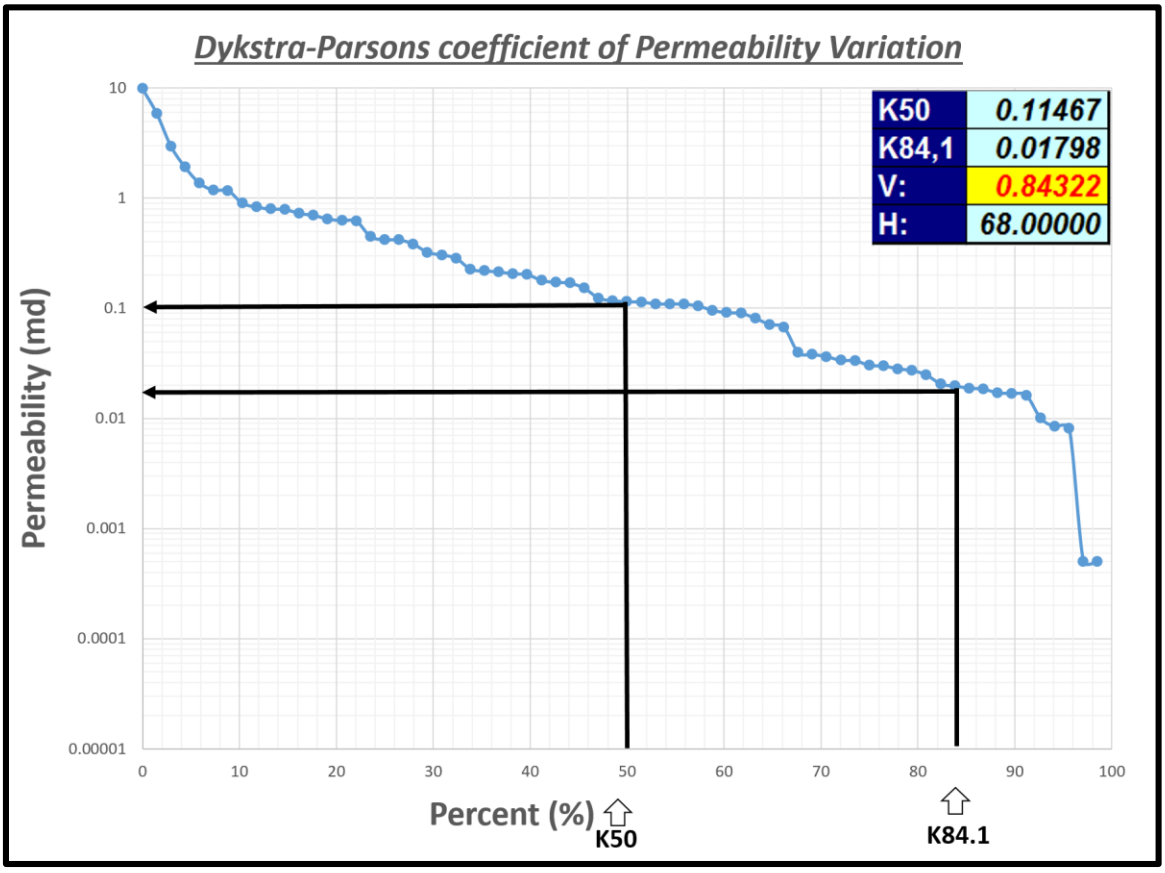


Figure 5.21: Dykstra-Parsons coefficient to test the heterogeneity in permeability of the reservoir.

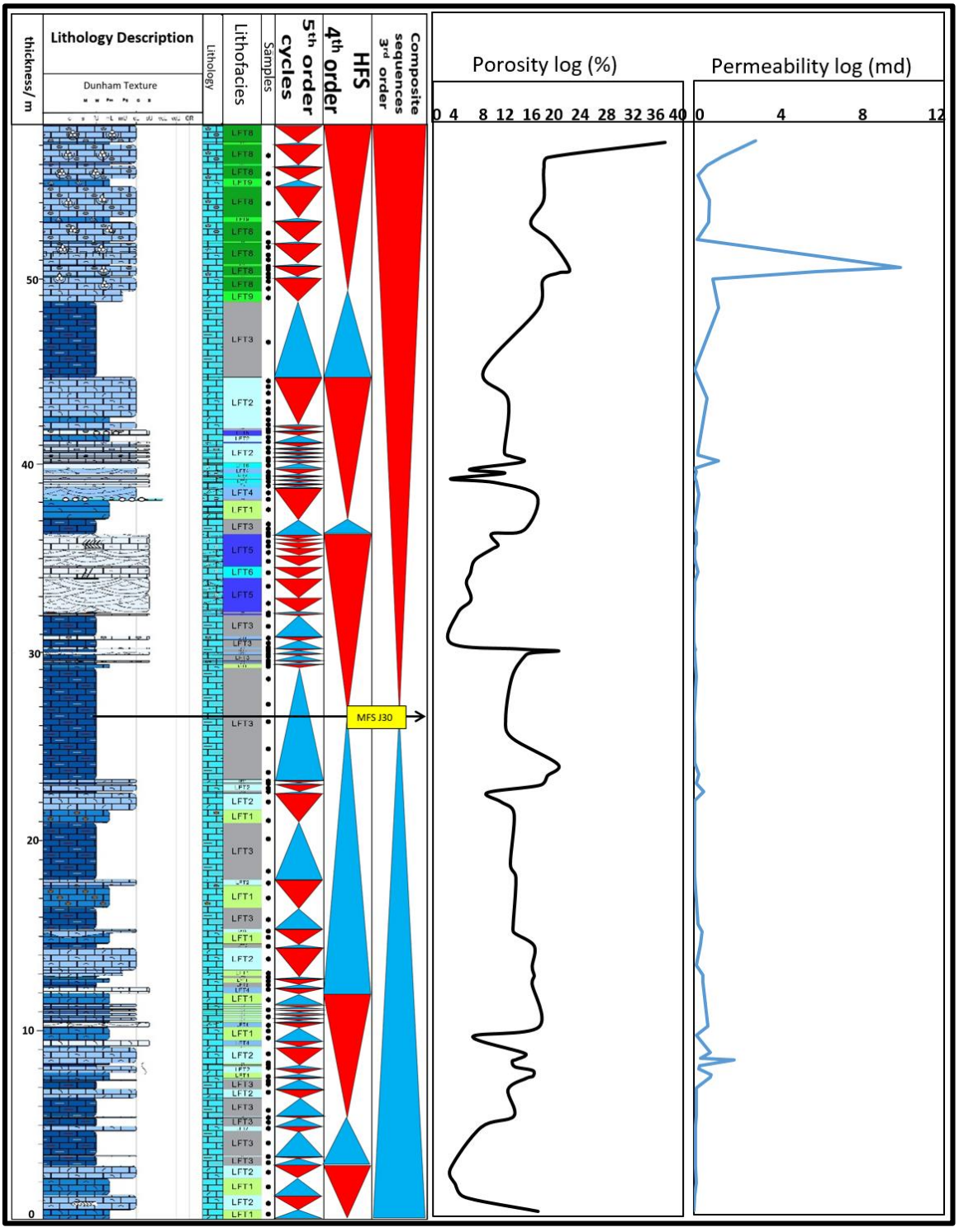


Figure 5.22: Vertical profiles of porosity and permeability along sequence stratigraphic framework of the D5 and D6 Members. The logs show clearly the heterogeneous nature of the reservoir units.

## 5.4 Rock-typing, hydraulic (Flow) units and global hydraulic elements (GHEs)

The classical methods to characterize the porosity and permeability, such as cross-plot relationship, are not always straightforward. However, it gives an idea about the variability within the dataset under investigation. The petrophysical data sets were classified into three groups based on rock texture which include: grain-dominated, muddy-grainy, and mud-dominated. The first group includes peloidal spiculitic echinoderm pack-grainstone (LFT4), cross-bedded peloidal oolitic grainstone (LFT5), oolitic grainstone (LFT6), and intraformational rudstone (LFT7). The second group comprises of only two lithofacies: skeletal foraminiferal peloidal packstone (LFT8) and peloidal echinoderm packstone (LFT2). The last group includes three lithofacies: skeletal spiculitic wackestone (LFT1), fissile shale (LFT3), and skeletal foraminiferal wackestone (LFT9). However, the boundaries between these groups are not sharp and crossed each other (Figure 5.23).

Porosity and permeability cross-plot based on rock texture show scattered pattern and it cannot easily relate them since same texture reflects different pattern (Figure 5.23). Furthermore, the mud-dominated lithofacies rocks have relatively the same range of porosity (0.1 to 0.2), while the grain-dominated and muddy-grainy lithofacies rocks have wide range of distribution. Generally, the three rock textures have permeability range from (0.01 to 1 md). These variabilities in distribution of the same rock texture and lithofacies are due to the complexity of pore geometry. Therefore, in order to better characterization and zonation of the reservoir body, the flow unit can be determined within the identified lithofacies. The flow units were calculated from the porosity and permeability data set of

the D5 and D6 Members based on reservoir quality index (RQI) and normalized porosity (Øn). The points located on the same straight line with the angle of 45 degrees from the horizontal axis will constitute a single flow unit. Therefore, nine hydraulic flow units (HU1-HU9) were defined for the D5 and D6 Members and each flow unit has a similar pore geometry and it tell us that there are many reservoir quality lithofacies and hence this mean their behavior for fluid flow is different (Figure 5.24).

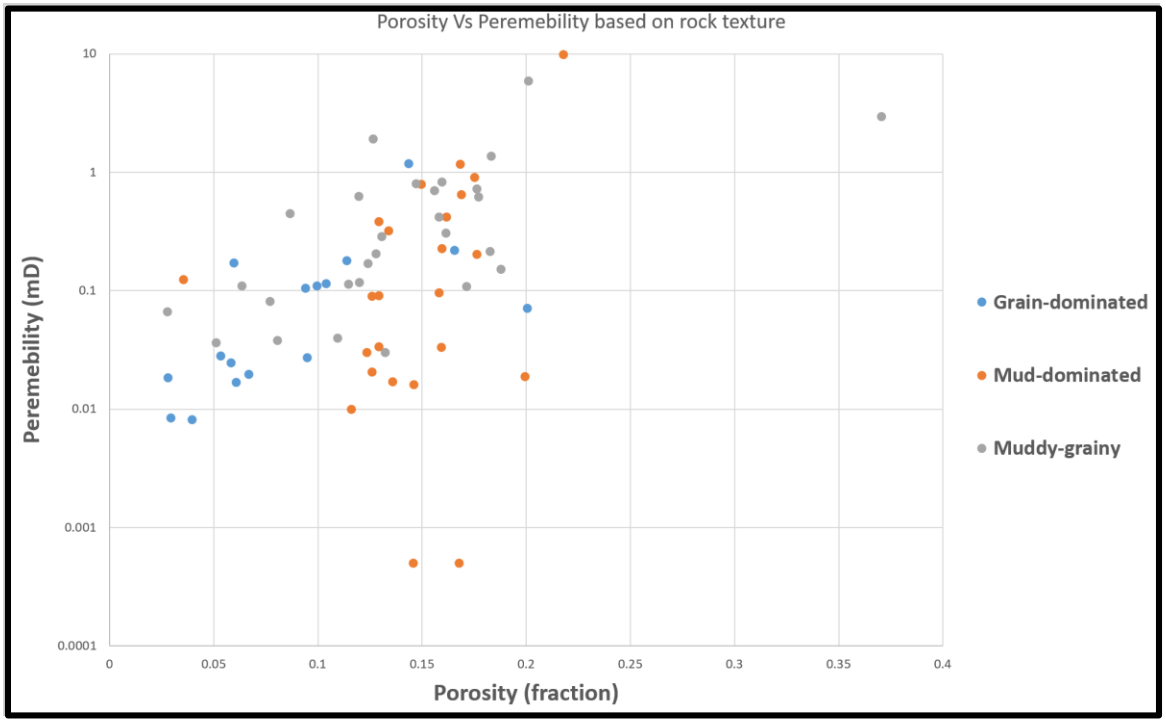


Figure 5.23: Porosity-permeability cross-plot based on rock texture of the D5 and D6 Members. Note that for specific porosity readings there are different permeabilities. Generally, the mud-dominated rocks have narrow range of porosity compared to the other rocks texture.

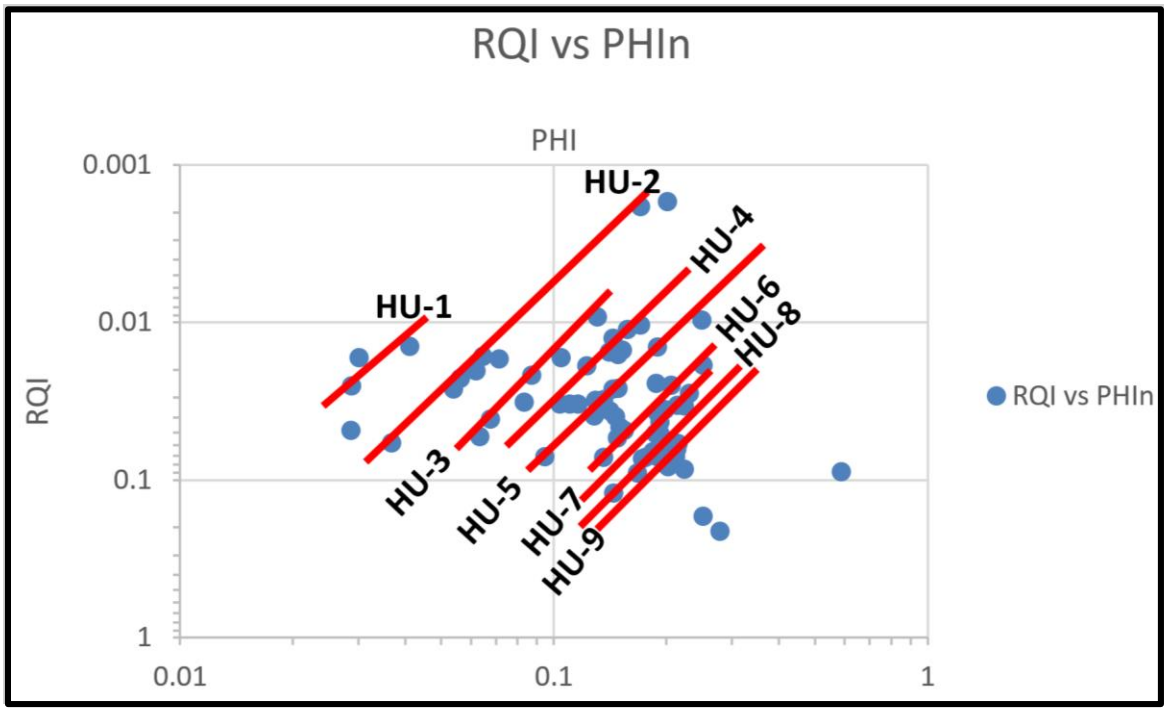


Figure 5.24: The hydraulic flow units of identified lithofacies of the D5 and D6 Members of Dhruma Formation.

To determine any trend and compare it with other reservoir, the researcher utilized the new approach introduced by Corbett and Potter (2004) namely petro-typing and Global Hydraulic Elements (GHEs) based on flow zone indicator (FZI). The lower boundaries of the hydraulic units were defined for the porosity and permeability (Figure 5.25). The global hydraulic elements defined based on porosity and permeability values and flow zone indicator (FZI). A systematic series of FZI will allow to determine the boundaries of hydraulic units, and this defines ten porosity-permeability elements with lower boundaries. In this study, we plotted our data in the global base map which introduced by Corbett and Potter, (2004). We defined (5) Global hydraulic elements (GHE1-GHE5) for the D5 and D6 Members. It has a flow zone indicator that range ranges from 0.0938 to 1.5, and can be described as multi-petrotype reservoir or mix global hydraulic elements (Figure 5.26).

However, most of the values are located within the GHE2 and GHE3. The plot also shows that our data set share part of the GHE with Middle East carbonates and occupy the lowest values (Figure 5.26).

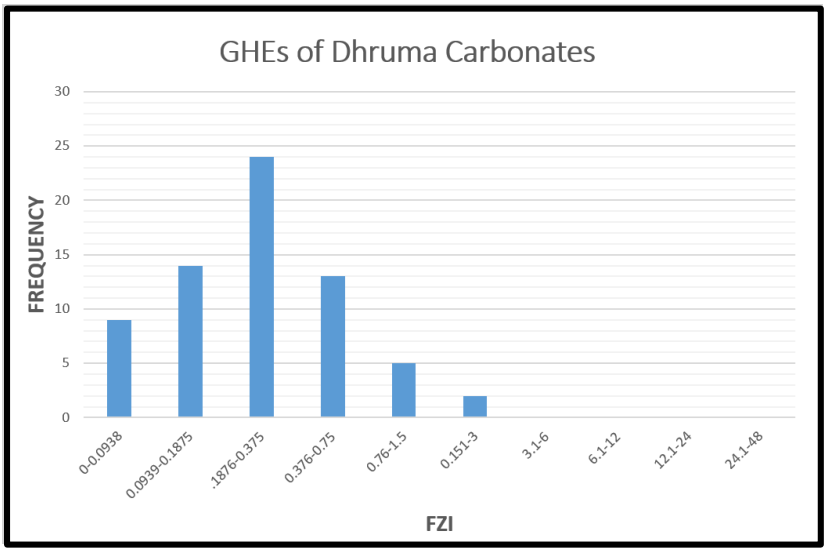


Figure 5.25: Distribution of the flow zone indicator (FZI) of carbonate Dhruma Formation.

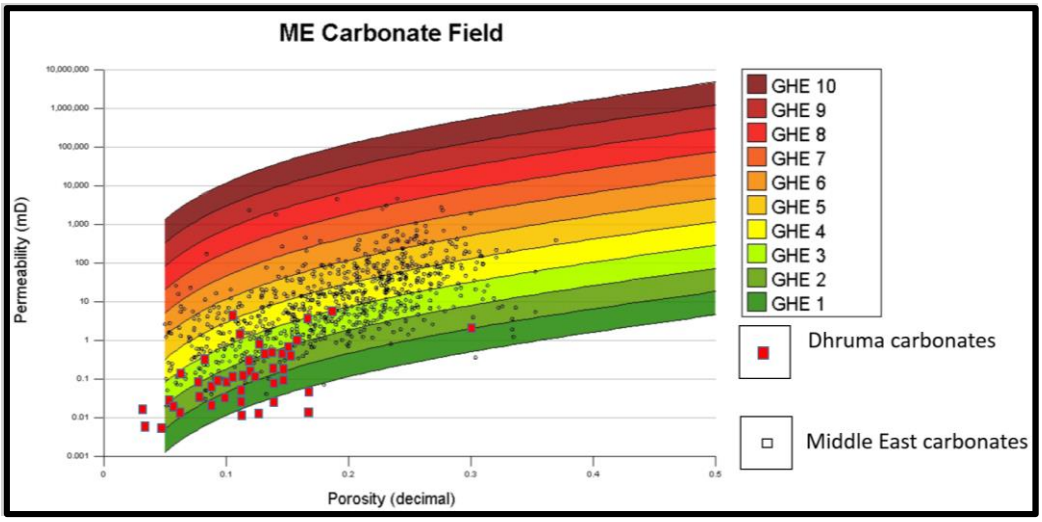


Figure 5.26: Global hydraulic trend in Dhruma Formation carbonate (red dots) and the Middle East carbonates (black dots). The Dhruma carbonates can be described as a multi-petrotype reservoir (modified from Corbett and Potter, 2004).

## 5.5 Geostatistical Modelling

The heterogeneity of the subsurface reservoirs represents a critical problem to understand. Tracing the architecture of reservoir in 3D as well as for management and predictions purposes of the reservoir is a challenge (Falivene et al., 2006). The studied 1D sections from wells and 2D and 3D seismic data have still limitations regarding vertical and horizontal resolution. However, for a better reservoir characterization of subsurface equivalents, outcrop analog can be used to offer a high-resolution framework of architecture and reservoir continuity.

Geostatistics provide a way to describe and understand the spatial variability of the geological problem (Isaaks and Srivastava, 1989). In this subsection, the geostatistical techniques were used to model the facies and to understand the variabilities in their petrophysical properties by using petrel software of Schlumberger. The model has been established following the same approach which introduced by Pringle et al. (2006). The authors used the standard surface-based modeling workflow based on outcrop stratigraphic sections to build their models. In this case, the stratigraphic sections were considered as pseudo wells to generate the models.

### 5.5.1 Input data and model flowwork

The field sample data have been georeferenced and coordinated (Table 5.4). Ten outcrop sections located on both side of road-cut to Saudi White cement factory and the cliffs around have been used as pseudo wells to generate the lithofacies and petrophysical static models (Figure 5.27, Figure 5.28 and Figure 5.29). The outcrop photomosaic was also used to get the thickness for each layer from the two sides of the outcrop and the cliffs around (Figure 4.24 and Figure 4.28). The identified nine lithofacies types of the D5 and D6 Members were statistically analyzed and coded (0 to 8). The histogram in (Figure 5.30) shows the percentage of each lithofacies types. The peloidal echinoderm packstone (1) is the most abundant lithofacies type which followed by fissile shale (2). The least abundant lithofacies type is intraformational rudstone lithofacies (6).

Generally, five steps have been followed and utilized to come up with the static model of the lithofacies and petrophysical properties and these steps include: 1) selection of the stratal horizons; 2) creation of the key surfaces by using $4^{th}$ order high-frequency sequences from the established stratigraphic framework and outcrop photo mosaic; 3) grid construction of the model; 4) import and upscaling of outcrop sections as pseudo wells and finally 5) these facies were populated within five stratigraphic zones to build the lithofacies model. Computed semivariograms parameters being used to establish the static lithofacies model by using Sequential Indicator Simulation algorithm (SIS). The petrophysical models of porosity and permeability were generated by assign their values on the lithofacies model.

Table 5.4: Shows the chosen outcrop sections location and their measured thickness.

| Section Name | Easting | Northing | Length (m) |
|---|---|---|---|
| DSW1 | 631447.10 | 2688964.06 | 57.05 |
| DSW2 | 631475.32 | 2689062.79 | 57.05 |
| DSW3 | 631540.88 | 2688950.70 | 57.05 |
| DSW4 | 631610.16 | 2688839.42 | 57.05 |
| DSW5 | 631681.14 | 2688689.71 | 57.05 |
| DSW6 | 631275.91 | 2689067.47 | 57.05 |
| DSW7 | 631327.95 | 2688994.62 | 57.05 |
| DSW8 | 631378.91 | 2688912.98 | 57.05 |
| DSW9 | 631430.72 | 2688830.82 | 57.05 |
| DSW10 | 631478.92 | 2688736.97 | 57.05 |

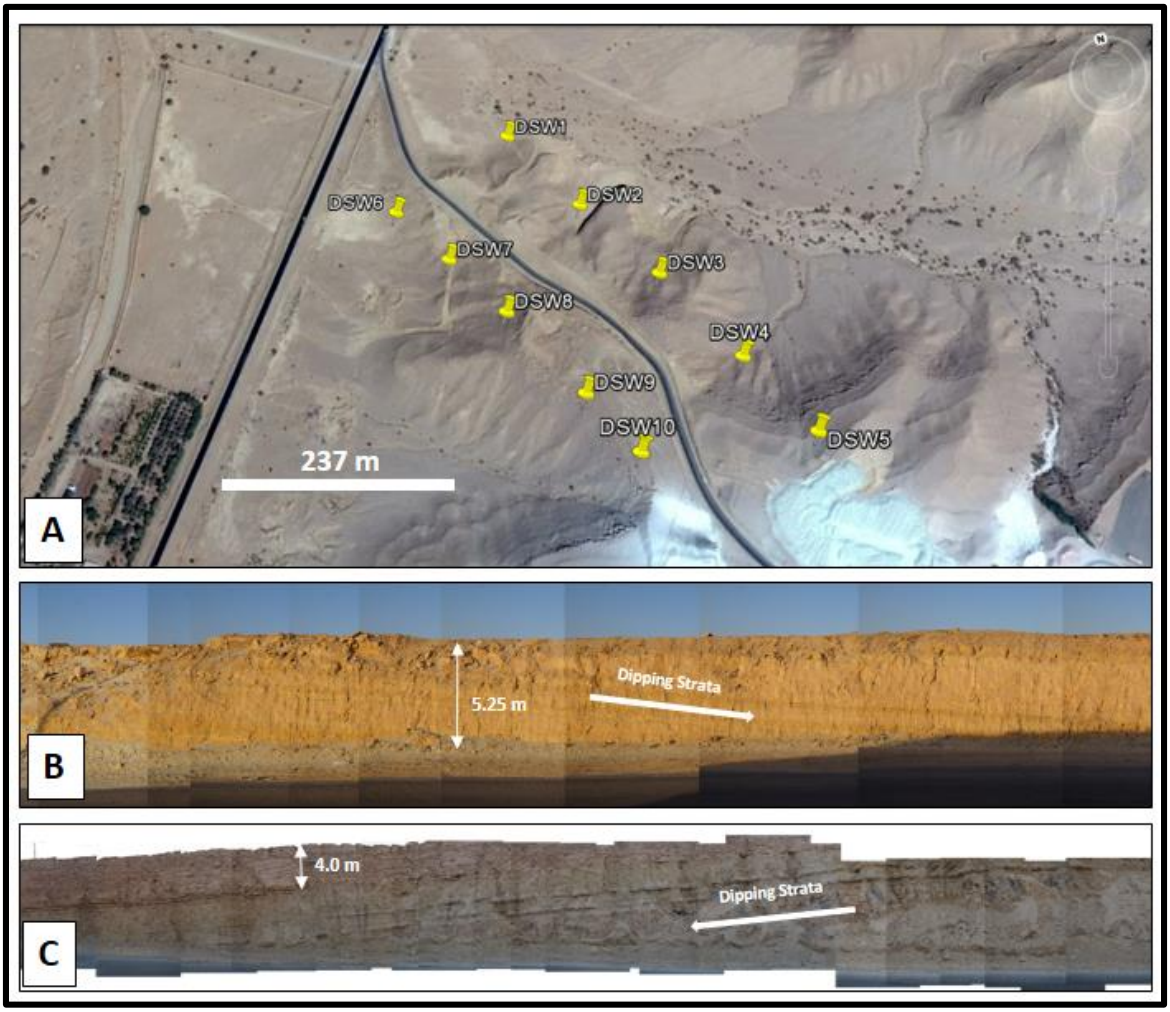


Figure 5.27: Study Area. (A) Satelite image showing the D5 and D6 Members of Dhruma Formation located in aroad-cut to Saudi White Cement Factory, southwest of Riyadh city, central Saudi Arabia. Ten outcrop sections (appers in yellow pins) were logged and used as pseduo wells to generate 3D lithofacies and petrophysical models (modified from google earth, 2017), (B) Outcrop photomozic of most probably D6 Member along a road-cut to cement factory, and (C) Outcrop photomozic of the D5/D6 Members along a road-cut to cement factory.

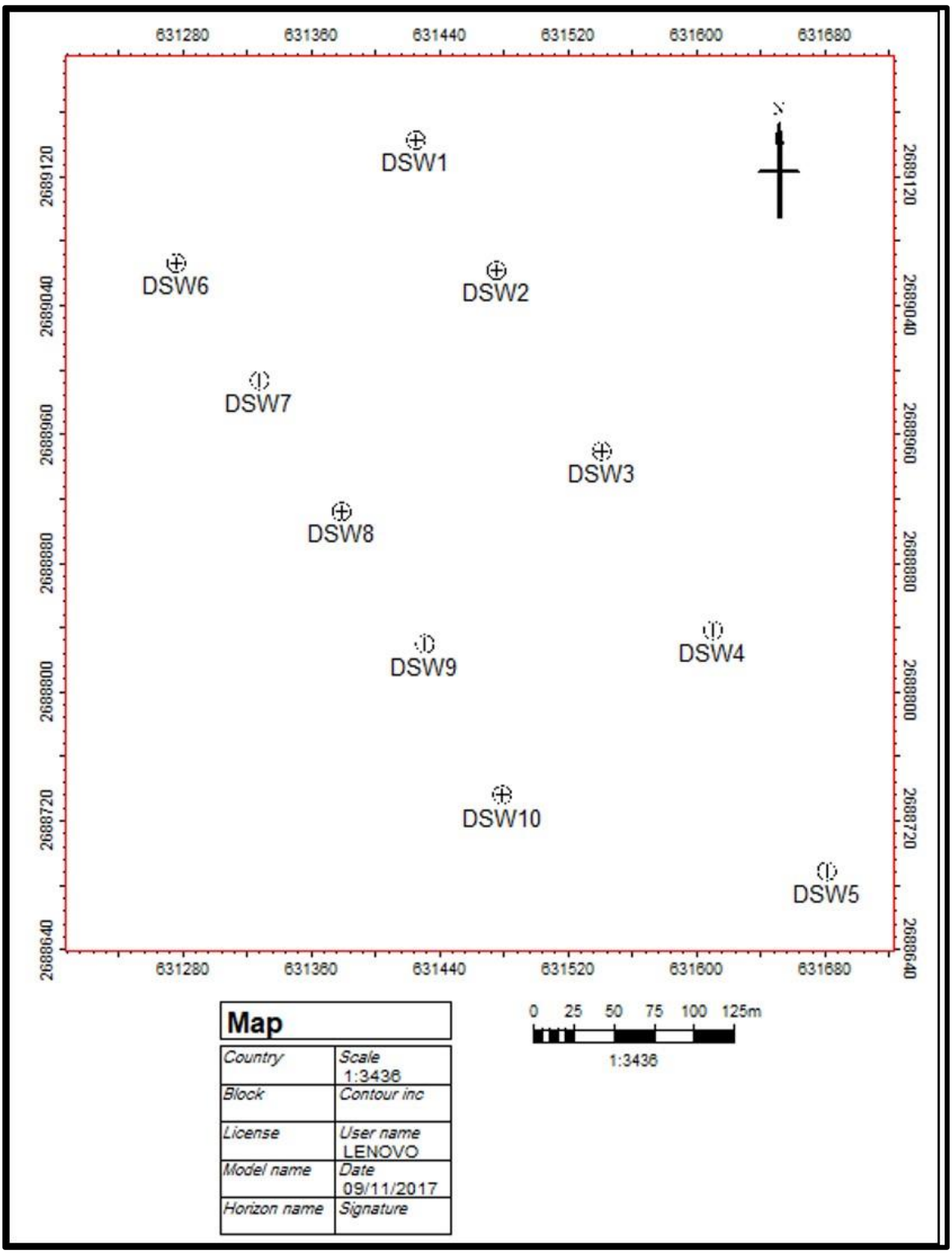


Figure 5.28: Base map shows the location of selected outcrop sections of the D5 and D6 Members in the Study Area (See figure 5.27).

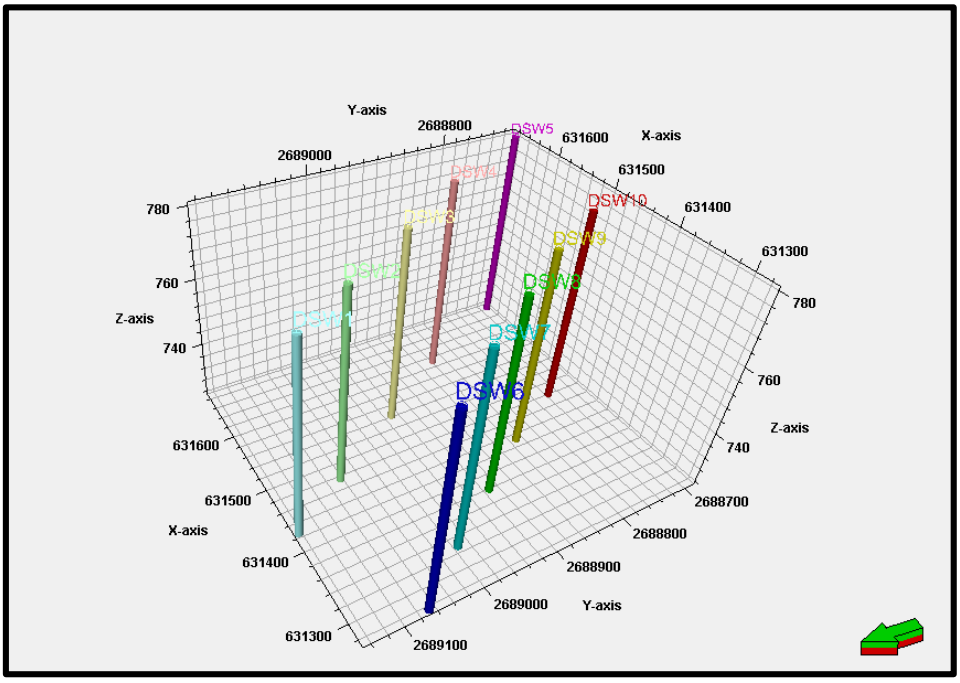


Figure 5.29: Ten outcrop sections were used as pseudo wells on the both sides of road-cut and cliffs around of the D5 and D6 Members.

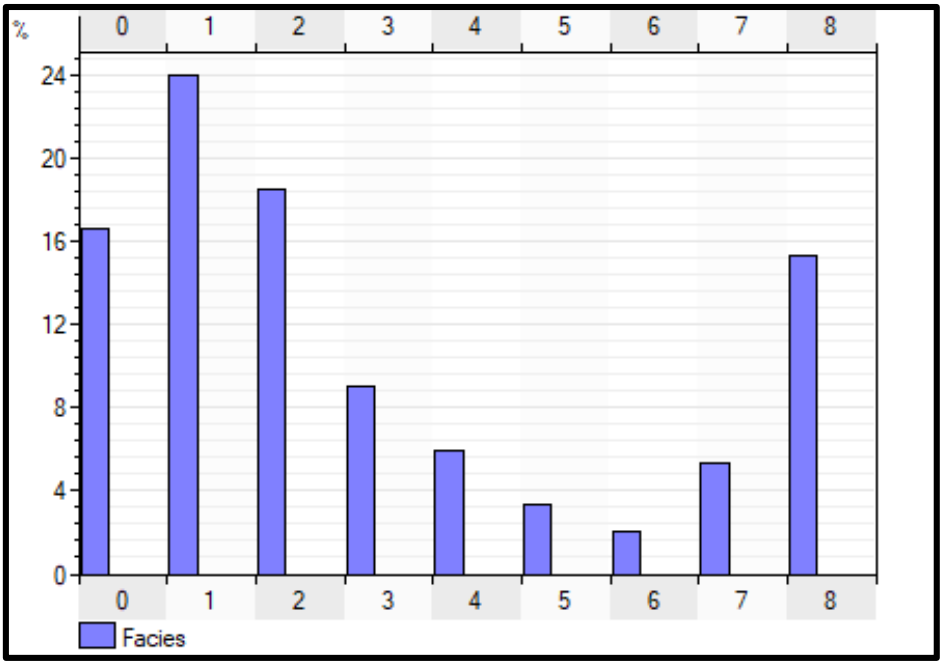


Figure 5.30: Histogram showing the distribution for individual facies percentage for the input data.

## 5.5.2 Data analysis and modeling

### 5.5.2.1 Data analysis

The variogram algorithm was utilized to understand and to measure the variability in geology properties like facies or petrophysical parameter such as porosity in specific trend. However, the variabilities in these rock properties have various behaviors in different directions. Variogram are commonly used in reservoir characterization as geostatistical tool to study and model the spatial variability in geological properties (Gringarten and Deutsch, 1999). Prior to construct semivariograms for the 3D model, a simple grid cell dimension of (1×1) with total cell number of 21315008 has been selected to build the 3D outcrop model. The next step was designing the model zones. Therefore, stratigraphic zonation was achieved based on sequence stratigraphic framework of the fourth order high-frequency cycles (HFS) of studied intervals. Each zone represents a transgressive-regressive cycle. The outcrop photomosaic and 2D outcrop panel were used in spatial correlation. The outcrop was divided into six surfaces and five zones (Figure 5.31) and (Table 5.5) from the correlated stratigraphic sections**.** Those are from bottom to top zone 1, 2, 3, 4 and 5. Each zone was then subdivided into layers. The number of layers within zone 2 and zone 3 are greater compared with other zones (Table 5.5). The total number of layers in all zones is 88 layer and the majority of them are small and very thin layers. The data was upscaled for each pseudo well (Figure 5.32). In the vertical distribution of the layers of the D5 and D6 Members, it appears that the small layers were hidden by the effect of the thick layers, and causes a problem in upsacling **(Figure 5.33).**

Table 5.5: Defined zones of the D5 and D6 Members and number of layers in each zone

| Zone | Number of layers |
|---|---|
| Zone1 | 17 |
| Zone2 | 24 |
| Zone3 | 28 |
| Zone4 | 15 |
| Zone5 | 4 |

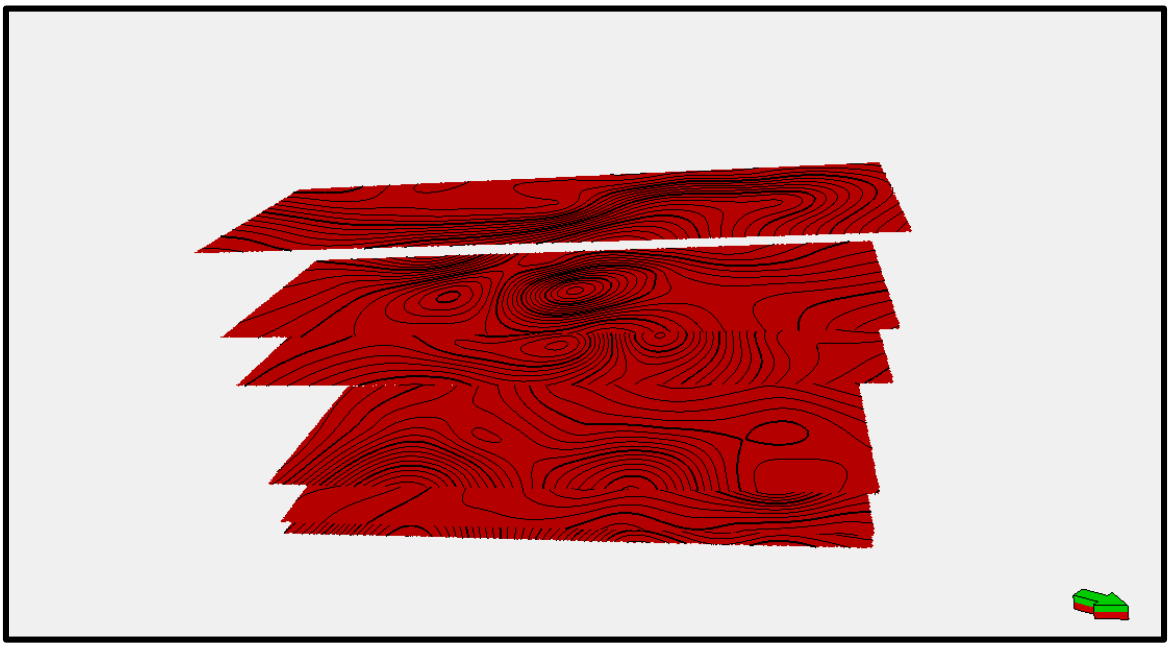

Figure 5.31: Six surfaces that chosen based on 4$^{th}$ order stratigraphic surfaces (HFS) , within it 5 zones were defined.

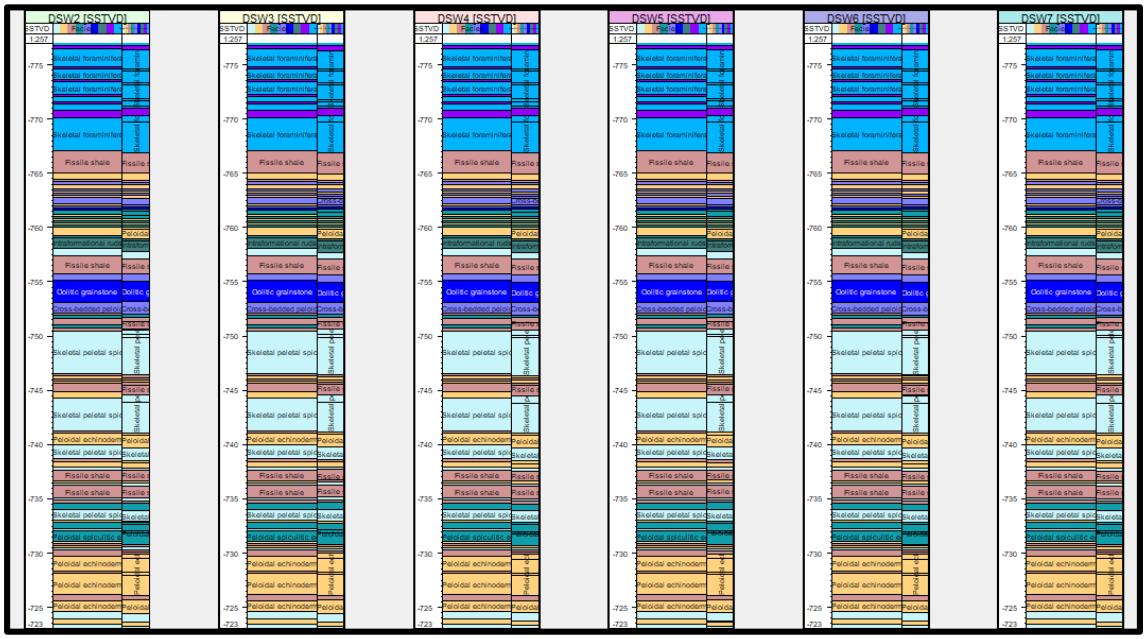


Figure 5.32: Part of the upscaled pseudo wells. Thin layers affected the upscaling.

Table 5.6: Shows variogram models paramters for the defined zones based on the stratigraphic surfaces and sequence stratigraphic freamework of thr fourt order HFS.

| Zone No. | Major Range | Minor Range | Vertical Range | Sill | Nugget | Model Type |
|---|---|---|---|---|---|---|
| Zone 1 | 523 | 125 | 10.7 | 1.13 | 0 | Exponential |
| Zone 2 | 500 | 191 | 8.76 | 1.09 | 0.7 | Exponential |
| Zone 3 | 553 | 524 | 14.5 | 1.03 | 0.3124 | Exponential |
| Zone 4 | 521 | 201 | 8.58 | 1.12 | 0.938 | Exponential |
| Zone 5 | 548 | 192 | 0.863 | 1.11 | 0.933 | Exponential |

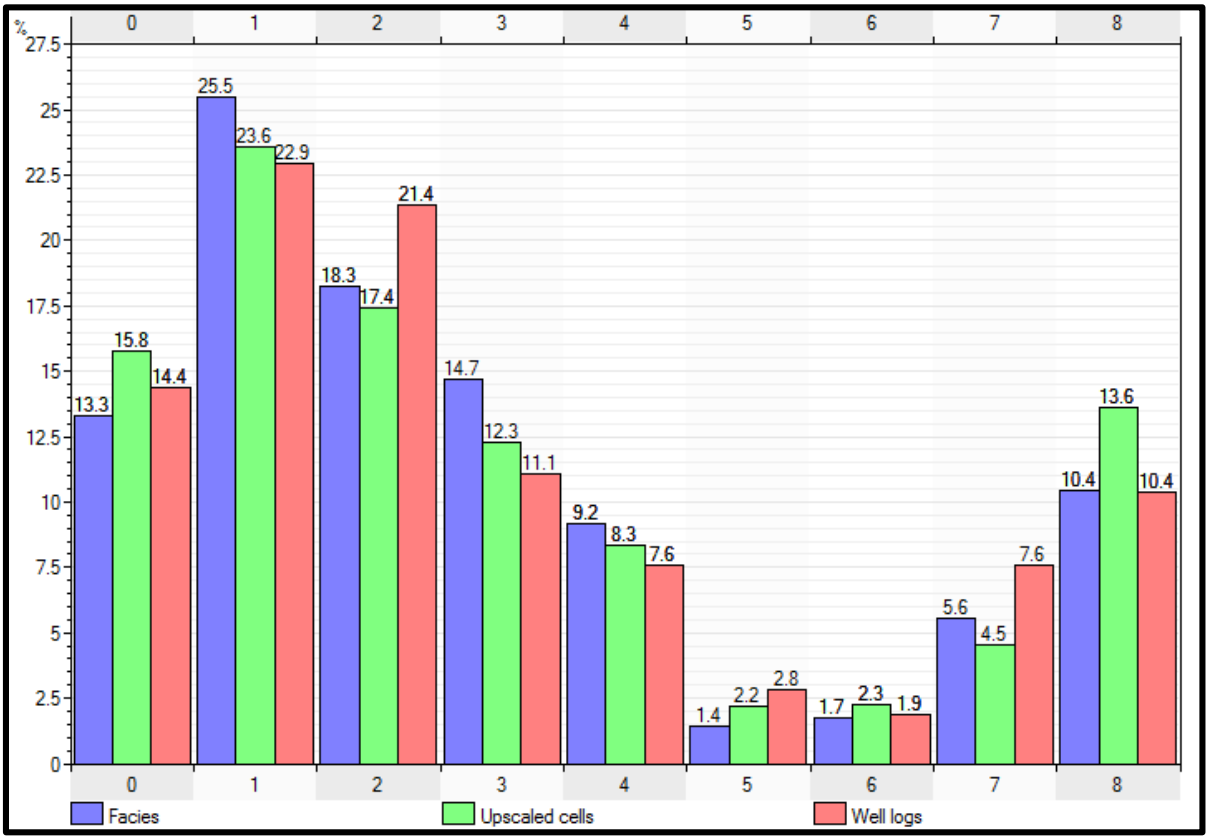


Figure 5.33:Histogram of the facies model data, upscaled data and well logs.

Several indicator semivariograms parameters were calculated for each zone by using the upscaled lithofacies in pseudo wells. The parameters, which include: nugget, sill and range, were estimated in the major, minor and vertical directions (Table 5.6). The presence of small layers have cause a problem in fitting of the variogram and it give high nugget value for each zone. The most commonly used variogram functions in literature are spherical, exponential, Gaussian and hole effect models (e.g. see Deutsch, 2002). However, the researcher utilized the exponential variogram model for all zones since it gives low nugget value. In PETREL software, the process of fitting the variogram requires adjusting variogram parameter's (nugget, sill and range) until to achieve the best fit of variogram curve.

#### 5.2.2.2 3D Lithofacies and petrophysical model

The established outcrop lithofacies model illustrate the distribution of the D5 and D6 Members in three dimensions based on the variogram. The model was achieved by utilizing sequential indicator simulation algorithm (SIS) on the nine identified lithofacies (Figure 5.34). Generally, the model shows layer cake style in low resolution as expected from different studies dealt with Jurassic carbonates reservoirs (e.g. Eltom et al. (2013); Elzain et al (2015)). However, the resulted model did not visualize the thin layers in a good way and this might be as result of grid resolution that been selected to generate the model and the effect of the thicker beds. For the model validation the field data have been compared with the output generated realizations of the lithofacies. Then these realizations have been ranked based on their close similarity to the input field data, and two realizations were selected since a good match between these realizations and the upscaled data were found (Table 5.7) and (Figure 5.35). The qualitative model validation was achieved by omparing

the real outcrop photo mosaic with slice of the 3D model (Figure 5.36). Generally, a good match was found between the 3D facies model cross section with equivalent outcrop stratigraphy.

The 3D porosity and permeability models of the D5 and D5 Members were established by assign the average porosity and permeability values for each lithofacies in the model (Figure 5.37 and Figure 5.38).

The readings of porosity and permeability were obtained from core plugs of collected rock samples from the field. The 3D models were generated by following the same variogram parameters in the previous facies model. Therefore, the spatial distribution of the petrophysical properties is controlled by lithofacies. Good reservoir quality was found in the upper most part of the model which characterized by relatively high porosity and permeability readings as result of intensive dissolution as discussed previously. This zone is mainly lagoonal lithofacies of skeletal peloidal foraminiferal packstone and skeletal foraminiferal wackestone.

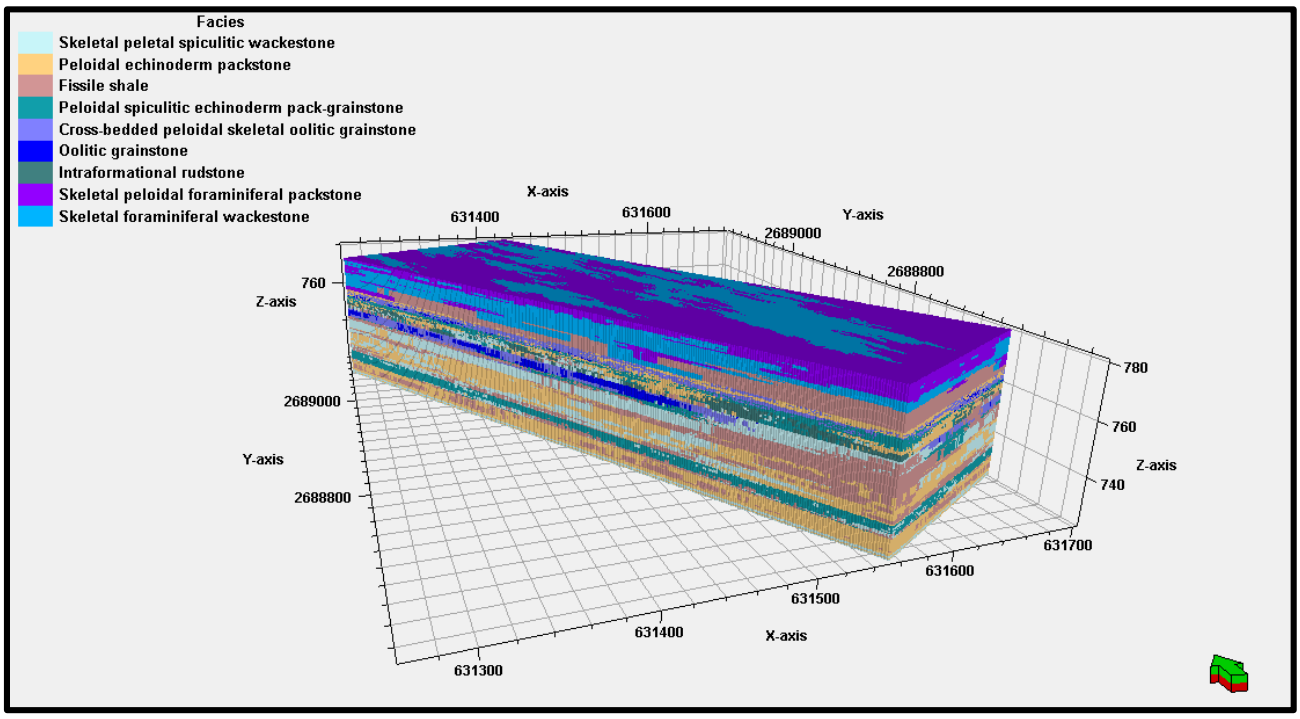


Figure 5.34: 3D outcrop lithofacies model of the D5 and D6 Members of Dhruma Formation generated by using sequential indicator simulation (SIS).

Table 5.7: Summary of simple statistics of the upscaled lithofacies and the top-two ranked realizations.

| Ups./R. | Code | Name | % | Min. | Mean | Max. | Std. |
|---|---|---|---|---|---|---|---|
| Upscaled Facies | 0 | Skeletal peletal spiculitic wackestone | 15.76 | 0.2 (1) | 1.2 (1.28) | 4.2 (3) | 1.316 |
| | 1 | Peloidal echinoderm packstone | 23.56 | 0.2 (1) | 0.7 (1.39) | 3.9 (4) | 0.914 |
| | 2 | Fissile shale | 17.42 | 0.2 (1) | 0.8 (1.28) | 1.9 (2) | 0.5515 |
| | 3 | Peloidal spiculitic echinoderm pack-grainstone | 12.27 | 0.2 (1) | 0.7 (1.8) | 2.2 (4) | 0.6763 |
| | 4 | Cross-bedded peloidal skeletal oolitic grainstone | 8.33 | 0.2 (1) | 0.6 (1.25) | 1.2 (4) | 0.3962 |
| | 5 | Oolitic grainstone | 2.2 | 0.2 (1) | 1.1 (1) | 1.9 (1) | 0.823 |
| | 6 | Intraformational rudstone | 2.27 | 1.2 (2) | 1.2 (2) | 1.2 (2) | 0.003473 |
| | 7 | Skeletal peloidal foraminiferal packstone | 4.55 | 0.2 (1) | 0.6 (1) | 1.1 (1) | 0.3177 |
| | 8 | Skeletal foraminiferal wackestone | 13.64 | 0.9 (1) | 2.7 (3) | 5.4 (8) | 1.851 |

| Ups./R. | Code | Name | % | Min. | Mean | Max. | Std. |
|---|---|---|---|---|---|---|---|
| Realiz.1 | 0 | Skeletal peletal spiculitic wackestone | 12.69 | 0.2 (1) | 1.3 (1.64) | 12.0 (13) | 1.316 |
| | 1 | Peloidal echinoderm packstone | 26.72 | 0.2 (1) | 1.5 (2.39) | 15.8 (22) | 1.828 |
| | 2 | Fissile shale | 17.89 | 0.2 (1) | 1.4 (2.04) | 11.1 (14) | 1.385 |
| | 3 | Peloidal spiculitic echinoderm pack-grainstone | 14.05 | 0.2 (1) | 1.0 (2.29) | 9.9 (17) | 0.9506 |
| | 4 | Cross-bedded peloidal skeletal oolitic grainstone | 7.19 | 0.2 (1) | 0.9 (1.91) | 4.4 (15) | 0.8625 |
| | 5 | Oolitic grainstone | 2.15 | 0.2 (1) | 0.9 (1.53) | 5.6 (11) | 0.962 |
| | 6 | Intraformational rudstone | 1.66 | 0.2 (1) | 1.4 (1.8) | 4.5 (7) | 0.9717 |
| | 7 | Skeletal peloidal foraminiferal packstone | 4.65 | 0.2 (1) | 1.6 (2.08) | 6.9 (9) | 1.284 |
| | 8 | Skeletal foraminiferal wackestone | 13 | 0.2 (1) | 4.0 (5.12) | 15.1 (17) | 3.193 |
| Realiz.2 | 0 | Skeletal peletal spiculitic wackestone | 13.28 | 0.2 (1) | 1.2 (1.63) | 10.9 (14) | 1.241 |
| | 1 | Peloidal echinoderm packstone | 25.47 | 0.2 (1) | 1.4 (2.26) | 13.4 (19) | 1.681 |
| | 2 | Fissile shale | 18.27 | 0.2 (1) | 1.6 (2.13) | 16.4 (18) | 1.821 |
| | 3 | Peloidal spiculitic echinoderm pack-grainstone | 14.69 | 0.2 (1) | 1.1 (2.57) | 8.6 (16) | 1.111 |
| | 4 | Cross-bedded peloidal skeletal oolitic grainstone | 9.16 | 0.2 (1) | 0.9 (2.1) | 5.6 (18) | 0.9107 |
| | 5 | Oolitic grainstone | 1.4 | 0.2 (1) | 1.3 (1.42) | 3.9 (8) | 1.106 |
| | 6 | Intraformational rudstone | 1.73 | 0.2 (1) | 1.2 (1.6) | 4.6 (7) | 0.8366 |
| | 7 | Skeletal peloidal foraminiferal packstone | 5.58 | 0.2 (1) | 1.6 (2.18) | 6.9 (9) | 1.354 |
| | 8 | Skeletal foraminiferal wackestone | 10.42 | 0.2 (1) | 2.9 (3.87) | 15.1 (17) | 2.305 |

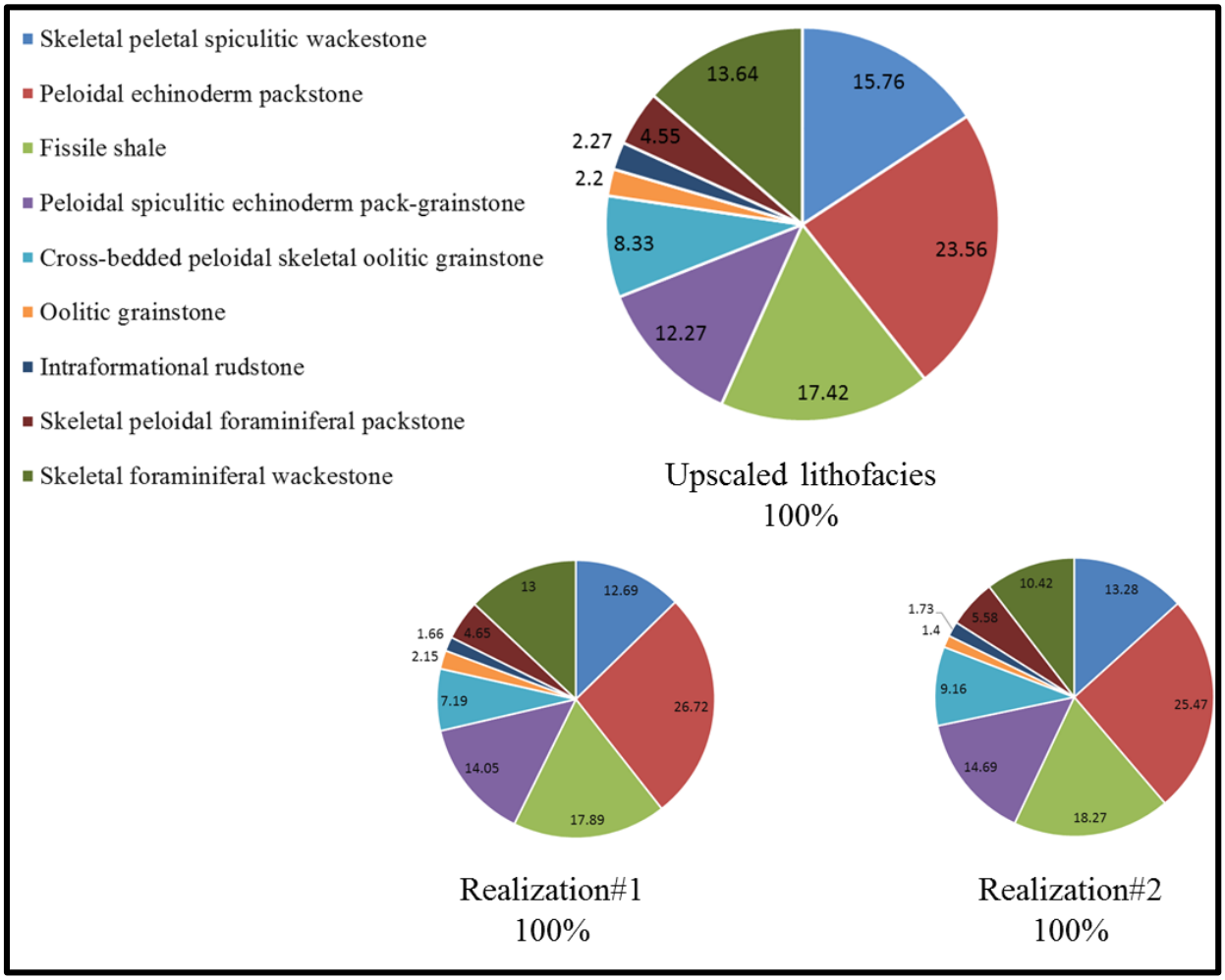


Figure 5.35: Top two-ranked lithofacies realizations compared with the upscaled lithofacies percentages of the input field data.

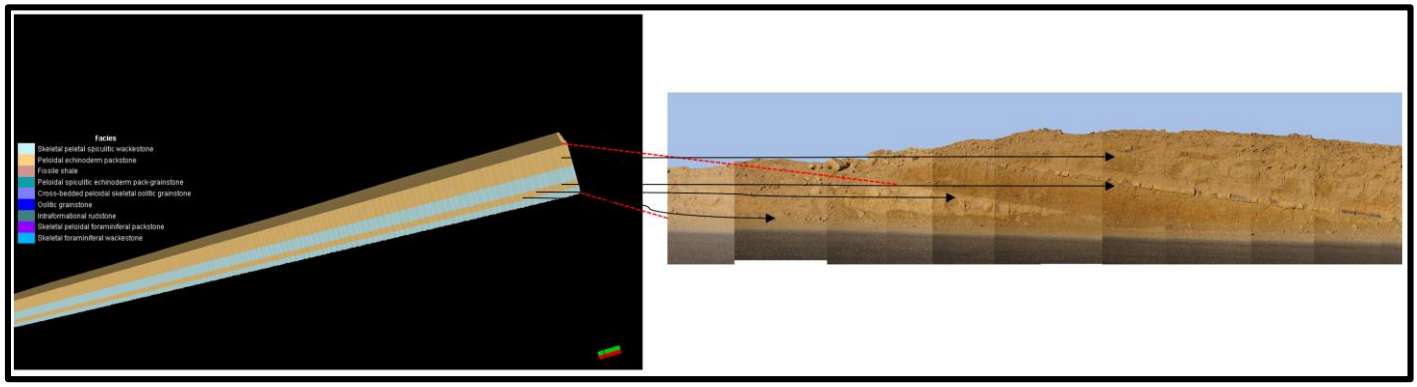


Figure 5.36: Outcrop photograph compared with 3D lithofacies model of zone 5 utilized for model validation. A great match was found between the two model and the outcrop stratigraphy.

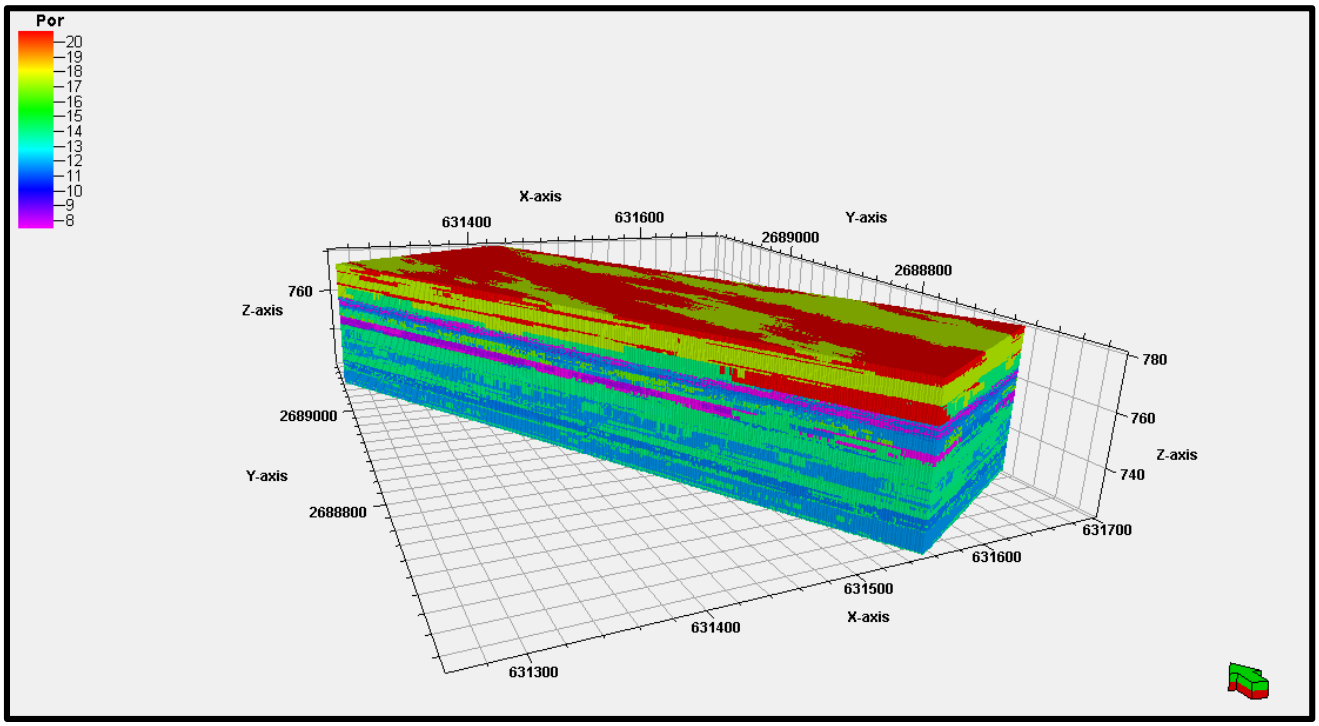


Figure 5.37: 3D porosity model of the D5 and D6 Members of Dhruma Formation generated by assign the average porosity values for each lithofacies in established lithofacies model.

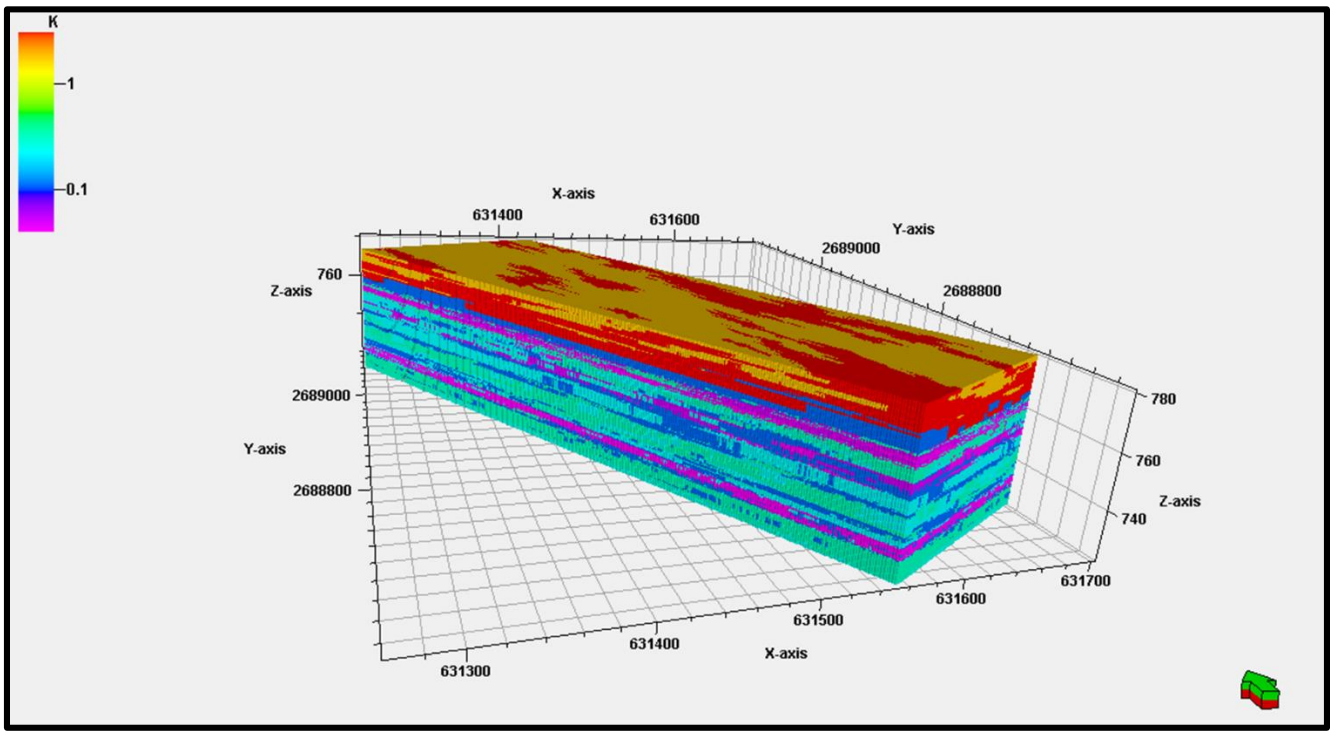


Figure 5.38: 3D permeability model of the D5 and D6 Members of Dhruma Formation generated by assign the average permeability values for each lithofacies in established lithofacies model.

# CHAPTER 6

# CONCLUSIONS AND RECOMMENDATIONS

## 6.1 Conclusions

- In this study the researcher investigated different aspects to enhance the reservoir characterization of the D5 and D6 Members of carbonate Middle Jurassic Dhruma Formation in outcrop in central Saudi Arabia. Detailed microfacies and stratigraphic architecture analysis were carried out. Moreover, diagenetic and reservoir quality analysis were combined with the 3D geostatistical modeling.
- The detailed lithofacies and stratigraphic analysis of studied sections of carbonates Dhruma Formation show that they are belong to the D5 and D6 Members based on lithofacies and bio component especially benthic foraminifera. The lithofacies analysis has been done based on Dunham (1962) classification of carbonate rocks and the standard microfacies of carbonate ramp that proposed by Flügel, (2004). Nine lithofacies types were identified which include: skeletal peletal spiculitic wackestone (LFT1), peloidal echinoderm packstone (LFT2), fissile shale (LFT3), peloidal spiculitic echinoderm pack-grainstone (LFT4), cross-bedded peloidal skeletal oolitic grainstone (LFT5), oolitic grainstone (LFT6), intraformational rudstone (LFT7), skeletal foraminiferal peloidal packstone (LFT8) and skeletal foraminiferal wackestone (LFT9). These lithofacies have been grouped into five major carbonate paleoenvironment that range from distal-to-proximal carbonate

ramp setting. The most abundant lithofacies types are: fissile shale (36%), peloidal echinoderm packstone (19%), skeletal peletal spiculitic wackestone (15%) and skeletal foraminiferal peloidal packstone (12%). The rest of the lithofacies types have abundance range from (<1 to 7%).

- The detailed stratigraphic analysis based high-resolution photo mosaic and identified lithofacies revealed around 53 cycle and cycle sets ($5^{th}$ to $6^{th}$ order), with thickness, ranges from centimeters to six meters with an average of 1.5 meter. These parasequences are stacked to form four high-frequency sequences (HFSs) with thickness ranges from one meter up to fourteen meters, and generally show shallowing upward nature. The latter was grouped into a single depositional sequence of $3^{rd}$ order magnitude. Furthermore, the Jurassic maximum flooding surface (MFS J30) was also captured, and it is located within a thick transgressive shale/ mudstone of the D5 Member. The stable isotope patterns of carbon and oxygen along the vertical composite stratigraphic section are relatively depleted in transgressive dominated compared with that in regressive dominated part. The abrupt shift in $\delta$ 18O values seem to be an indication of a subaerial exposure surface.
- Different pore types were recognized in studied intervals of the D5 and D6 Members which include: fracture, intraparticle, moldic and intercrystalline porosities. The dominant pore types are fracture and intraparticle porosities. The moldic porosity and intraparticle porosity are the dominant ones in the uppermost part of the vertical composite stratigraphic section which is equivalent to Lower Fadhili reservoir in the subsurface. The diagenetic alterations that controlled the

reservoir quality of Dhruma carbonates include: micritization, cementation, dissolution, dolomitization/ dedolomitization and burial diagenesis. These alterations have various effects on reservoir quality evolution. Relatively high porosity and permeability readings were observed in skeletal foraminiferal peloidal packstone (LFT8) and skeletal foraminiferal wackestone (LFT9) in the upper most part of the section. The reason of that is the development of intensive meteoric dissolution which creates abundant pores. In certain intervals intensive meteoric calcite cementation blocked most of the original pore space and significantly reduced the reservoir quality in grainy texture rock such as oolitic grainstone and echinoderm pack-grainstone lithofacies. The correlation between porosity and permeability shows poor relationship and reflects the heterogeneous nature of reservoir units of Dhruma Formation. However, heterogeneity measures show very heterogeneous nature of these two variables as result of primary depositional texture and subsequent diagenetic alterations. The variability in porosity profile along vertical stratigraphic section generally shows a positive correlation with carbon and oxygen isotope ratios. However, the transgressive part is dominated by heavier isotope composition compared with regressive dominated part.

- Further step toward better reservoir characterization has been achieved by utilizing two approaches: hydraulic flow units and rock-typing. Therefore, nine hydraulic flow units and five global hydraulic elements (GHEs) have been defined in D5 and D6 Members of Middle Jurassic carbonate Dhruma Formation. The GHEs have flow zone indicator range from 0.0938 to 1.5, and these variabilities reflect the complexity in pore geometry.

- To understand the reservoir architecture, continuity and quality in three dimensions, the geostatistics approaches have been utilized to generate the lithofacies and petrophysical static models. Generally, the model shows layer cake in low-resolution. The petrophysical models were established by assigning the average porosity and permeability readings for each lithofacies in the 3D outcrop lithofacies model. Relatively high porosity and permeability values were observed in zone 1 which is dominated by lagoonal lithofacies.

## 6.2 Recommendations

- We recommend to apply the same integrated approaches been used in this study to the remaining members of Dhruma Formation (D1-D4).
- Detailed regional microfacies analysis is needed in order to enhance the correlation between different members of Dhruma Formation in the surface outcrops with that of subsurface equivalent.
- To carry out detailed diagenetic analysis within sequence stratigraphic framework.
- Most of the high porosity readings seem to be related to micro porosity. Therefore, detailed micro porosity analysis is needed for better reservoir characterization.
- Applying geomechanical and geochemical tools to enhance the reservoir zonation and characterization.
- Enhancing the 3D lithofacies model by the integration of LiDAR data (Light Detection and Ranging) with the high-resolution outcrop photo mosaic. This technique provides high-resolution 3D digital outcrop dataset, and it has significant contribution for better reservoir architecture analysis and 3D Model construction.

# References


Abdulkadir, I., Sahin, A., 2010. DISTRIBUTION OF PETROPHYSICAL PARAMETERS IN THE CAMBRO- ORDOVICIAN DIBSIYAH MEMBER OF THE WAJID SANDSTONE, SW SAUDI ARABIA. J. Pet.

Al-fares, A.A., Bouman, M., Jeans, P., 1998. A new look at the Middle to Lower Cretaceous stratigraphy, offshore Kuwait. GeoArabia 3.4, 543–560.

Al-Husseini, M.I., 2000. Origin of the Arabian plate structures: Amar Collision and Najd Rift. GeoArabia 5, 527–542.

Al-Husseini, M.I., 1997. Jurassic sequence stratigraphy of the western and southern Arabian Gulf. GeoArabia 2, 361–382.

Al-Jallal, I., 1995. The Khuff Formation: its regional reservoir potential in Saudi Arabia and other Gulf countries; depositional and stratigraphic approach. Middle East Pet. Geosci. Conf. GEO 94, 103–119.

Al-Mojel, A., 2010. High-Resolution Sequence Stratigraphy of the Middle Jurassic Lower Fadhili Reservoir in Khurais Complex, Central Saudi Arabia. KFUPM. Master, Thesis.

Allan, J.R., Matthews, R.K., 1982. Isotope signatures associated with early meteroic diagensis. Sedimentology 29, 797–817. doi:10.1111/j.1365-3091.1982.tb00085.x

Alméras, Y., 1987. Les brachiopodes du Lias-Dogger: paléontologie et biostratigraphie. Geobios.

Alsharhan, A., Kendall, C., 1986. Precambrian to Jurassic rocks of Arabian Gulf and adjacent areas: their facies, depositional setting and hydrocarbon habitat. Am. Assoc. Pet. Geol. Bull. 70, 977–1002.

Alsharhan, A., Nairn, A., 2003. Sedimentary basins and petroleum geology of the Middle East, 1st editio. ed. Elsevier.

Alsharhan, A.S., Magara, K., 1995. Nature and distribution of porosity and permeability in jurassic carbonate reservoirs of the Arabian Gulf basin. Facies 32, 237–253. doi:10.1007/BF02536872

Amaefule et al., 1993. Enhanced reservoir description: using core and log data to identify hydraulic (flow) units and predict permeability in uncored intervals/wells. SPE 68th Annu. Tech. Conf. Exhib. Soc. Pet. Eng. 205–220. doi:http://dx.doi.org/10.2118/26436-MS

Bell, A., 2004. The creation of late Proterozoic basement highs and their subsequent influence on

sedimentation patterns of the Arabian Peninsula, abstract. GeoArabia 9 (1), 50.

Choquette, P.W., Pray, L.C., 1970. Geologic nomenclature and classification of porosity insedimentary carbonates. Am. Assoc. Pet. Geol. Bull. 54, 207–250. doi:10.1306/5D25C98B-16C1-11D7-8645000102C1865D

Corbett, P., Potter, D., 2004. Petrotyping: A basemap and atlas for navigating through permeability and porosity data for reservoir comparison and permeability prediction. Pap. SCA2004-30 Present. Int. Symp. Soc. Core Anal. (pp. 5-9).

Corbett, P.W.M., Jensen, J.L., 1992. Estimating the mean permeability: how many measurements do you need? First Break 10, 89–94.

Deutsch, C.V., 2002. Geostatistical Reservoir Modeling. Oxford University press.

Dubrule, O., 1998. Geostatistics In Petroleum Geology, AAPG Continuing Education Course Note Series #38.

Dunham, R.J., 1962. Classification of carbonate rocks according to depositional textures. A. A. P. G. Mem., 1, 108–121.

Dykstra, H., 1978. The Prediction of Oil Recovery by Gravity Drainage. J. Pet. Technol. 30, 160–174. doi:10.2118/6548-PA

Ebanks, 1987. Flow unit concept-integrated approach to reservoir description for engineering projects. AAPG (Am. Assoc. Pet. Geol.) Bull.;(United States).

Edgell, S., 1992. Basement tectonics of Saudi Arabia as related to oil field structures. Kluwer Acad. Publ. 169–193. doi:10.1007/978-94-011-2654-0_10

EL-Sorogy, A., Galmed, M., Al-Kahtany, K., 2017. Microfacies and diagenesis of the Middle Jurassic Dhruma carbonates, southwest Riyadh, Saudi Arabia. J. African Earth Sci. In press.

Eltom, H., Abdullatif, O., Makkawi, M., Abdulraziq, A., 2014. Characterizing and modeling the Upper Jurassic Arab-D reservoir using outcrop data from Central Saudi Arabia. Geo Arab (2)19, 53–84.

Eltom, H., Makkawi, M., Abdullatif, O., Alramadan, K., 2013. High-resolution facies and porosity models of the upper Jurassic Arab-D carbonate reservoir using an outcrop analogue, central Saudi Arabia. Arab. J. Geosci. 6, 4323–4335. doi:10.1007/s12517-012-0708-1

Embry, A.F., Klovan, J.S., 1971. A Late Devonian reef tract on northeastern Banks Island. N.W.T. Bull. Can. Pet. Geol. 4, 730–781.

Enay, R., Mangold, C., Almeras, Y., 2009. The Wadi ad Dawisir “delta”, central Saudi Arabia: A

relative sea-level fall of Early Bathonian age. GeoArabia 14, 17–52.

Enay, R., Nindre, Y. Le, Mangold, C., Manivit, J., Vaslet, D., 1987. Le Jurassique d'arabie saoudite centrale: Nouvellesdonnées sur la lithostratigraphie, les paléoenvironnements, les faunes d'Ammonites, les âges et les corrélations. Geobios, Lyons, Mem. Spec. 9, 13–65.

Evamy, B.D., 1967. Dedolomitization and the Development of Rhombohedral Pores in Limestones 37.

Falivene, O., Arbués, P., Howell, J., Muñoz, J.A., Fernández, O., Marzo, M., 2006. Hierarchical geocellular facies modelling of a turbidite reservoir analogue from the Eocene of the Ainsa basin, NE Spain. Mar. Pet. Geol. 23, 679–701. doi:10.1016/j.marpetgeo.2006.05.004

Fitch, P.J.R., Lovell, M.A., Davies, S.J., Pritchard, T., Harvey, P.K., 2015. An integrated and quantitative approach to petrophysical heterogeneity. Mar. Pet. Geol. 63, 82–96. doi:10.1016/j.marpetgeo.2015.02.014

Flügel, E., 2010. Diagenesis, Porosity, and Dolomitization. In: Flugel, E., (ed.). Microfacies of Carbonate Rocks, in: Microfacies of Carbonate Rocks. Springer Berlin Heidelberg, Berlin, Heidelberg, pp. 267–338.

Flügel, E., 2004. Microfacies of Carbonate Rocks, Depositional Models, Facies Zones and Standard Microfacies. Springer Berlin Heidelb. 657–724.

Gringarten, E., Deutsch, C. V, 1999. Methodology for Improved Variogram Interpretation and Modeling for Petroleum Reservoir, in: SPE-56654-MS. Society of Petroleum Engineers, pp. 1–33.

Hughes, G.W., 2009a. Biofacies and palaeoenvironments of the Jurassic Shaqra Group of Saudi Arabia. Vol. Jurassica 6, 33–45.

Hughes, G.W., 2009b. Using Jurassic Micropaleontology To Determine Saudi Arabian Carbonate Paleoenvironments. SEPM Spec. Publ. 127–152.

Hughes, G.W., 2004. Middle to Upper Jurassic Saudi Arabian carbonate petroleum reservoirs: Biostratigraphy, micropaleontology, and paleoenvironments. GeoArabia 9, 79–114.

Isaaks, E.H., Srivastava, R.M., 1989. Applied Geostatistics, New York. Oxford University press. doi:10.1016/0040-1951(74)90006-7

Jordan, C., Wilson, J.L., 1994. Carbonate reservoir rocks. Pet. Syst. source to trap.

Konert, G., Afifi, A., Al-Hajri, S., et al., 2001. Paleozoic Stratigraphy and Hydrocarbon Habitat of the Arabian Plate. GeoArabia 6, 483–515.

Konert et al., 2001. Paleozoic Stratigraphy and Hydrocarbon Habitat of the Arabian Plate. GeoArabia 6, 483–515.

Lake, L., Jensen, J., 1991. A review of heterogeneity measures used in reservoir characterization. situ.

Longman, M., 1980. Carbonate Dlagenetlc Textures from Nearsurface Dlagenetic. Am. Assoc. Pet. Geol. Bull. 64, 461–487.

Lorenz, M., 1905. Methods of measuring the concentration of wealth. Publ. Am. Stat. Assoc.

Moore, C.H., Wade, W.J., 2013. Carbonate reservoirs : porosity and diagenesis in a sequence stratigraphic framework, 2nd ed. Elsevier Science, Amsterdam.

Nindre, Y. Le, Manivit, J., Manivit, H., Vaslet, D., 1990. Stratigraphie sequentielle du Jurassique et du Cretace en Arabie Saoudite. Bull. la Soc. Geol.

Nurmi, R., Charara, M., Waterhouse, M., 1990. Heterogeneities in carbonate reservoirs: detection and analysis using borehole electrical imagery. Geol. Soc.

Powers, R., 1968. Saudi Arabia: Lexique stratigraphique international: Paris. Fr. Cent. Natl. la Rech. Sci.

Powers, R., Ramirez, L., Redmond, C., 1966. Geology of the Arabian peninsula. Geol. Surv.

Pringle, J.K., Howell, J.A., Hodgetts, D., Westerman, A.R., Hodgson, D.M., 2006. virtual outcrop modeling.pdf. First Break 24, 33–42.

Reid, R.P., Macintyre, I.G., 2000. Microboring Versus Recrystallization: Further Insight into the Micritization Process. J. Sediment. Res. 70, 24–28.

Sahin, A., Saner, S., 2001. Statistical distributions and correlations of petrophysical parameters in the Arab-D reservoir, ABQAIQ oilfield, Eastern Saudi Arabia. J. Pet. Geol. 24, 101–114. doi:10.1111/j.1747-5457.2001.tb00663.x

Saller, A., Henderson, N., 2001. Distribution of porosity and permeability in platform dolomites: Insight from the Permian of west Texas: Reply. Am. Assoc. Pet. Geol. Bull.

Saner, S., Sahin, A., 1999. Lithological and zonal porosity-permeability distributions in the Arab-D reservoir, Uthmaniyah field, Saudi Arabia. Am. Assoc. Pet. Geol. Bull. 83, 230–243. doi:10.1306/A9673EAA-1738-11D7-8645000102C1865D

Schlaich, M., Aigner, T., 2015. The Geology of the Middle Jurassic Dhruma Formation in Outcrops of the Oman Mountains ( Sultanate of Oman ) The Geology of the Middle Jurassic Dhruma Formation in Outcrops of the Oman Mountains ( Sultanate of Oman ). pp. 8–11.

Schlumberger, 2007. Carbonate reservoirs: Meeting unique challenges to maximize recovery. Schlumberger Mark. Anal. 1–12.

Schmalz, J., Rahme, H., 1950. The variation of waterflood performance with variation in permeability profile. Prod. Mon.

Sharland, P., Archer, D.M., Casey, R.B., Davies, S.H., Hall, A.P., Heward, A.D., Horbury, A.D., Simmons, M.D., 2001. Arabian plate sequence stratigraphy, GeoArabia Special Publication 2, Gulf PetroLink, Bahrain.

Soleimani, B., Nazari, K., Bakhtiar, H., Haghparast, G., 2008. Three-Dimensional Geostatistical Modeling of Oil Reservoirs: A Case Study From the Ramin Oil Field in Iran. J. Appl. Sci.

T. Ahmed, 2006. RESERVOIR ENGINEERING HANDBOOK, Third Edit. ed. Elsevier.

Tiab, D., Donaldson, E., 2015. Petrophysics: theory and practice of measuring reservoir rock and fluid transport properties, 2nd ed.

Vaslet, D., Delfour, J., Manivit, J., Nindre, Y. Le, Brosse, J., 1983. Geologic Map of the Wadi a Rayn Quadrangle.

Vaslet, D., Pellaton, C., Manivit, J., Le Nindre, Y.-M., Brosse, J.-M., Fourniguet, J., 1985. Geologic map of the Sulayyimah quadrangle, sheet 21H, Kingdom of Saudi Arabia. Saudi Arab. Deputy Minist. Miner. Resour. Geosci. Map GM-100 A, scale 1250,000, with text 32 pp.

Wilson, J.L., 1975. Carbonate Facies in Geologic History. Springer, Verlag, New York.

Ziegler, M. a, 2001. Late Permian to HoIocene PaIeofacies EvoIution of the Arabian PIate and its Hydrocarbon Occurrences. GeoArabia 6, 445–504.

# Vitae

**Name** : Ibrahim Mohamed Yousif Mohamed

**Nationality** : Sudanese

**Date of Birth** :4/17/1988

**Email** : abrhomayousif@yahoo.com

**Address** : Khartoum-Sudan

**Academic Background** : B.Sc. in Petroleum Geology from Faculty of Petroleum & Minerals, Al Neelain University, Khartoum, Sudan (2011).

## Accepted Conference Papers

Ibrahim Yousif, Osman Abdullatif, Mohammad Makkawi, and Waleed Abdulghani, 2017, Sedimentology and High-Resolution Sequence Stratigraphy of the Middle Jurassic Dhruma Formation Carbonates Outcrops in the Central Saudi Arabia, in: EGU General Assembly, Vienna, Austria.

Ibrahim Yousif, Osman Abdullatif, Mohammad Makkawi, and Waleed Abdulghani, 2017, Lithofacies, Paleoenvironments, and Diagenesis of the Middle Jurassic Carbonate Dhruma Formation: Implications on Reservoir Quality, Outcrop Analog Approach, Central Saudi Arabia, in: AAPG/SEG International Conference & Exhibition, London, England.

Ibrahim Yousif, Osman Abdullatif, Mohammad Makkawi, and Mazin Bashri, 2018, Lithofacies and Reservoir Heterogeneity and Architecture of Carbonates D5 and D6 Members, Upper Dhruma Formation (Middle Jurassic), Outcrop Analog from Central Saudi Arabia, in: GEO 2018 13$^{th}$ Middle East Geosciences Conference & Exhibition, Manama, Bahrain.

## Journal Manuscripts (Under review)

Ibrahim M. Yousif, Osman M. Abdullatif, Mohammad H. Makkawi, Mazin Bashri and Waleed Abdulghani, 2017, Lithofacies, paleoenvironment and high-resolution stratigraphy of the D5 and D6 Members of the Middle Jurassic carbonates Dhruma Formation, outcrop analog, central Saudi Arabia, Journal of African Earth Sciences.